Elucidating the Mechanisms and Biological Consequences of Exogenous Fatty Acid Utilization by *Staphylococcus aureus*

Emily L. Pruitt

A dissertation

submitted in partial fulfillment of the

requirements for the degree of

Doctor of Philosophy

University of Washington

2024

Reading Committee:

Libin Xu, Chair

Matthew Bush

Bo Zhang

Program Authorized to Offer Degree:

Chemistry

University of Washington

Abstract

Elucidating the Mechanisms and Biological Consequences of

Exogenous Fatty Acid Utilization by *Staphylococcus aureus*

Emily L. Pruitt

Chair of the Supervisory Committee:

Libin Xu

Departments of Medicinal Chemistry and Chemistry

Staphylococcus aureus is a significant human pathogen known for its ability to cause a range of infections, from minor skin conditions to life-threatening diseases. The ability of *S. aureus* to utilize exogenous fatty acids (eFAs) from the host environment has emerged as a crucial factor in its pathogenesis and antibiotic resistance. This dissertation explores the mechanisms and biological consequences of eFA utilization by *S. aureus* by employing advanced lipidomic techniques to elucidate the underlying processes. Chapter 2 investigates the substrate specificity of *S. aureus*-secreted lipases, the effect of human serum albumin on eFA incorporation, and the effect of the FASII inhibitor AFN-1252 on eFA, highlighting the adaptive mechanisms *that S. aureus* employs to maintain membrane integrity and resist antimicrobial agents. Chapter 3 introduces a novel analytical approach integrating an online Paternó-Büchi (PB) reaction with hydrophilic interaction liquid chromatography-ion mobility-mass spectrometry (HILIC-IM-MS)

to determine the position of carbon-carbon double bonds in unsaturated lipids. This technique enhances the resolution and accuracy of lipidomic analyses, and provides detailed insights into the structural modifications of lipids produced by *S. aureus* under different growth conditions and treatments. Chapter 4 summarizes the key findings and discusses the broader implications of eFA use in *S. aureus.* These results underscore the importance of lipid metabolism in bacterial adaptation and resistance, and suggest potential targets for therapeutic intervention. Overall, this dissertation contributes to a deeper understanding of the metabolic strategies employed by *S. aureus* to thrive in various host environments. By elucidating the mechanisms of eFA utilization and its effects on membrane dynamics, this study provides a foundation for the development of novel antimicrobial therapies aimed at disrupting bacterial lipid metabolism and mitigating the threat of antibiotic-resistant infections.

DEDICATION

To my loving husband

and

To Bernie & Jack

and

To Phoebe & Moose

ACKNOWLEDGEMENTS

There are many incredible people who have changed my life in the last few years, from those who simply exchanged a smile with me in the hallway to those who let me cry on your shoulder. Graduate school has been a rollercoaster of a journey, and I would not be here today or have made any of these accomplishments without all of you. Thank you.

To my graduate research advisor, Libin- thank you for your unwavering guidance, patience, and encouragement throughout this journey. My graduate school experience took a complete 180° turn in the best way when you agreed to let me join your lab. Thank you for taking a chance on me, teaching me, supporting me, and never giving up on me. Your insights have been invaluable to my research and for both my personal and professional development. Thank you for demonstrating such genuine care, compassion, and enthusiasm.

To my wonderful lab mates- thank you for your camaraderie, collaboration, and friendships. You all welcomed me into the lab with open arms, and I am forever grateful that you did. Thank you for helping me with research projects, teaching me all the science, and always saying yes to a coffee break. I truly admired your brilliance, hard-work ethics, and kindness. I am so excited to see where life takes you- each one of you is going to do incredible things.

To my sweet friends, Sarah, Vanessa, and Cyan- thank you for loving and encouraging me through all the ups and downs. Sarah, I could not be more grateful that the universe brought you into my life, first as my mentor and now as my best friend. You are my person. I would not have made it here without you. Vanessa, you are one of the most generous, supportive, and strongest people I know. I cannot imagine going through graduate school without you by my side. Thank you for always being there for me, venting and celebrating over wine, loving my

little family, and cheering me on. Cyan, you were such a constant light through some of the hardest times. Thank you for sticking with me, having weekly wine Wednesdays, making me laugh, and creating some of the most fun memories together.

To my fantastic family, both in Northa Carolina and Washington- I truly owe you a profound debt of gratitude. Thank you for your encouragement and for always showing an interest in my research, even when you did not understand it. Mom and Dad, you were here from the very beginning. Thank you for showing me unwavering love and giving me every opportunity to succeed. Your belief in me is a constant source of motivation. Lolli and Pop, thank you for your thoughtful cards and for supporting me no matter what. Benjamin, thank you for being the coolest broski around and always telling me how proud you were of me. To the Leong family, thank you for adopting me into your family and making Seattle feel like home.

To my undergraduate chemistry professor, Dr. Hall- thank you for inspiring, challenging, and supporting me. Your words of encouragement before I left for graduate school have stuck with me every step of the way, “Em, you got through p-chem, now you can do anything.” Thank you for continuing to show up for me and being a special part of my life to this day.

To my loving husband, Seth- thank you for everything. Thank you for moving across the country to be with me, provide for me, and show up every day as my number-one fan. Thank you for picking me up from school countless times late at night, supplying me with never ending Coke Zeros, supporting my crazy endeavors, and taking me on the grandest adventures. You are my pillar of strength, and your encouragement has been the driving force behind my success. I could not have done this without you.

TABLE OF CONTENTS

LIST OF FIGURES

LIST OF TABLES

CHAPTER 1: Introduction

1.1. Overview of *Staphylococcus aureus* as a Significant Human Pathogen

Staphylococcus aureus is a formidable gram-positive bacterium known for its opportunistic pathogenicity, genetic diversity, and adaptability to diverse host environments. Discovered in 1880 by Scottish surgeon Sir Alexander Ogston during his investigations of surgical wound infections, *Staphylococcus* was named for its characteristic growth pattern resembling grape clusters (from the Greek *Staphyle*- "bunches of grapes" and *kokkos*- "berry") (1, 2). Soon after, the German physician Friedrich Julius Rosenbach isolated a staphylococci strain identified as *Staphylococcus aureus,* which he named for its distinguishable golden-yellow colored colonies (from the Latin *aurum*- "gold") (3). By the early 1900s, *S. aureus* infections had reached a fatality rate of almost 82%, piquing the interest of investigators in studying the course of action and diseases caused by this bacterium (4).

Penicillin was introduced against *S. aureus* infections in the 1940s, and although it initially improved treatment outcomes, resistant bacterial strains quickly evolved, presenting significant challenges to the new age of antibiotics (5–9). In response to the spread of penicillin-resistant strains, the antibiotic methicillin was introduced in 1961 for clinical use; however, this marked a critical point because methicillin-resistant *Staphylococcus aureus* (MRSA) emerged within the same year and has since become a leading cause of healthcare-associated and community-acquired infections worldwide (9–12).

S. aureus is a common commensal organism of the human microbiota and a potent pathogen capable of causing life-threatening infections (13–16). Colonization occurs in approximately 30% of the general population and primarily affects the human skin and nose (17–19). When the mucosal membrane or dermal barrier is compromised, such as through wounds, surgical procedures, or persistent skin disorders, *S. aureus* can penetrate the underlying tissues,

organs, or bloodstream, causing a range of superficial and invasive infections (13, 15, 20, 21). Foreign implants, such as catheters and prosthetic joints, are also vulnerable to bacterial and biofilm-related infections, which comprise complex bacterial communities that adhere to surfaces (14, 15, 22–26). The versatility of *S. aureus* to infiltrate nearly every host biological system poses the most significant risk of infection in individuals with compromised immune systems, chronic illnesses, and those undergoing invasive procedures. However, *S. aureus* strains capable of causing invasive, life-threatening infections in previously healthy individuals have emerged in community settings (16, 17).

Despite decades of dedicated research and antimicrobial development, the treatment of *S. aureus* infections remains a substantial and urgent medical challenge worldwide. The complexity of MRSA strains, in particular, presents significant hurdles, leading to higher healthcare costs, extended hospital stays, and tragically, higher mortality rates (27, 28). The USA300 strain first emerged in community settings but has now become the primary source of both community- and hospital-associated infections (29–31). To date, more than 20 years have passed since a new class of antibiotics was clinically introduced to treat these infections (32). Owing to its substantial impact on morbidity and mortality, the World Health Organization (WHO) has classified MRSA as a high-priority pathogen, and the Centers for Disease Control and Prevention (CDC) have deemed it a serious threat to public health (12, 33). This burden of MRSA and its threat to global health underscores the urgent need for effective infection control measures, education, and the development of novel therapeutics.

1.2. Host-Pathogen Interaction

There is a great deal of interest in deciphering host-pathogen interactions with *S. aureus* and their subsequent consequences, although the emphasis has primarily been on how

mammalian hosts detect or react to bacterial pathogens and less on understanding the pathways by which potential pathogens respond to environmental cues or the immune system (19, 34). However, an expanding area of research focuses on how *S. aureus* senses the environment to adapt to individual niches on and within the host, utilizes these cues to express specific virulence factors, and alters the host response to infection, thereby providing key insights into the molecular mechanisms of infectious diseases (19). This is vital for identifying novel targets to develop therapeutics to reduce pathogen virulence.

S. aureus deploys an arsenal of virulence factors to promote pathogenesis across various host environments and has evolved the ability to resist host defense antimicrobial components (25, 31, 35–39). Lipids play a crucial role in *S. aureus* pathogenesis in addition to their role in other cellular processes. They modulate the production of virulence factors and are involved in biochemical cell signaling, membrane protein function, respiratory energy metabolism, and bacterial membrane formation. This link between lipid metabolism and pathogenesis provides a potential avenue for the development of novel therapeutics (19, 22, 34, 38, 40–43). In *S. aureus,* the cytoplasmic membrane is primarily composed of the major lipids diglycosyldiacylglycerols (DGDG), phosphatidylglycerol (PG), lysyl-phosphatidylglycerol (LysylPG), and cardiolipin (CL), with PGs being the most abundant (44–46).

S. aureus acclimates to diverse host environments by continuously adjusting its membrane composition according to environmental cues such as changes in temperature, salinity, osmolarity, pH, and presence or absence of oxygen, thereby directly influencing the biophysical properties of the membrane with modifications to phospholipid headgroups and fatty acid chain structures (42, 47–53). These modulations play crucial roles in the survival and virulence of *S. aureus* throughout the host and in its resistance to antimicrobial agents (43, 54,

55, 45, 52). Further understanding of the multifaceted mechanisms involved in bacterial fatty acid synthesis, phospholipid structural modifications, and the consequential change in lipid packing and membrane fluidity is vital to provide insight into the adaptations of *S. aureus* in host-pathogen interactions and reveal potential targets to combat antimicrobial resistance.

1.3. Lipid Metabolism in *Staphylococcus aureus*

1.3.1. *Overview of Bacterial Lipids*

Staphylococcus aureus sustains the function and integrity of its membrane by regulating its total phospholipid content and fatty acid composition. Saturated straight-chain or branched-chain fatty acids (SCFAs or BCFAs) are synthesized by the bacterium through the *de novo* Type II fatty acid synthesis (FASII) pathway (56). Lipid packing levels in organisms are typically modulated using unsaturated fatty acids (UFAs), acyl chains that contain one or more double bonds. A vital caveat of *S. aureus* phospholipid synthesis is its inability to synthesize UFAs endogenously (42, 44). Instead, it uses branching to regulate membrane fluidity by synthesizing iso- and anteisobranched-chain fatty acids derived from amino acid precursors (42, 57–59). Additionally, *S. aureus* can incorporate exogenous fatty acids (eFAs) from the host into its phospholipids, reducing energy consumption from *de novo* fatty acid biosynthesis and modifying the membrane composition to bypass the innate immune response and withstand drug activity (56, 59–65, 46). Using host sources for eFA can directly impact FASII regulation and lipid metabolism in *S. aureus*; therefore, it is important to first consider how the bacterium synthesizes *de novo* fatty acids and endogenous phospholipids.

1.3.2. *Fatty Acid Synthesis Pathway*

Unlike the mammalian Type I fatty acid synthesis system, which is characterized by a single multifunctional polypeptide, *S. aureus* presents a unique case. It employs a discrete set of genes, with each gene encoding a specific enzyme for individual steps in FASII (40, 41, 49). Fatty acid synthesis in *S. aureus* consists of an initiation phase and elongation cycle to produce SCFAs or BCFAs. Precursors of SCFA are derived from acetyl-CoA, which is converted to malonyl-CoA by acetyl-CoA carboxylase (ACC). FabD (malonyl-CoA-ACP transacylase) transfers the malonyl group of malonyl-CoA to an acyl carrier protein (ACP), forming malonyl-ACP (40). The branched-chain amino acids leucine, isoleucine, and valine are acetyl-CoA precursors used in BCFA synthesis (66).

Initiation of FASII in *S. aureus* is facilitated by a single 3-ketoacyl-ACP synthase III (FabH), utilizing malonyl-ACP and acetyl-CoA to form β-ketoacyl-ACP (40, 66). The FASII elongation pathway involves a series of four enzymatic reactions that progressively extend the acyl chain attached to ACP by two carbons per cycle, as depicted in **Figure 1.1** (41)**.** Upon introduction by FabH, β-ketoacyl-ACP is reduced using FabG (β-ketoacyl-ACP reductase), dehydrated by FabZ (β-hydroxyacyl-ACP dehydratase), and then reduced by FabI (enoyl-ACP reductase I) to complete the cycle. The enzymatic activity of β-Hydroxyacyl-ACP dehydratases typically produces unsaturated fatty acids. However, in contrast to other microorganisms, *S. aureus* contains only one isoform of this enzyme, FabZ, which is considered unable to introduce double bonds into the growing acyl chain (41, 57). The acyl-ACP molecule produced from FASII either undergoes subsequent rounds of elongation facilitated by condensation with malonyl-ACP using FabF (β-ketoacyl-ACP synthase II), or continues into the bacterial phospholipid biosynthesis pathway (40, 41).

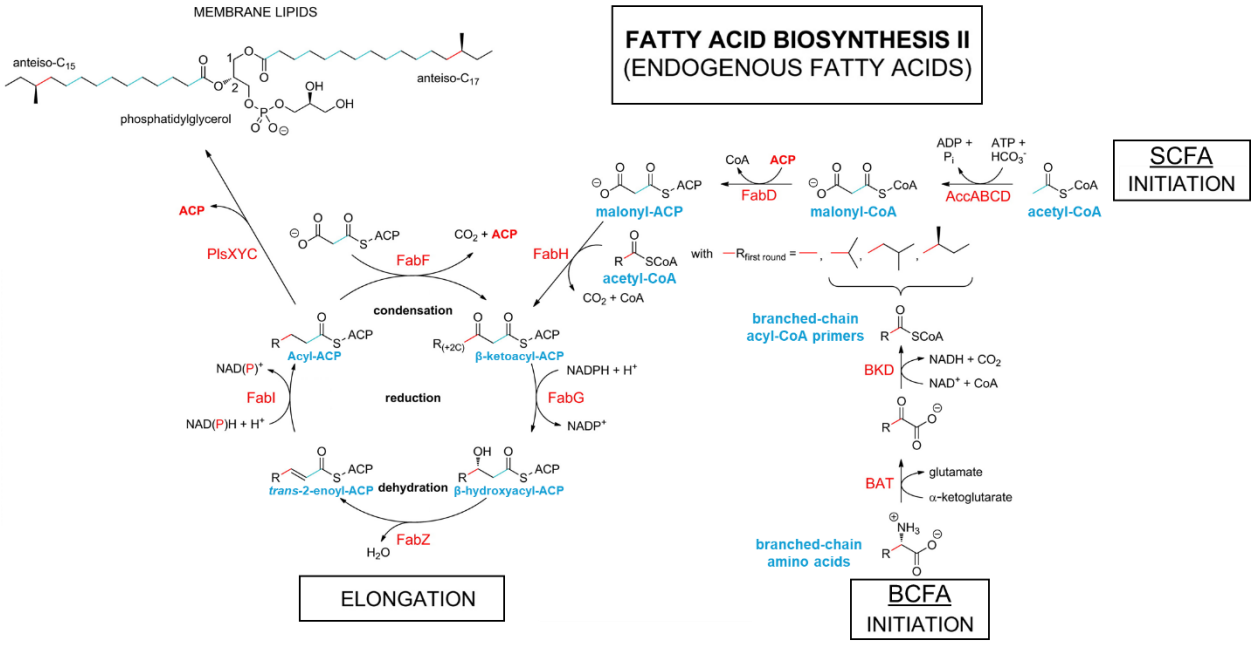

Figure 1.1. Bacterial type II fatty acid (FASII) biosynthesis pathway.

This figure has been adapted from Schiebel J, Chang A, Lu H, Baxter MV, Tonge PJ, Kisker C. 2012. Staphylococcus aureus FabI: Inhibition, Substrate Recognition, and Potential Implications for In Vivo Essentiality. Structure 20:802–813. (© 2012), with permission from Elsevier.

1.3.3. *Membrane Lipid Synthesis Pathway*

Membrane phospholipid synthesis in *S. aureus* begins with acylation of glycerol-3-phosphate (G3P). Acyl-ACP end-products of the FASII elongation pathway are converted to acyl-PO_4 by PlsX (acyl-acyl carrier protein: phosphate transacylase) by transferring the acyl group to inorganic phosphate. Acyl-phosphate is then converted to the universal bacterial phospholipid precursor phosphatidic acid by PlsY (glycerol-3-phosphate acyltransferase) and PlsC (1-acyl-sn-glycerol-3-phosphate acyltransferase) (43, 60, 67).

Phosphatidic acid can be converted to glycolipids, such as diglycosyldiacylglycerols (DGDG) and monoglucosyldiacylglycerol (MGDG), or phospholipid phosphatidylglycerol (PG), which is the most abundant lipid species in *S. aureus* (**Figure 1.2**) (43, 44). PG is then used as the central phospholipid from which other phospholipids are derived. Lysyl-phosphatidylglycerol (Lysyl-PG) is formed through the transfer of L-lysine to PG, catalyzed by the transmembrane enzyme multi-peptide resistance factor *MprF* (68). Cardiolipins (CLs) are synthesized from the condensation of two PG molecules using cardiolipin synthase 1 and 2 (*cls1* and *cls2*) (69). *S. aureus* can change the lipid species content within its membrane in response to external stimuli, altering the sensitivity of host-pathogen interactions and dictating antibiotic efficacy.

1.3.4. *Exogenous Fatty Acid Utilization*

Staphylococcus aureus has adapted alternate metabolic pathways to incorporate eFAs from the host environment to support its growth and virulence (63). The bacterium can only synthesize saturated fatty acids, but can also utilize host-derived SCFAs and UFAs. These eFAs play an essential role in providing an additional source of energy and building components for membrane biosynthesis, especially in environments where endogenous synthesis may be limited or inhibited. To facilitate the incorporation of eFAs into the membrane, *S. aureus*

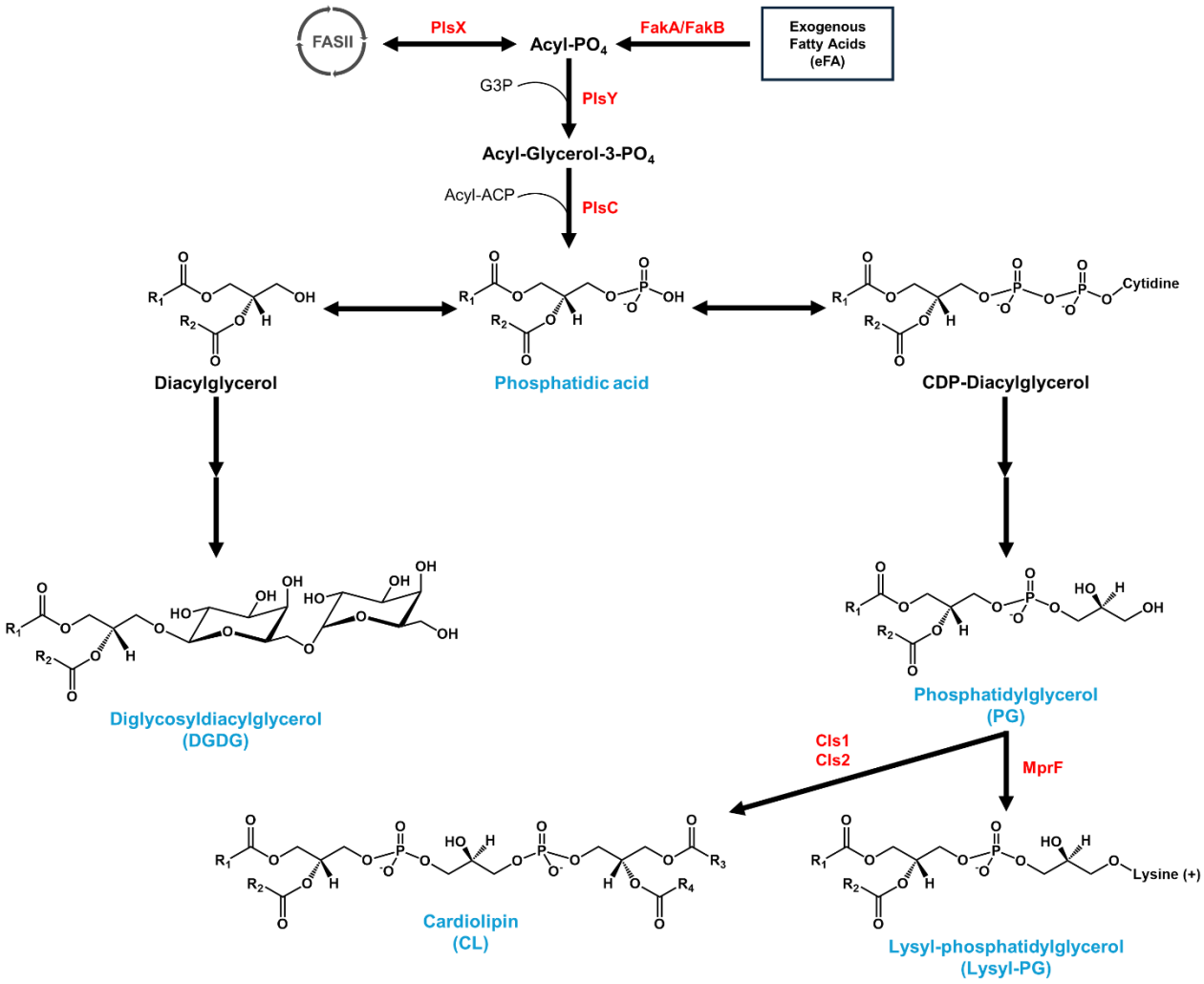

Figure 1.2. Membrane lipid biosynthetic pathway in *S. aureus*.

secretes at least three main lipases, SAUSA300_2603 (Sal1, encoded by *gehA*), SAUSA300_0320 (Sal2 or Geh, encoded by *gehB),* and SAUSA300_0641 (Sal3 or 0641, encoded by *gehE),* to release fatty acids from lipids found in the serum and low-density lipoproteins (63, 64, 70–73). Once FFAs are released by lipases, they can be taken up by bacteria, phosphorylated by fatty acid kinase (FakA), and incorporated into bacterial lipids, with or without further elongation via the FASII pathway (**Figure 1.3**) (46, 59, 60, 63, 74).

1.3.5. *Effect on Antimicrobial Resistance*

Resistance to some cell wall-and cell membrane-targeting antimicrobials in *S. aureus* has been associated with variations in phospholipid and fatty acid content. PGs are anionic, carrying a unit negative charge, and, as the most abundant lipid species, they significantly contribute to membrane stability and electrostatic interactions (43, 75, 76). Cationic compounds, such as host-generated cationic antimicrobial peptides (CAMPs), are a class of antimicrobial agents that utilize the negative charge of PG phospholipids to adhere to and insert into the bacterial membrane, leading to compromised structural integrity and the breakdown of essential microbial processes (77–79). To escape this innate immune attack, *S. aureus* increases the production of Lysyl-PG, adding a positively charged lysine residue to PG lipids. Upregulation of lysyl-PG inherently decreases the amount of PG lipids available for binding and increases the membrane positive charge, which may aid in repelling cationic compounds (36, 43, 78, 80).

Daptomycin is a membrane-targeting cyclic lipopeptide approved by the United States Food and Drug Administration in 2003 and used as a last-resort treatment for severe MRSA infections (81, 82). The efficacy of this antibiotic depends on its complex formation with calcium, which facilitates oligomerization and insertion into the bacterial membrane, forming

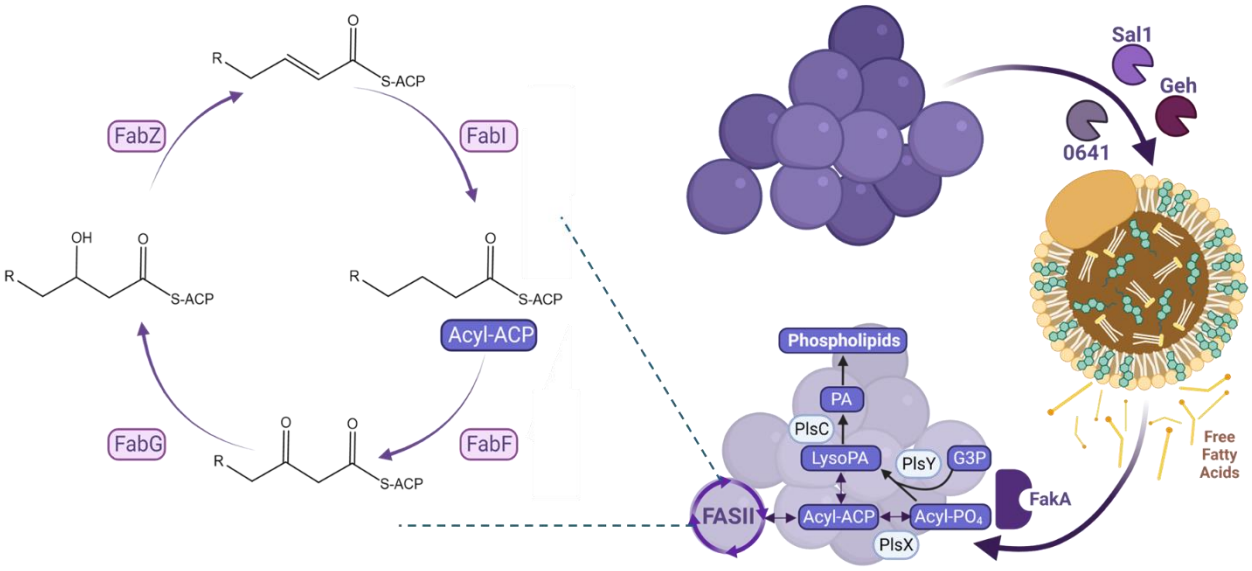

Figure 1.3. Pathways of exogenous fatty acid uptake and incorporation.

pores, which subsequently leads to cell death (81, 83, 84). Infection treatment failure and *S. aureus* resistance have been correlated with membrane adaptations, such as alterations in charge and fluidity, mutations related to the cell wall or lipid synthesis, and the release of membrane phospholipid decoys (45, 83, 85–89). One such metabolic adaptation resulting in decreased daptomycin susceptibility is characterized by a mutation in cardiolipin synthase (*cls2*), which increases CL content and decreases PG lipids (45). An increase in CLs has also been associated with decreased membrane fluidity and inhibition of daptomycin pore-formation activity (69, 83, 85, 90). While *S. aureus* cannot endogenously synthesize UFAs, it can incorporate exogenous UFAs, altering lipid packing in the membrane by increasing bacterial membrane fluidity and, in turn, affecting the binding of membrane-targeting antimicrobials, such as daptomycin (81).

As the bacterial FASII metabolic pathway is distinctly different from the mammalian fatty acid synthesis system, the unique mechanisms and enzymes of FASII have become targets for antimicrobial drug development (91–94). AFN-1252 is a FASII-targeting antibiotic developed to inhibit the FabI enzyme, thereby inhibiting the endogenous phospholipid synthesis in *S. aureus* (94). Its effect on broad lipidomic changes has not yet been well characterized, and the therapeutic efficacy of AFN-1252 is still debated, as it shows promising treatment for skin and soft-tissue bacterial infections, but FASII bypassing variants that utilize host-derived eFAs raise questions about its long-term effectiveness (94–97, 74, 98–102). Revealing the changes in phospholipids and fatty acid composition within *S. aureus* from the utilization of eFAs has significant implications for the nature of the bacterial cell surface, its effect on membrane biophysical properties, function and activity of antimicrobials, and its interaction with the host defense system (46).

1.4. Lipidomic Methods

Lipidomics is a widely used approach for investigating the mechanisms underlying the utilization of host-derived fatty acids and their effects on the susceptibility of *S. aureus* to membrane-targeting antimicrobials. Lipids are hydrophobic or amphipathic small molecules characterized by their structural and biosynthetic complexities into eight main classes: fatty acyls, glycerolipids, glycerophospholipids, sphingolipids, sterol lipids, prenol lipids, saccharolipids, and polyketides (103). The main lipid classes can be further divided into numerous subclasses and combinations of modifications, reflecting a diverse range of functions (103–106). However, most lipids occupy a narrow mass range of approximately 600-900 *m/z*, which makes it difficult to resolve the majority of the lipid species (105, 107). Previously, we developed a hydrophilic interaction liquid chromatography (HILIC) ion mobility-mass spectrometry (IM-MS) method to identify changes in the lipidome with increased resolution of isobaric lipid species (107).

Normal-phase and reverse-phase chromatography systems have previously been used to separate lipids; however, the gradients were long, sometimes longer than 30 min, and did not achieve reliable separation (104, 107). By combining polar stationary phase columns with a highly organic gradient separation, HILIC can resolve lipid species based on the polarity of the head groups (on a scale of seconds) and then by acyl chain length and the degree of unsaturation within the subclass (85, 105, 107). Despite an impressive improvement from previous methods, HILIC coupled with MS alone is unable to effectively separate all lipid species in a single run (108).

To further increase the separation of lipids, an orthogonal gas-phase separation, ion mobility (IM), is coupled with HILIC and MS. In IM separation, ions are driven through a

mobility drift region by an applied electric field while an inert background gas (most commonly helium or nitrogen) impedes ion motion (107). Compact structures undergo fewer collisions with the gas and move rapidly through the drift region, whereas extended structures undergo more collisions and move more slowly. Ions with the same charge are separated by size and shape, which is reflected by their collision cross section (CCS) with the background gas (105, 107). Traditionally, CCS values have been directly measured using drift-tube IM (DTIM) instruments, where CCS (or Ω) is linearly proportional to the time required for an ion to traverse the drift region (drift time, t_d) in a static electric field (109). On the other hand, traveling-wave IM (TWIM) instruments use a migrating low-voltage wave to push ions through the buffer gas, offering higher sensitivity and a faster duty cycle (107, 109). While this dynamic electric field does not allow for direct CCS measurements, CCS calibrants with similar physical properties to analytes and known values can be used to calibrate the relationship between CCS and drift time through a modified Mason–Schamp equation:

$$\Omega = \left(\frac{18\pi}{16}\right)^{\frac{1}{2}} \frac{ze}{(k_B T)^{\frac{1}{2}}} \left[\left(\frac{1}{\mu}\right)^{\frac{1}{2}} \frac{760}{P} \frac{T}{273} \frac{1}{N_0} A(t_d)^B\right] = ze\left[\left(\frac{1}{\mu}\right)^{\frac{1}{2}} A'(t_d - t_0)^B\right]$$

Ω is the CCS, *ze* is the ion charge, μ is the reduced mass of the ion and drift gas, t_d is the drift time, t_0 is the ion flight time outside the drift cell, *B* is a constant determined from fitting with known DTIM CCS calibrants, and *A'* combines the fit term (A) and Boltzmann constant (k_B), drift gas temperature (T), pressure (P), and drift-gas number density (N_0) (109). Thus, by using lipid standards as calibrants, accurate CCS values of lipid ions can be obtained, which can be used to enhance the confidence of lipid identification. Herein, we report a multidimensional HILIC-IM-MS-based lipidomics approach to characterize the factors affecting the utilization of eFAs by *S. aureus*.

1.5. Overview of Following Dissertation Chapters

The studies detailed in this dissertation aimed to elucidate the influence of various host environments on the metabolism of *S. aureus.* Further understanding of the adaptive mechanisms and subsequent biological consequences of the utilization of exogenous fatty acids by the bacterium is presented using comprehensive lipidomic profiling methods. **Chapter 2** investigates the substrate specificity of the secreted bacterial lipases Sal1, Geh, and 0641 in the presence of human serum and the major donors of fatty acids in serum. Human serum albumin was assessed as a viable source of exogenous fatty acids for *S. aureus* and its ability to restrict or enhance host fatty acid utilization. The effects of AFN-1252, a FASII inhibitor, on the incorporation of eFAs into the bacterial membrane and possible adaptive mechanisms are presented. Building upon the observed lipid changes that occur in *S. aureus*, the formation of reactive oxygen species and cell membrane fluidity were also explored, emphasizing the metabolic adaptations of *S. aureus* in the host environment. **Chapter 3** presents an innovative analytical approach for determining the carbon-carbon double bond position in unsaturated lipids and fatty acids by integrating an online photochemical Paternó-Büchi reaction with HILIC-IM-MS. This approach uses 2-acetylpyridine as the reagent and demonstrates its applicability in tracking the metabolic adaptation of *S. aureus*, resulting in more detailed lipid characterization. Overcoming analytical challenges in lipidomics is necessary to gain insight into the adaptive mechanisms of resistant bacterial strains. **Chapter 4** summarizes the overall findings and describes the future directions for this project and related research. Together, these studies provide valuable insight into identifying potential targets for the development of novel therapeutics, further the understanding of exogenous fatty acids utilized by *Staphylococcus aureus* and subsequent biological consequences, and contribute to unraveling the complexity of the host-pathogen interaction.

CHAPTER 2: Elucidating the Impact of Bacterial Lipases, Human Serum Albumin, and FASII Inhibition on the Utilization of Exogenous Fatty Acids by *Staphylococcus aureus*

This chapter has been reproduced with permission from Pruitt EL, Zhang R, Ross DH, Ashford NK, Chen X, Alonzo F III, Bush MF, Werth BJ, Xu L. Elucidating the Impact of Bacterial Lipases, Human Serum Albumin, and FASII Inhibition on the Utilization of Exogenous Fatty Acids by *Staphylococcus aureus*. *mSphere*. 2023; 8(6):e0036823. (©2023). with minor edits.

2.1. Introduction

Antibiotic-resistant bacteria pose a major threat to global health, killing more people than HIV/AIDS or malaria (110). Among them, *Staphylococcus aureus* has been deemed one of the most serious threats, infecting the skin, soft tissue, and blood. It causes nearly 120,000 bloodstream infections with 20,000 associated deaths per year in the United States alone (111). *S. aureus* adapts to the host environment by incorporating exogenous fatty acids (eFAs) into its cell membrane, thereby allowing the bacteria to reduce energy consumption from *de novo* fatty acid biosynthesis, bypass the innate immune response, and withstand drug activity (98–100, 112–117). Elucidating the effects of host fluids on the metabolism of the bacteria is critical to understanding the host-pathogen interaction and evolution of antimicrobial resistance (112, 118–120).

S. aureus only synthesizes straight-chain or branched-chain saturated fatty acids (SCFAs or BCFAs) via the type II fatty acid synthesis pathway (FASII) but can also utilize host-derived SCFA and unsaturated fatty acids (UFAs) or free fatty acids (FFA) (113, 115, 117, 121, 122). In our recent study, lipidomics analysis of *S. aureus* grown in human serum showed that bacteria incorporate UFAs into the bacterial membrane lipids, and cholesteryl esters and triglycerides are the major donors of fatty acid substrates in serum (112). Human serum albumin, an abundant carrier protein in the bloodstream that binds to acidic and lipophilic compounds, has been shown to sequester FFAs to restrict their exploitation by the bacteria (101, 123), but we hypothesize that it may also serve as a reservoir of fatty acids.

To facilitate the incorporation of eFAs into its membrane, *S. aureus* secretes three lipases, *S. aureus* lipase 1 (Sal1), glycerol ester hydrolase (Geh), and SAUSA300_0641 (0641 or sal3), to release FFA from lipids found in serum (**Figure 2.1**) (113, 114, 121, 124–127). Once FFAs are

released by the lipases, they can be taken up by the bacteria, phosphorylated by the fatty acid kinase (FakA), and incorporated into the bacterial lipids, with or without further elongation via the FASII pathway (Figure 2.1) (112–116). When using triglycerides (TGs) as substrates, Geh can release both short- (4-carbon) and long-chain substrates (16 and 18-carbon), with a preference for the long-chain fatty acids linoleic acid (18:2) and oleic acid (18:1), whereas Sal1 prefers short-chain fatty acid (4-carbon) substrates (113, 114, 124–126). 0641 was also found to prefer hydrolyzing short-chain fatty acids (4-carbon or fewer) from triglycerides (127). Several studies have revealed the importance of these lipases as multifaceted virulence factors in *S. aureus* infections; however, the substrate specificity of Geh, Sal1, and 0641 on cholesterol esters and the impact of Geh, Sal1, or 0641 knockouts on eFA utilization have not been examined previously.

Incorporated serum UFAs can alter lipid packing, affecting the binding of membrane-targeting antimicrobials, and as an adaptive mechanism to drug exposure, *S. aureus* has been shown to modify its membrane and cell wall composition (98, 128–131). AFN-1252, a FabI inhibitor, has been developed as a FASII-targeting antibiotic, but its effect on broad lipidomic changes has not been well characterized (116). The therapeutic efficacy of AFN-1252 also remains in debate, as it shows promising treatment for skin and soft-tissue bacterial infections, but FASII bypassing variants that utilize host-derived eFAs, bring into question its long-term effectiveness (94–96, 98–101). Although *S. aureus* can uptake eFAs and use them to evade the effects of FASII inhibitors and antibiotics, UFAs have also long been known to be toxic to the bacteria (113, 132–134). Polyunsaturated fatty acids (PUFAs), such as the abundant mammalian fatty acid arachidonic acid, can inflict damage on *S. aureus* upon incorporation into its membrane and kill the pathogen through a lipid peroxidation mechanism (132, 135, 136).

Despite previous work on the effect of exogenous fatty acids on *S. aureus,* several significant questions remain. First, the substrate specificity of the released lipases toward cholesterol esters remains unknown. Second, the comprehensive lipidomic changes resulting from eFA utilization have not been completely elucidated. Third, the role of albumin as a reservoir for fatty acids and its impact on eFA incorporation efficacy has not yet been determined. Fourth, the effect of the FASII inhibitor, AFN-1252, on eFA utilization has not yet been investigated. To answer these questions, we grew *S. aureus* and *geh*, *sal1*, *0641*, or *fakA* knockout (KO) mutant strains in tryptic soy broth (TSB) supplemented with eFAs under various conditions and conducted comprehensive lipidomic analyses of these bacteria. We further characterized the changes in membrane fluidity and formation of reactive oxygen species resulting from the incorporation of unsaturated eFAs.

We found that a) Geh is the primary lipase responsible for hydrolyzing cholesteryl esters, and, to a less extent, triglycerides; b) exogenous fatty acids were incorporated into the bacterial membrane when grown in serum regardless of the lipase knockout; c) human-serum albumin can serve as a buffer of eFA for *S. aureus*, facilitating the use of eFAs at a low concentration but inhibiting eFA utilization at high concentrations; d) AFN-1252 leads to an increase of UFAs in its membrane with or without eFAs; e) incorporation of unsaturated eFAs leads to increased membrane fluidity during the exponential growth phase; and f) incorporation of unsaturated eFAs increases reactive oxygen species formation, inhibiting *S. aureus* growth.

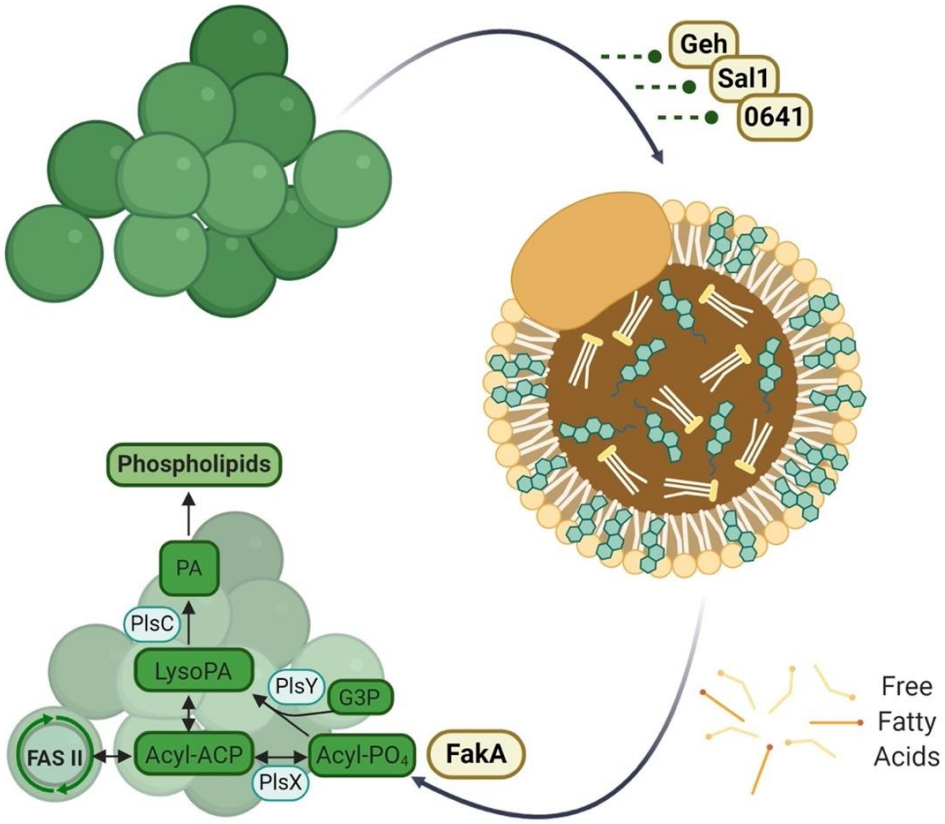

Figure 2.1. Schematic overview of exogenous fatty acid utilization by *S. aureus*.

2.2. Results

2.2.1. *S. aureus lipase knockouts grown in serum still incorporate UFAs.*

S. aureus and *geh*-, *sal1*-, *0641*-, or *fakA*- knockout mutant strains (Δ*geh*, Δ*sal1*, Δ*0641*, or Δ*fakA*) were grown in the presence and absence of human serum, and changes in the lipidome were identified through hydrophilic-interaction liquid chromatography (HILIC) ion mobility-mass spectrometry (IM-MS) to determine the role of each enzyme in this environment. HILIC first resolves lipid species on a scale of seconds based on the polarity of the head groups and then by acyl chain length and degree of unsaturation within the subclass (137–139). Lipid separation is further increased through ion mobility, a gas-phase separation orthogonal to liquid chromatography (LC). As described previously, lipid identification is enhanced by using collisional cross section (CCS) values obtained from the IM-MS analysis (137, 138). Some serum-derived lipids, such as phosphatidylcholines, phosphatidylethanolamines, and sphingomyelins, are not incorporated into the bacterial membrane (112). Thus, major lipids that are synthesized by *S. aureus,* diglucosyldiacylglycerols (DGDGs), lysyl-phosphatidylglycerols (LysylPGs), phosphatidylglycerols (PGs), and cardiolipins (CLs), were examined (139–141).

We determined the total carbon and unsaturation degrees of the lipid acyl side chains for the major lipid species in the wild type (WT) and Δ*geh*, Δ*sal1*, Δ*0641*, Δ*fakA* mutants (**Figure 2.2**). As seen in the figure, *S. aureus* grown in TSB-only displayed higher levels of fully saturated lipid species compared to those grown in human serum for each lipid class. This is not surprising since without exogenous fatty acids, the bacteria can only synthesize saturated SCFA or BCFA *de novo.* Consistent with previous studies, the Δ*fakA* mutant possessed a higher abundance of long acyl side chains (117). All strains contained DGDG, PG, and LysylPG saturated lipids with 32 to 37 total carbons, with 33 and 35 carbons being the major species across classes in each strain.

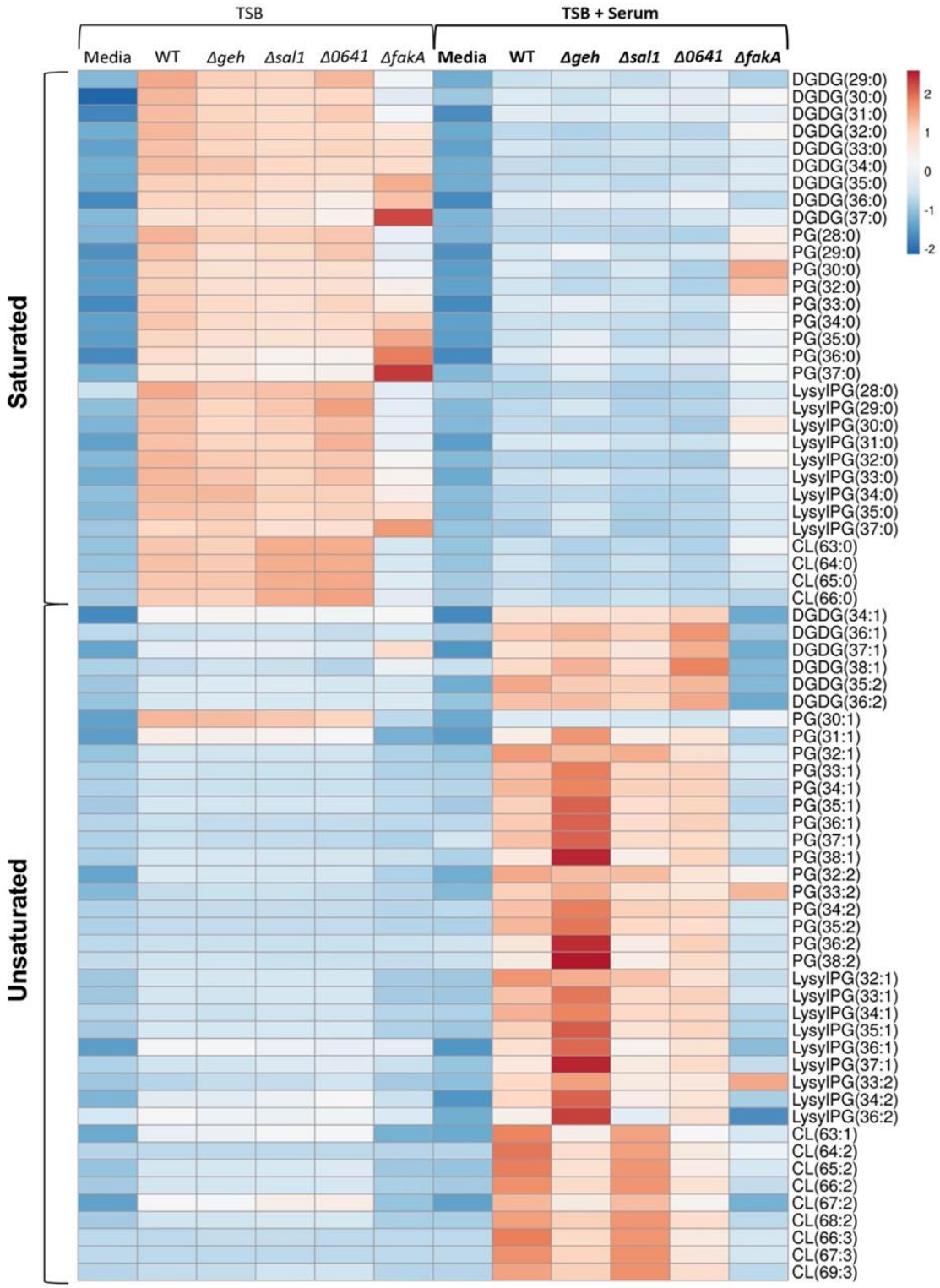

Figure 2.2. Relative abundances of lipids of WT (USA300 LAC) and *geh*-, *sal1*-, *0641*-, or *fakA*-knockout mutant strains grown in TSB or TSB + 20% human serum. DGDG: diglucosyldiacylglycerol; PG: phosphatidylglycerol; LysylPG: lysyl-phosphatidylglycerol; CL: cardiolipin. Results are row-centered and scaled by unit variance scaling. N=3 per group.

Upon further targeted fragmentation experiments using tandem MS (MS/MS) on select DGDG and PG lipids, no differences in acyl chain composition were observed across the most abundant lipids of the wild type, Δ*geh*, Δ*sal1*, Δ*0641* and Δ*fakA* strains grown in TSB-only. C15:0 was consistently identified as the major component of saturated PGs while C20:0 was the most abundant FA moiety in DGDGs.

When WT *S. aureus* was grown in TSB supplemented with 20% human serum, lipid profiles of all membrane lipid classes contained elevated levels of UFAs (such as 33:1, 34:1, 35:1, 36:1, 33:2, 34:2, 35:2, and 36:2) that were absent from strains grown in TSB-only (**Figure 2.2**). Linoleic acid (C18:2), palmitic acid (C16:0), and oleic acid (C18:1) comprise the majority of fatty acids found in human serum, along with a slightly lower amount of stearic acid (18:0) and arachidonic acid (C20:4) (142, 143). MS/MS experiments confirmed C18:1 and C18:2 were the dominant UFAs utilized by the WT and lipase mutants. Comparable levels of C20:1 and C20:2 were also observed, suggesting elongation of oleic and linoleic acids by *S. aureus*. When grown in the presence of serum, PG lipids in the WT and lipase KOs with odd-numbered total carbons (e.g, 33 and 35) contain C15:0 as the most abundant acyl side chain while PGs with even-numbered total carbons (e.g., 34 and 36) contain C16:0, instead of C15:0, as a major fatty acid. This pattern was not seen in the Δ*fakA* mutant, however, indicating the increase in C16:0, palmitic acid, likely arose from the serum. As expected, the Δ*fakA* mutant prevented the incorporation of eFAs into the bacterial membrane (**Figure 2.2**). This is consistent with previous reports of *S. aureus* incorporating serum-derived UFAs into the bacterial lipids and the necessity of FakA to incorporate eFAs into membrane lipids (112, 116, 117). We noted that Δ*fakA* showed similar intensities to the WT and lipase KOs for PG 32:2, PG 33:2, and LysylPG 33:2 only when grown in TSB-containing human serum. Although individual lipase knockouts did not

completely prevent the incorporation of host-derived UFAs, the Δ*geh* mutant exhibited the least UFA abundance in DGDGs and CLs. However, Δ*0641* also displayed lower UFA levels than the WT, implying possible overlapping functions exist between the lipases (113, 114). Interestingly, there was an overall increase of UFAs in Δ*geh*, suggesting an upregulation of eFA incorporation-related genes in the absence of Geh. Much higher levels of saturated lipids, especially lipids with saturated chains 30:0 and 32:0, were observed in the Δ*fakA* strain grown in serum, which could indicate upregulation of *de novo* fatty acid synthesis caused by the loss of FakA.

2.2.2. *Substrate specificity of S. aureus secreted lipases.*

To further elucidate the overlapping substrates among the lipases, the WT and Δ*geh*, Δ*sal1*, Δ*0641*, Δ*fakA* mutants were grown in the presence of cholesteryl esters (CEs) and triglycerides (TGs), the major donors of eFAs in serum (112). TSB was supplemented with CE and TG standards containing the unsaturated fatty acids C18:1, C18:2, or C20:4 at a final concentration of 100 μM for each lipid. Comprehensive lipidomics was conducted in the same way as described above (**Figure 2.3** and **Figure 2.4**).

When grown in the presence of CEs, the WT, Δ*sal1*, and Δ*0641* strains displayed similar eFA incorporation in PG (**Figure 2.3 B**), DGDG, LysylPG, and CL (**Figure 2.4**) lipid species. Neither the Δ*fakA* nor Δ*geh* strain contained UFAs in any major lipid classes. This suggests that Geh is the lipase responsible for hydrolyzing cholesteryl esters. Elongation of the supplemented CE unsaturated fatty acids was observed in the wild type, Δ*sal1*, and Δ*0641* mutants as evidenced by the presence of C20:1, C20:2, and C22:4. MS/MS of DGDG and PG lipid species confirmed the fatty acyl composition of 34:1 and 34:2 (**Figure 2.3 E and F**) to be C14:0 and C20:1 or C20:2, 35:1 and 35:2 contained C15:0 and C20:1 or 20:2, and PG 36:4 contained C14:0 and C22:4.

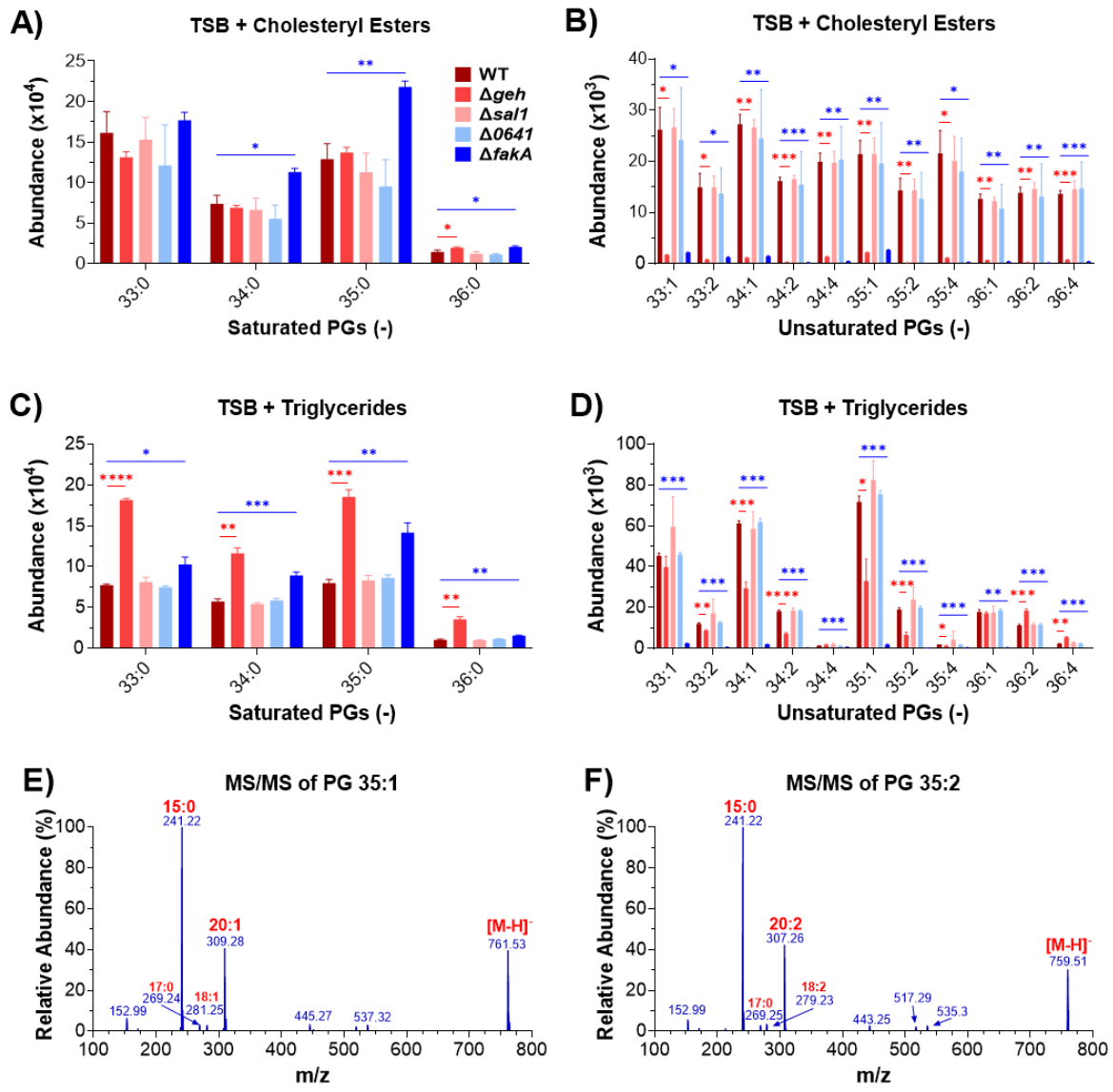

Figure 2.3. Relative abundance of lipids of WT (USA300 LAC) and *geh*-, *sal1*-, *0641*-, or *fakA*-knockout mutant strains grown in the presence of cholesteryl esters or triglycerides containing C18:1, C18:2, or C20:4 at 100 μM for each lipid. (A) and (B): saturated and unsaturated lipids in the strains grown in the presence of cholesteryl esters, respectively. (C) and (D): saturated and unsaturated lipids in the strains grown in the presence of triglycerides. (E) and (F): MS/MS fragmentation spectra of two unsaturated PGs. Statistical analysis was conducted using unpaired *t* tests. *, $P \leq 0.05$; **, $P \leq 0.01$; ***, $P \leq 0.001$; ****, $P \leq 0.0001$. N = 3 per group.

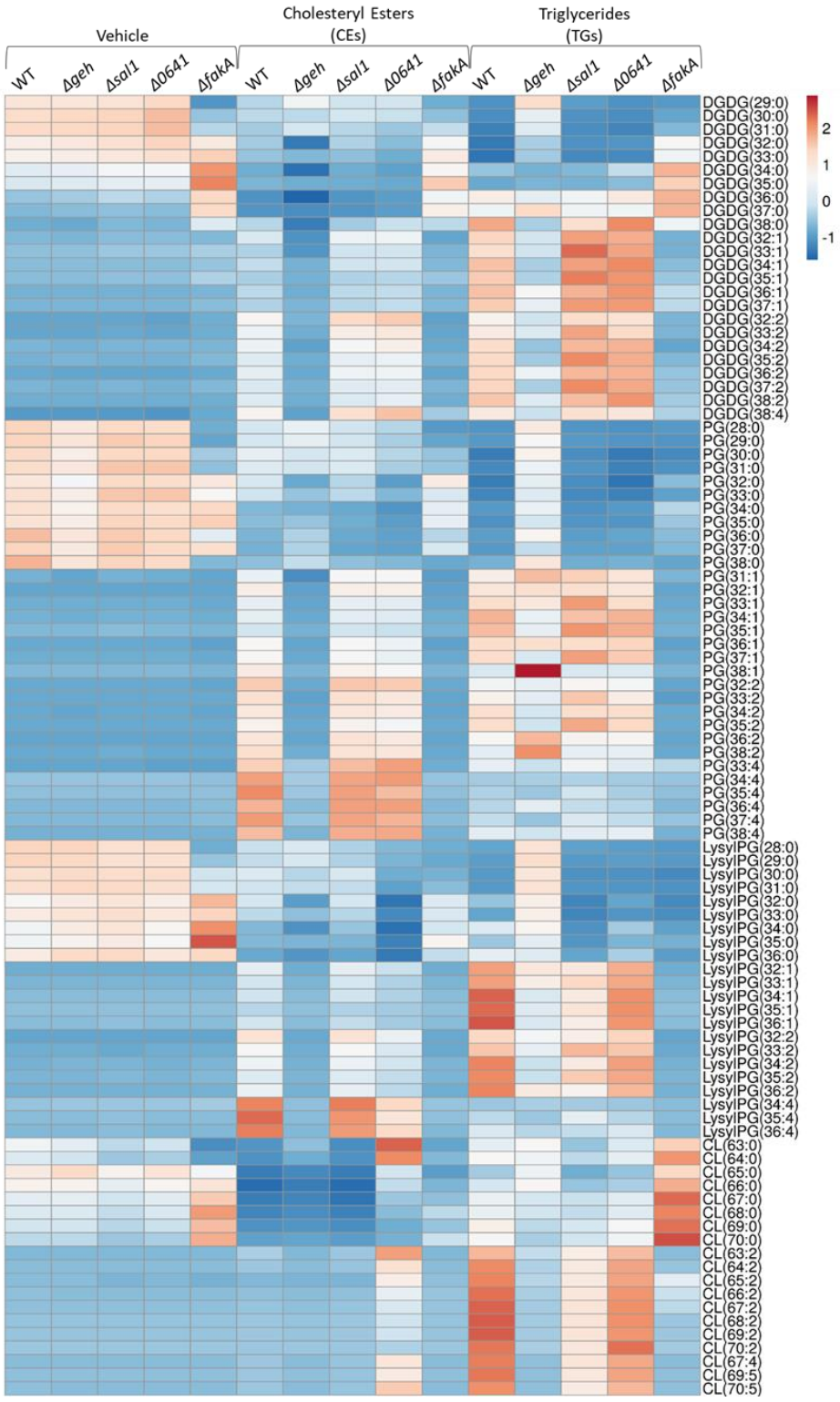

Figure 2.4. Relative abundances of lipids of WT (USA300 LAC) and *geh*-, *sal1*-, *0641*-, or *fakA*-knockout mutant strains grown in TSB or TSB + cholesteryl esters (CEs) or triglycerides (TGs) containing C18:1, C18:2, or C20:4 at 100 μM for each lipid. Results are row-centered and scaled by unit variance scaling. N = 4 per group.

In the presence of TGs, the Δ*geh* strain again had the most significant impact on the incorporation of eFAs (**Figure 2.3 C and D**). However, Δ*geh* did not completely abolish eFA incorporation within PG and LysylPG lipids. Differences in the fatty acid composition of PG 36:1 and PG 36:2 between the wild-type, Δ*sal1*, Δ*0641* strains and Δ*geh* were identified with C18:1 being the most abundant acyl side chain in the Δ*geh* strain and C20:1 for Δ*sal1* and Δ*0641* strains. Interestingly, increased levels of saturated lipids were observed in Δ*geh*, indicating an upregulation of *de novo* fatty acid synthesis in this lipase KO. Overall, this suggests Geh is the major enzyme hydrolyzing the long-chain triglycerides, but other lipases can also hydrolyze such TGs. To further affirm the role of the Geh lipase, the Δ*geh*+*geh* complement strain was grown with CEs and TGs. Complementation of the lipase mutant restored the abundance of eFA incorporation, with no notable differences in relation to the WT in the presence of cholesteryl esters or triglycerides (**Figure 2.5**).

2.2.3. *Human serum albumin as a source of eFAs and its effect on eFA incorporation.*

Figure 2.2 showed that eFAs were incorporated into the bacterial membrane when grown in serum, regardless of the lipase knockout, indicating that there may be sufficient amounts of FFAs in the serum, so lipases may not be as necessary in this nutrient-rich environment. FFAs in the bloodstream are typically bound to human serum albumin (HSA), a carrier protein present at high concentrations (35-50 mg/mL) in human blood (144). Albumin concentrations vary throughout the body and sites of infection and decrease with increasing age, highlighting the importance of understanding the effect of HSA on the utilization of serum fatty acids in *S. aureus* (101, 144–146). Here, the WT and Δ*fakA* strains were grown in the presence and absence of fatty acid-containing and fatty acid-free HSA.

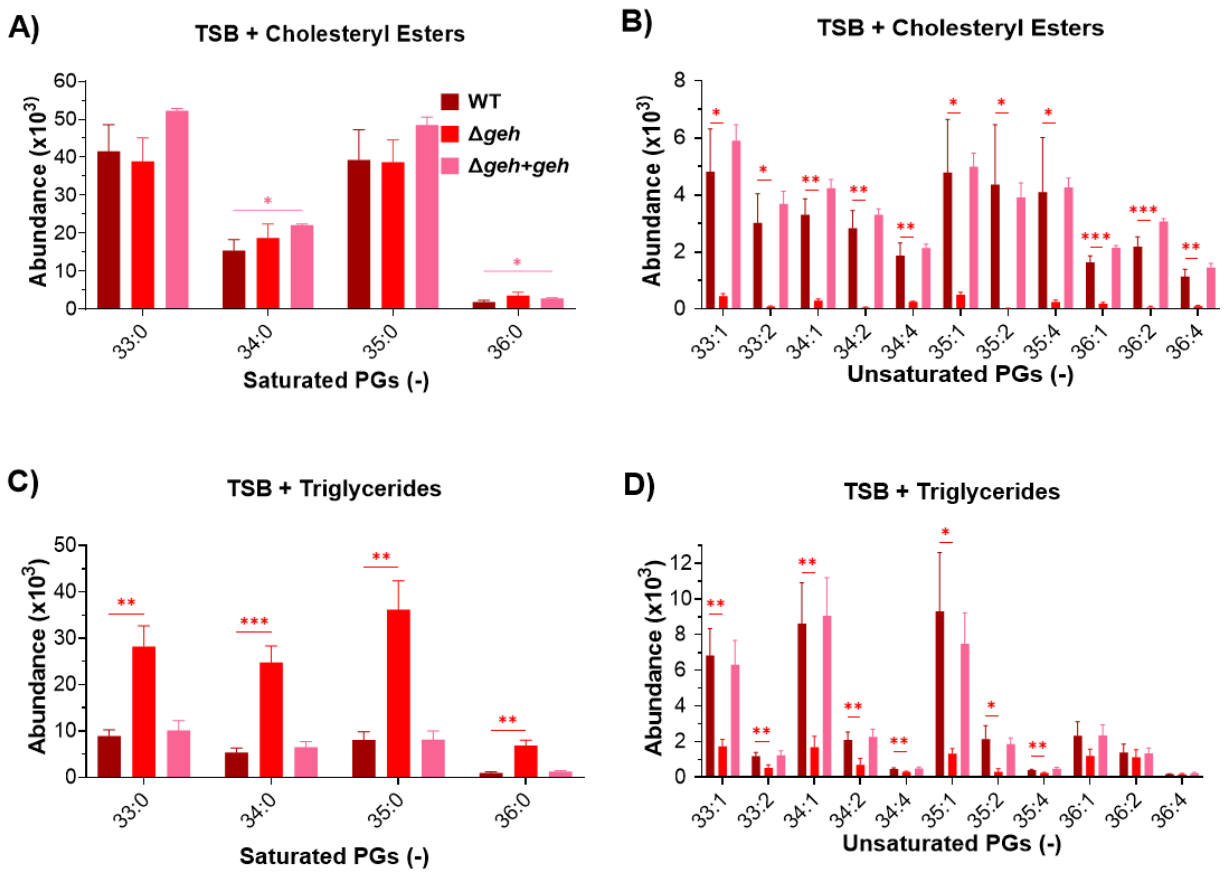

Figure 2.5. Relative abundance of lipids of the WT, Δ*geh*, and Δ*geh*+*geh* strains grown in the presence of cholesteryl esters or triglycerides containing C18:1, C18:2, or C20:4 at 100 μM for each lipid. (A) and (B): saturated and unsaturated lipids in the strains grown in the presence of cholesteryl esters, respectively. (C) and (D): saturated and unsaturated lipids in the strains grown in the presence of triglycerides. Statistical analysis was conducted using unpaired *t* tests. *, $P \leq 0.05$; **, $P \leq 0.01$; ***, $P \leq 0.001$. N=4 per group.

We found that fatty acid-containing albumin can indeed serve as a source of eFAs, indicated by the incorporation of UFAs in the WT when grown in the presence of fatty acid-containing HSA (**Figure 2.6 A** for PGs and **Figure 2.7** for other lipid classes). However, we note that most unsaturated lipids observed when grown in the presence of fatty acid-containing HSA only contain one or two double bonds, much less than those observed when grown in the presence of eFA standards, indicating the majority of fatty acids carried by HSA are mono-unsaturated fatty acids (147, 148). As expected, there were no UFAs incorporated into the membrane lipids with the Δ*fakA* strain or when the WT was grown in the presence of fatty acid-free HSA.

To determine if albumin aids *S. aureus* with incorporating FFAs into the bacterial membrane, the WT and Δ*fakA* mutant were grown in media containing FA-free HSA with the eFA standards: oleic acid (18:1), linoleic acid (18:2), and arachidonic acid (20:4). As seen in **Figure 2.6 A** and **Figure 2.7**, we found that FA-free HSA at 10 mg/mL significantly enhanced the incorporation of UFAs as indicated by the higher levels of unsaturated lipids. However, concentrations of albumin vary throughout the body, so in a separate experiment, a range of 20 to 40 mg/mL was used. We found that FA-free HSA proportionately decreased the incorporation of UFAs as its concentration increased (**Figure 2.6 B** and **Figure 2.8**). As observed with FA-free HSA at 10 mg/mL, the WT grown with FA-free HSA at both 20 and 30 mg/mL showed greater levels of PG 33:1 and 33:2 than the WT grown with eFAs only. These results suggest that HSA could enhance the utilization of eFAs by *S. aureus* at low concentrations but inhibit the utilization at high concentrations.

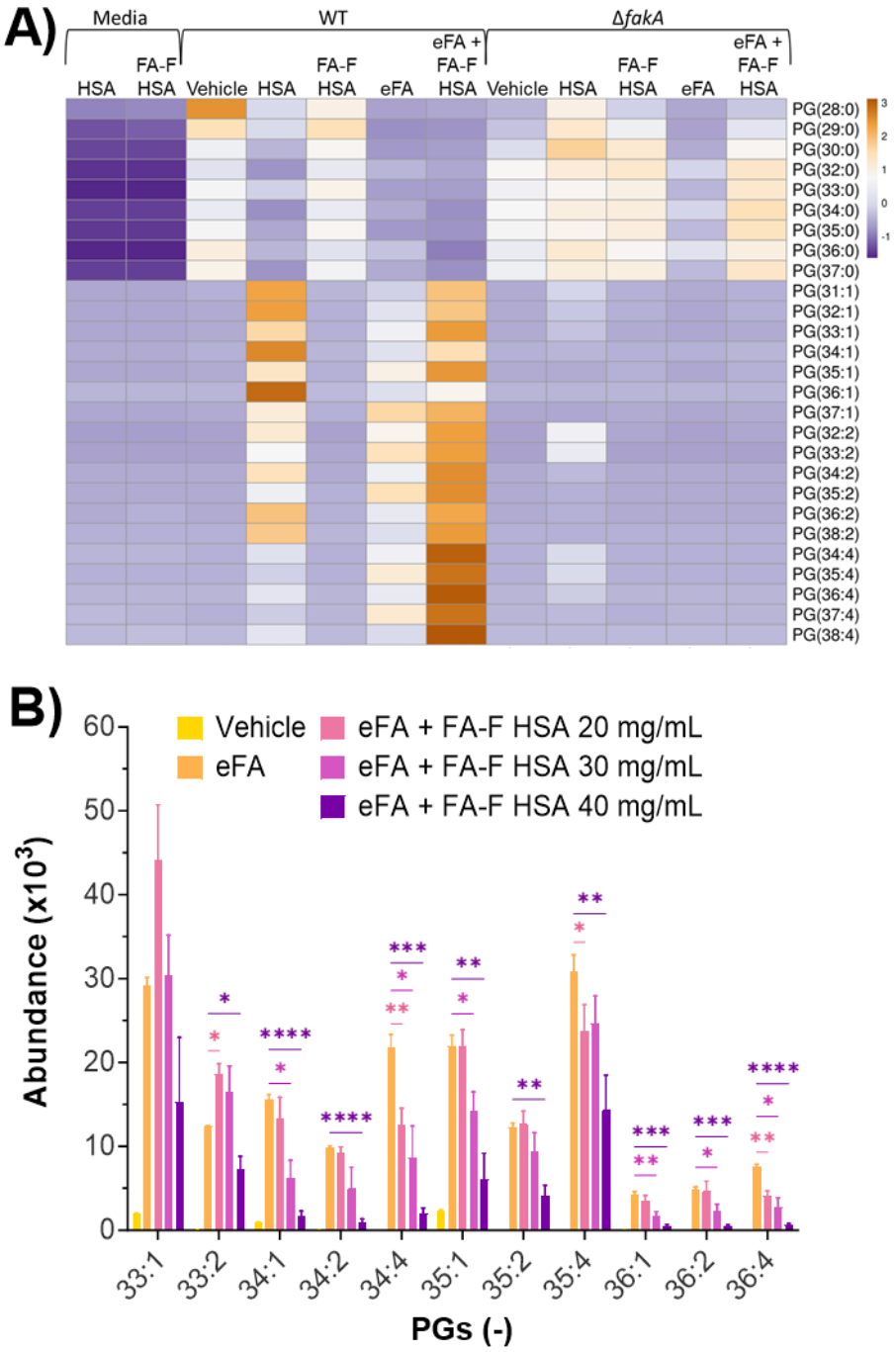

Figure 2.6. Effect of human serum albumin (HSA) on the incorporation of exogenous fatty acids (eFAs) to WT and *fakA*-knockout strains. (A) Effect of 10 mg/mL fatty acid-containing HSA and 10 mg/mL fatty acid-free (FA-F) HSA on the incorporation of eFAs mixture (oleic acid 18:1, linoleic acid 18:2, and arachidonic acid 20:4). (B) The effect of increasing concentrations of FA-F HSA (20-40 mg/mL) on the incorporation of eFAs. Statistical analysis was conducted using unpaired *t* tests. *, $P \leq 0.05$; **, $P \leq 0.01$; ***, $P \leq 0.001$; ****, $P \leq 0.0001$. N = 3 per group.

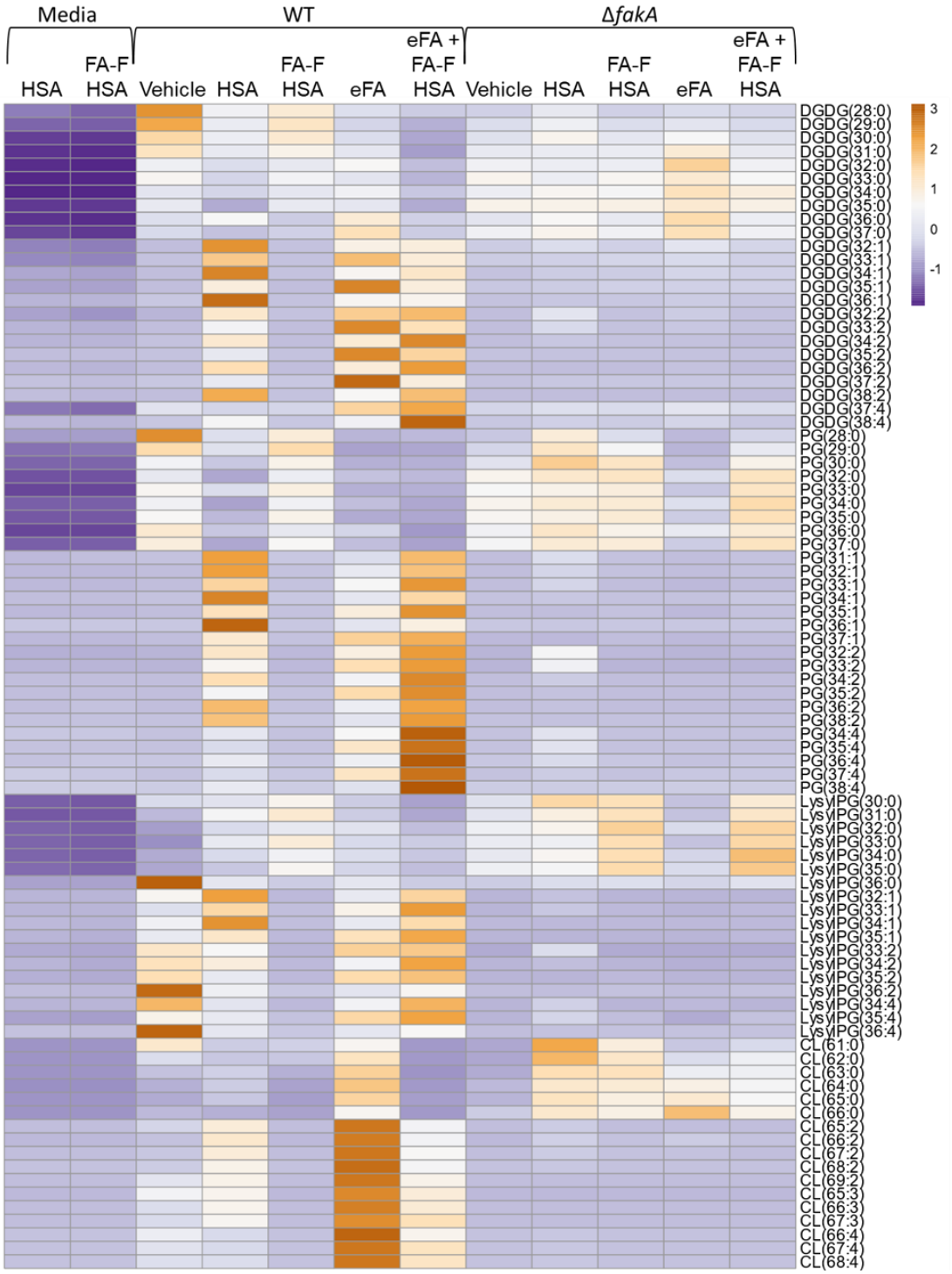

Figure 2.7. Effect of fatty acid-containing HSA and fatty acid-free (FA-F) HSA at 10 mg/mL on the incorporation of eFAs mixture (oleic acid 18:1, linoleic acid 18:2, and arachidonic acid 20:4) into bacterial lipids. Results are row-centered and scaled by unit variance scaling. N = 4 per group.

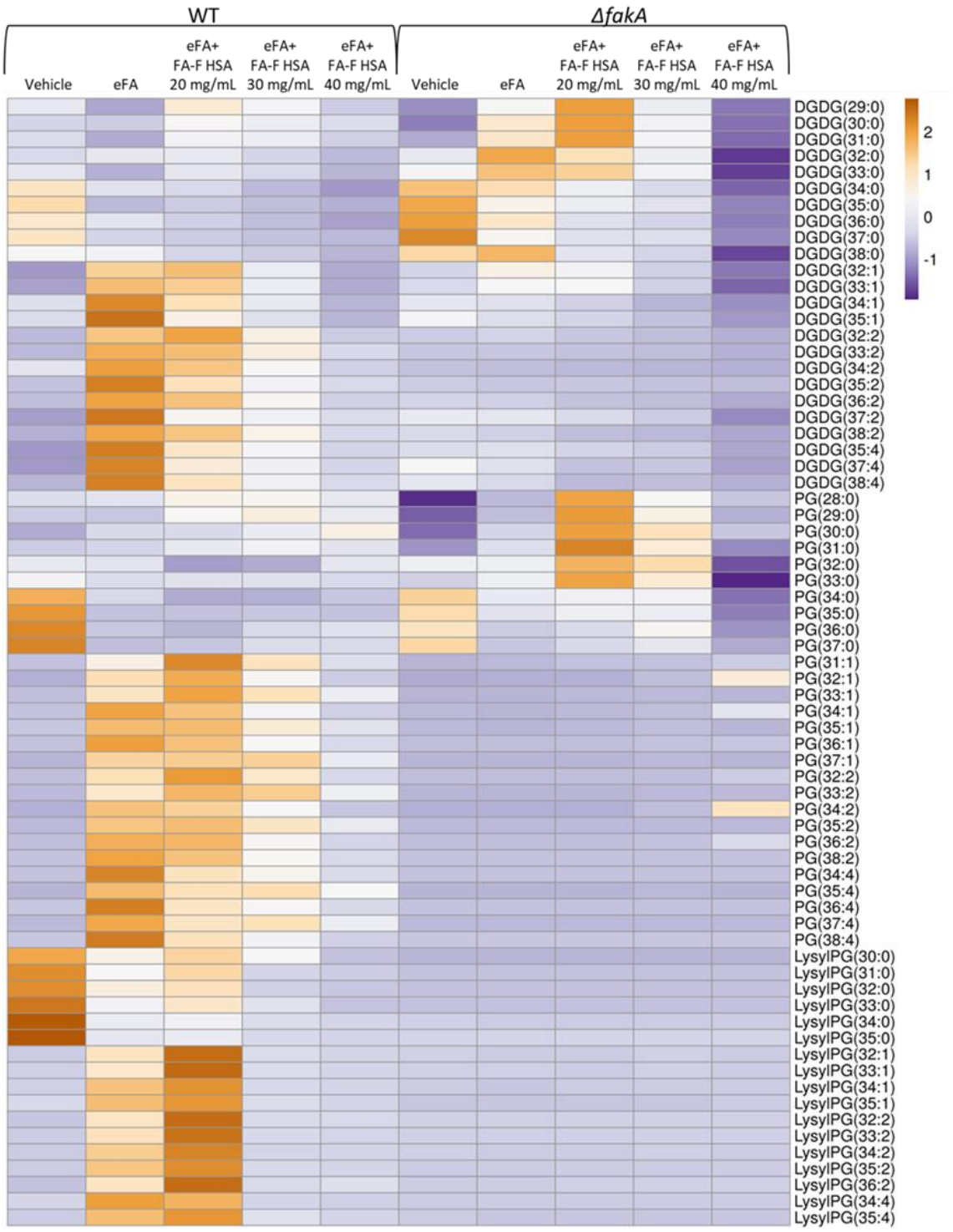

Figure 2.8. The effect of increasing concentrations of FA-F HSA on the incorporation of eFAs mixture (oleic acid 18:1, linoleic acid 18:2, and arachidonic acid 20:4) into bacterial lipids. Results are row-centered and scaled by unit variance scaling. N = 4 per group.

2.2.4. *Effect of eFAs on membrane fluidity.*

Antibiotics, such as daptomycin, have been shown to have increased bactericidal activity against *S. aureus* with incorporated UFAs, which corresponds to increased membrane fluidity, and decreased daptomycin bactericidal activity against *S. aureus* with a high percentage of saturated FAs (128). The membrane fluidity was assessed in the WT and Δ*fakA* mutant at two time points, 5 hours and 24 hours of growth, with the fluorescent probe 1,6-diphenyl 1,3,5-hexatriene (DHP) in the presence and absence of eFA standards or human serum.

As expected, an increase in membrane fluidity was observed at 5 hours in the WT when grown in the presence of eFAs or serum than without, indicated by a decrease in polarization value (**Figure 2.9 A**). Comparatively, Δ*fakA* consistently displayed a significantly more rigid membrane compared to the WT in eFAs ($P < 0.05$) and in serum ($P < 0.05$). This is consistent with incorporation of UFAs into the *S. aureus* membrane. However, the Δ*fakA* mutant also displayed overall increases in membrane fluidity when grown with eFAs or serum compared to growth in TSB-only at 5 hours (**Figure 2.9 A**). Although UFAs are not incorporated in the Δ*fakA* mutant, it is possible that the presence of eFAs could lead to a change in endogenous fatty acid synthesis regulation, including synthesis of branched-chain fatty acids, resulting in a more fluid membrane overall. In contrast to the mid-exponential phase of growth, no significant differences in fluidity were found between the WT and Δ*fakA* mutant during the stationary phase (**Figure 2.9 B**), which may result from the varied lipid composition with growth phases (117, 149). Little difference was displayed between strains in TSB only and TSB containing eFA standards, but both strains were more fluid in the presence of human serum, indicating the impact of the nutritional environment on responses within the membrane composition.

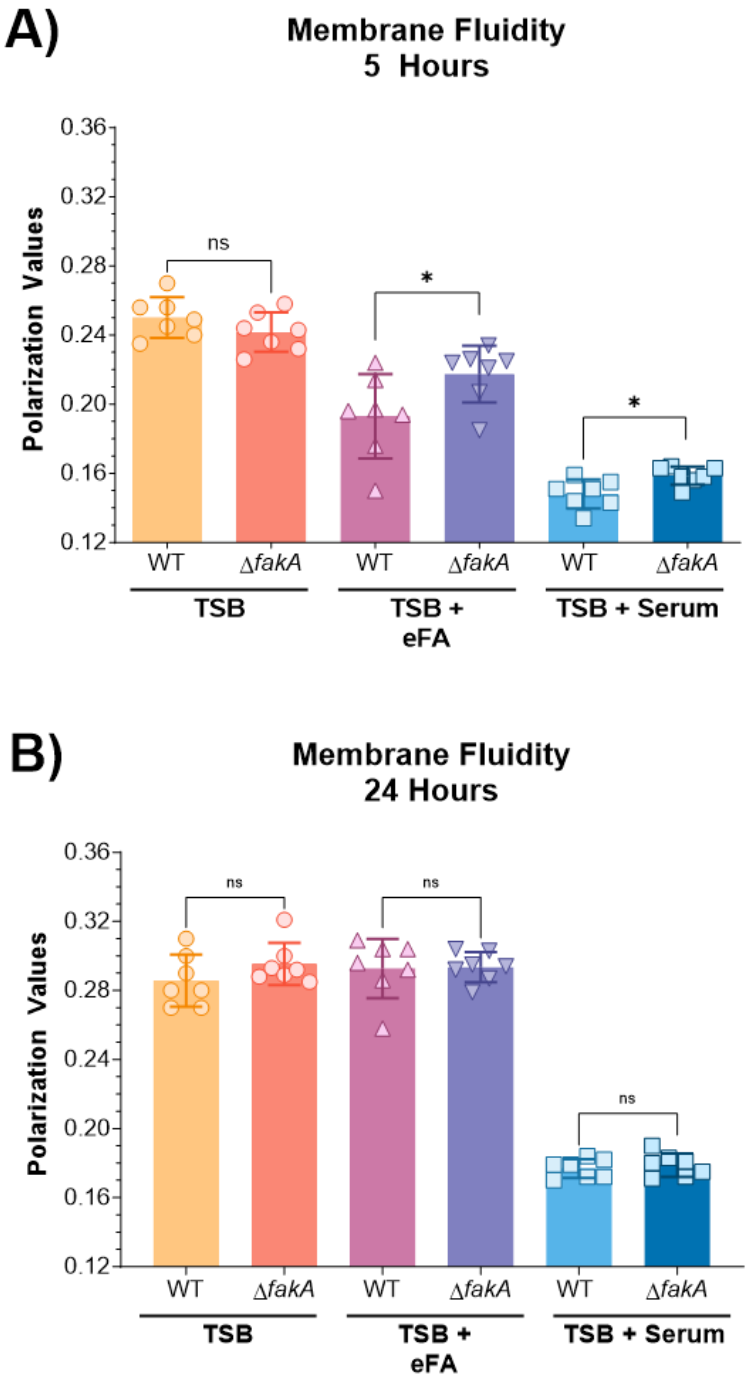

Figure 2.9. Membrane fluidity of WT and *fakA*-KO (Δ*fakA*) strains grown to 5 hours (A) or 24 hours (B) in the presence of eFA standards (18:1, 18:2, and 20:4) or 20% human serum. Statistical analysis was conducted using unpaired *t* tests. *, $P \leq 0.05$. N = 4.

2.2.5. *AFN-1252 enhances UFAs with or without eFA source.*

An attractive target for drug discovery is the FASII pathway in *S. aureus.* AFN-1252 is an inhibitor that targets the FabI enzyme, an enoyl-acyl carrier protein (ACP) reductase that is essential in the final elongation step of FASII (96, 150, 151). We hypothesized that the FASII inhibitor would enhance the incorporation of eFAs due to suppression of endogenous FA synthesis. Thus, *S. aureus* was grown in the presence of AFN-1252, eFAs, or a combination of both. Exposure of *S. aureus* to AFN-1252 and eFAs resulted in bacterial membrane composed predominantly of UFAs (**Figure 2.10**), confirming promotion of eFA incorporation by AFN-1252 (100).

Interestingly, the UFA content in the WT grown with only AFN-1252 in the absence of eFAs also increased although displaying a different lipid profile from that of eFA only group (**Figure 2.10**, **Figure 2.11**, and **Figure 2.12**). Upon MS/MS fragmentation, these UFA-containing lipids exhibited different patterns from those grown in the presence of eFAs, mostly containing fatty acids with one double bond. As also seen in prior experiments when *S. aureus* is exposed to eFAs, PG 33:1 was found to be composed of C15:0 (241 *m/z*) and C18:1 (281 *m/z*), but in the presence of AFN-1252 only, PG 33:1 was found to be composed of C14:0 (227 *m/z*) and C19:1 (295 *m/z*) (**Figure 2.13**). This is not surprising as AFN-1252 inhibits FabI, which reduces a double bond to a saturated carbon-carbon bond in the FASII cycle, indicating possible accumulation of the ACP intermediate (151). PG 33:2 in *S. aureus* with AFN-1252 contained C14:1 (225 *m/z*), C19:1 (295 *m/z*), C16:1 (253 *m/z*) and C17:1 (267 *m/z*), further suggesting accumulations of the unsaturated ACP intermediate (**Figure 2.13 B**). Such fatty acid compositional changes reveal a different aspect of the mechanism of action of AFN-1252, which warrants further investigation in the future.

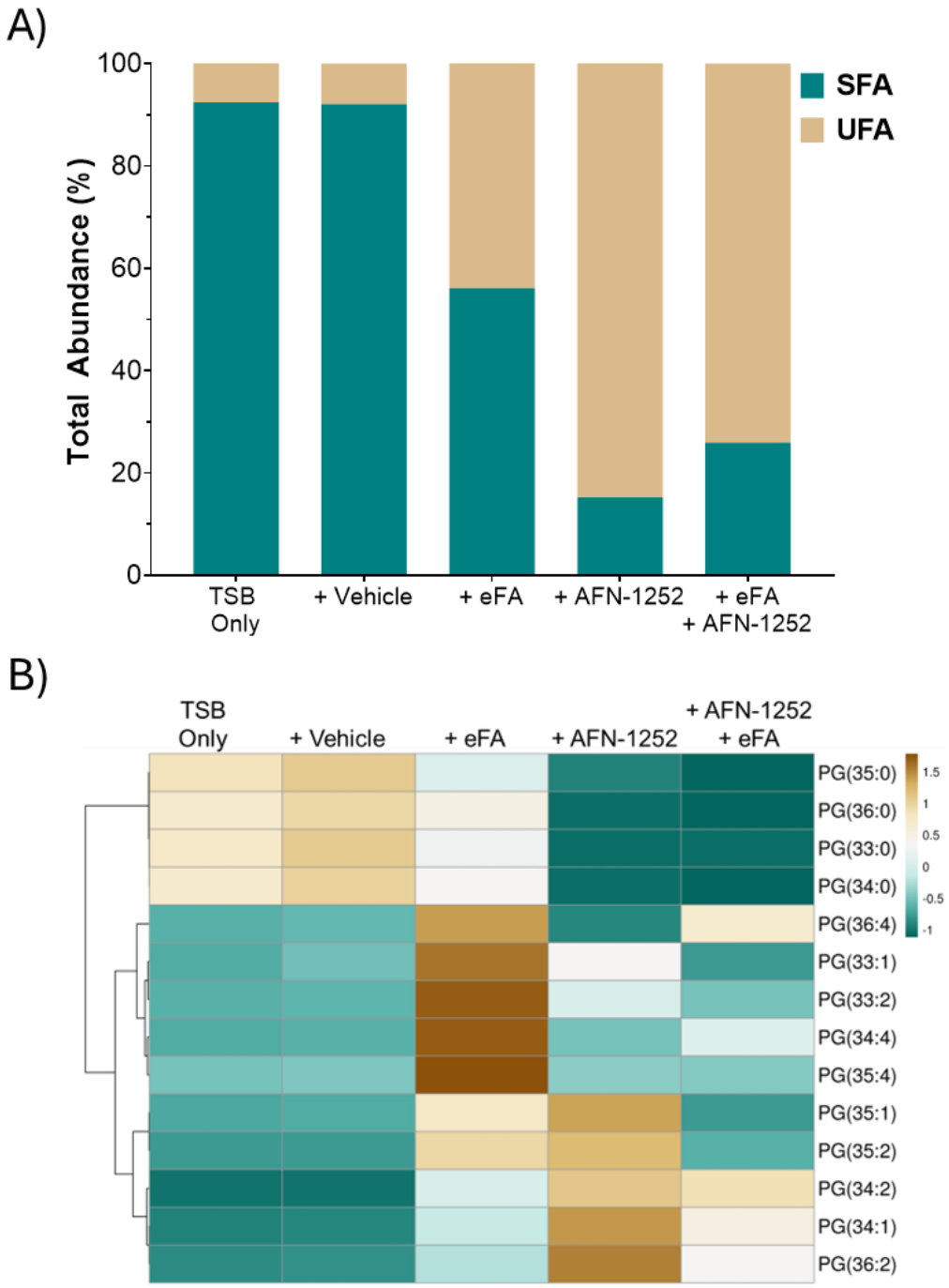

Figure 2.10. Effect of AFN-1252 on the incorporation of eFA standards containing fatty acids 18:1, 18:2, and 20:4. (A) Comparison of the sum of all saturated and unsaturated lipids; (B) comparison of individual PGs under various conditions. N=3 per group.

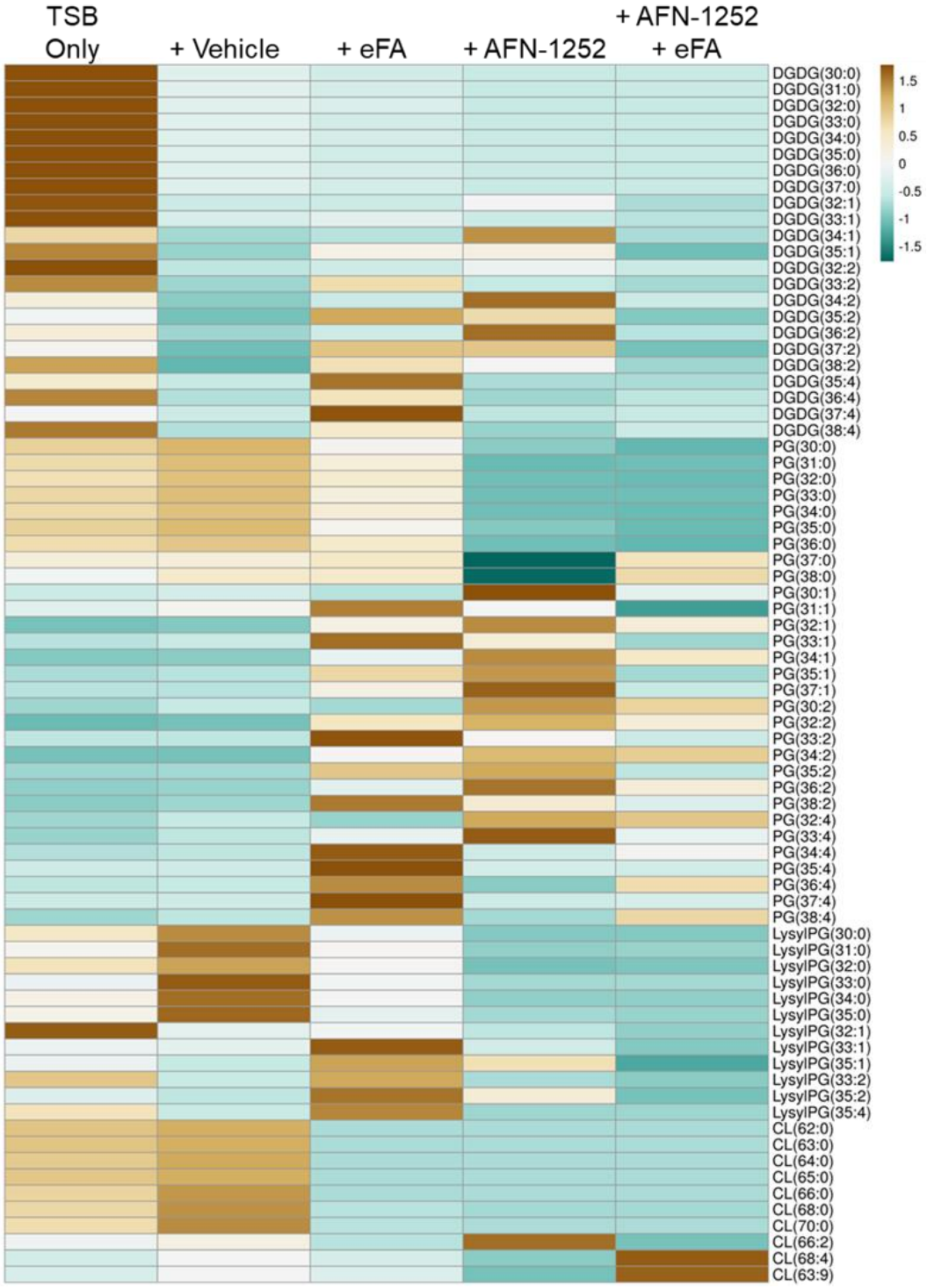

Figure 2.11. Effect of AFN-1252 on the incorporation of eFA standards containing fatty acids 18:1, 18:2, and 20:4 into various lipid classes in *S. aureus*. Results are row-centered and scaled by unit variance scaling. N = 3-4 per group.

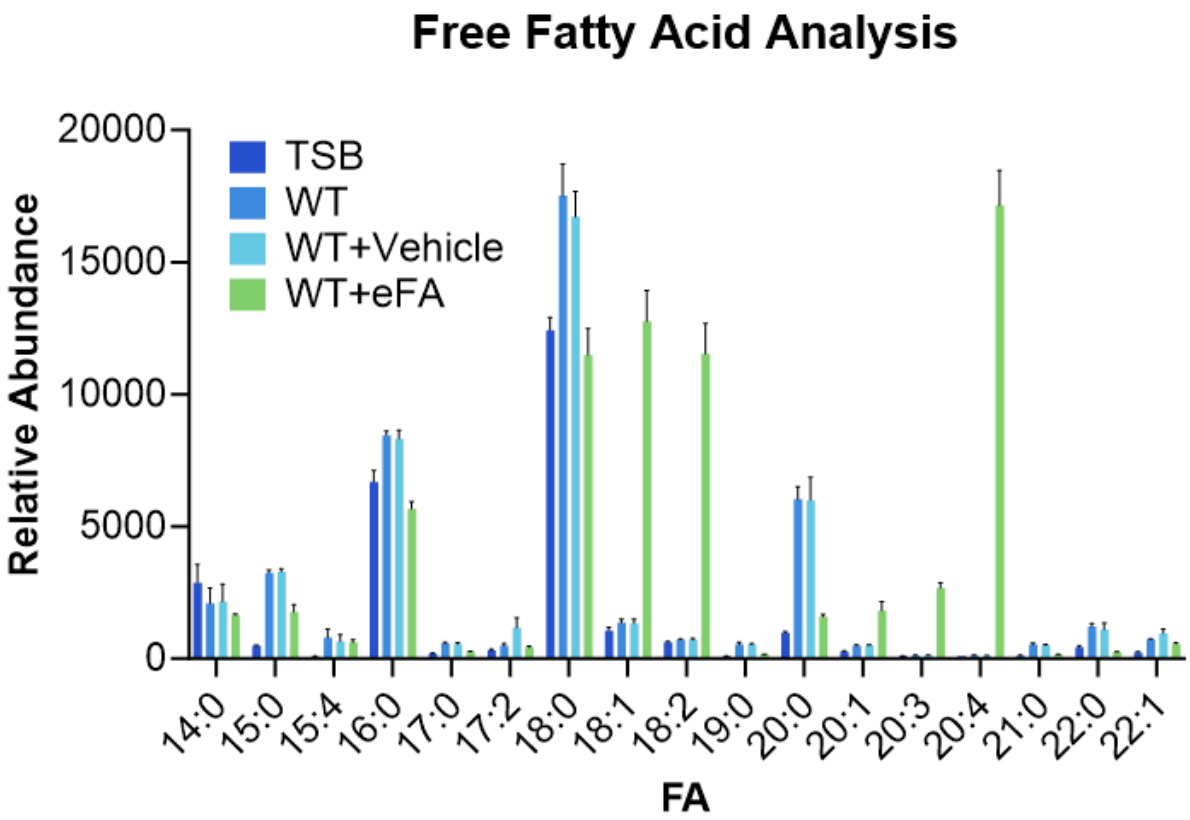

Figure 2.12. Relative abundances of fatty acids identified in the WT grown in TSB with eFA standards containing fatty acids 18:1, 18:2, and 20:4. N=3-4 per group.

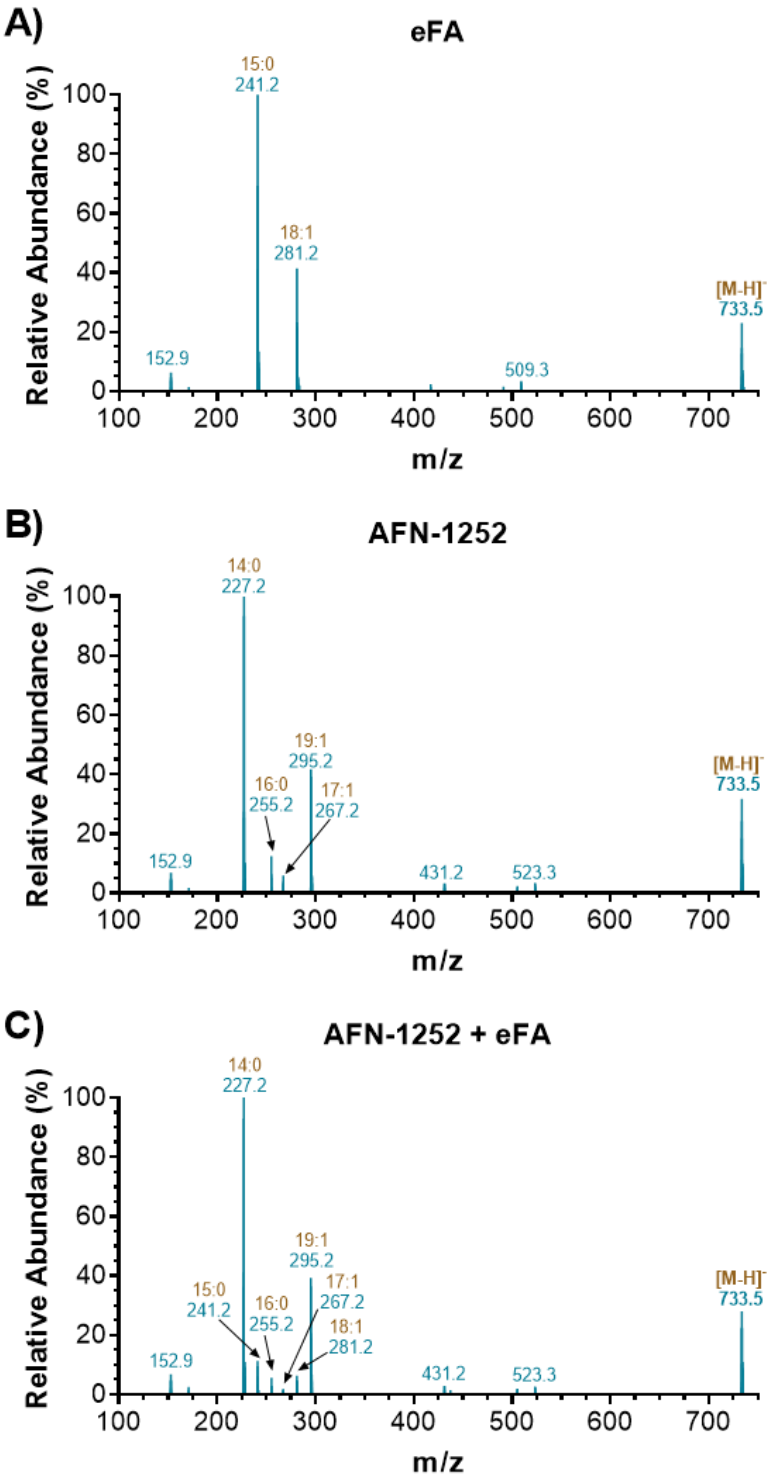

Figure 2.13. Fatty acid composition of PG 33:1 informed by MS/MS fragmentation of the parent $[M+H]^-$ ion from WT grown in the presence of (A) eFA only, (B) AFN-1252 only, or (C) AFN-1252+eFA.

2.2.6. *Effect of eFAs on ROS formation.*

When *S. aureus* was grown with exogenous fatty acid sources, host-derived fatty acids were incorporated into the membrane, resulting in increased levels of PUFAs (**Figure 2.2, Figure 2.3, and Figure 2.4**) and growth inhibition by UFAs (**Figure 2.14**). PUFAs such as linoleic acid (18:2), a major UFA found in human skin, and arachidonic acid (20:4), which is released in humans during inflammatory responses, have been shown to be toxic to the bacteria and kill through lipid peroxidation (132, 136). Reactive oxygen species (ROS), produced by phagocytes in PUFA-rich environments, also play an integral role in bacterial killing by oxidative damage (152, 153). To examine the effect of incorporated eFAs on ROS formation in the bacterial cells, the WT and Δ*fakA* mutant were grown with and without eFA standards, and ROS production was measured using the fluorogenic dye, H_2DCFDA. We observed a significant increase of ROS in the WT strain when the measurements were taken in an eFA-rich environment (**Figure 2.15**). Small increases in ROS formation were also observed in Δ*fakA* mutant, but not as significant as in the WT strain. This suggests that the incorporation of PUFAs into the membrane lipids is necessary to increase oxidative stress and enhance their killing activity. To confirm if ROS were responsible for growth inhibition, we cotreated the *S. aureus* strains with the radical-chain-terminating antioxidant α-tocopherol (Vitamin E) (136). Extended lag phases observed with UFAs were partly eliminated by α-tocopherol treatment (**Figure 2.14**).

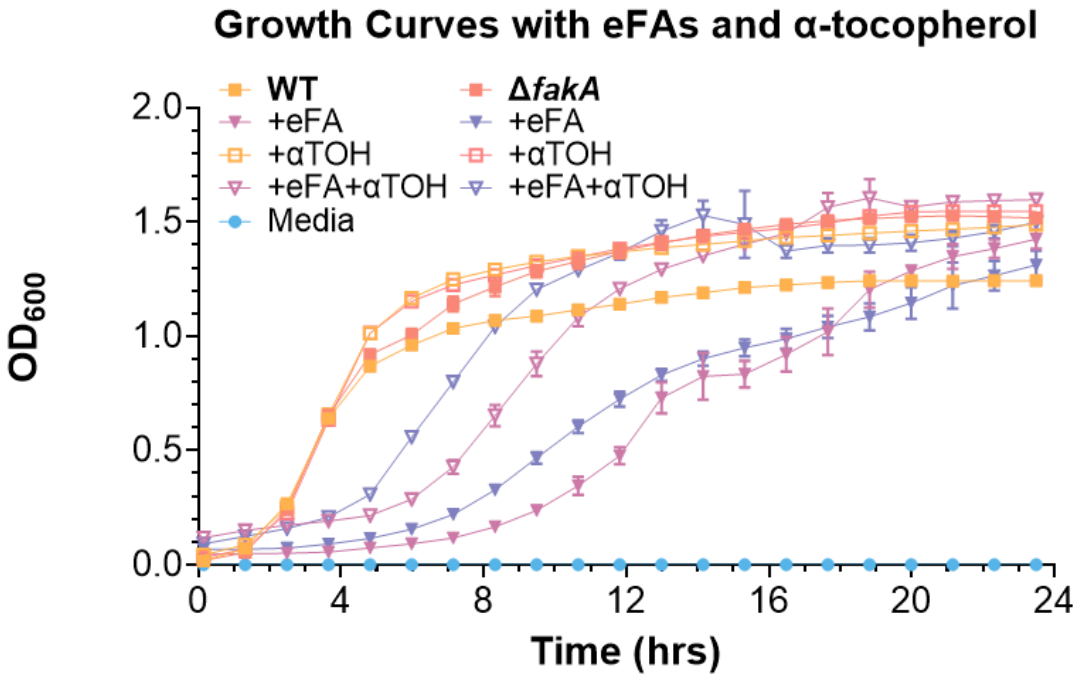

Figure 2.14. Growth curves of the WT and fakA-KO strains grown in the presence or absence of the eFA standard mixture containing fatty acids 18:1, 18:2, and 20:4 at 100 μM and treated with 80 μM α-tocopherol (Vitamin E). All data represent means ± standard deviations for conditions measured in biological triplicate.

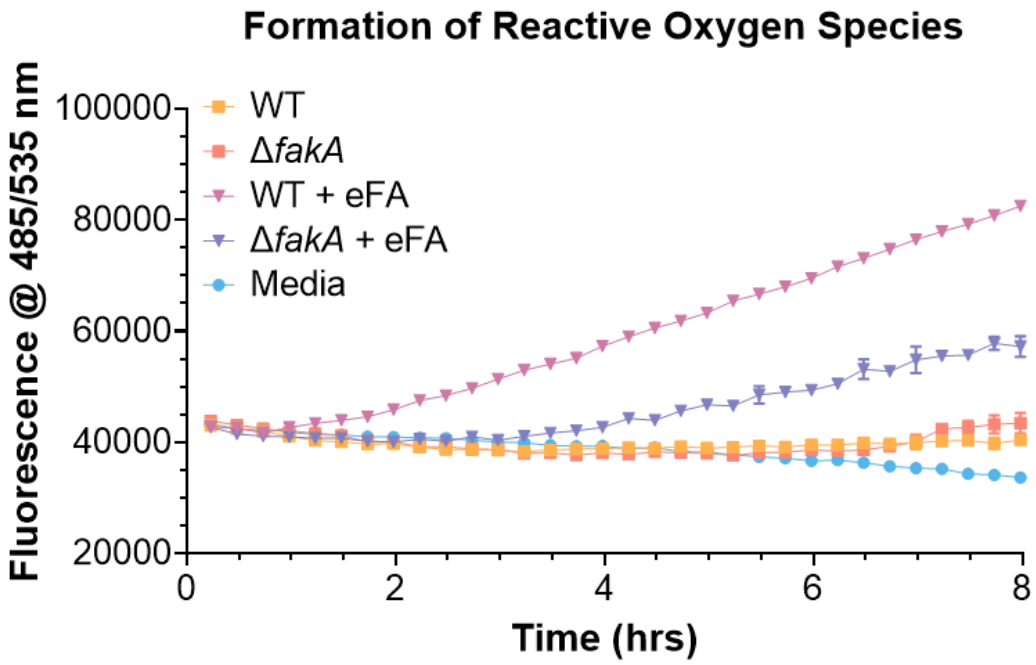

Figure 2.15. Formation of reactive oxygen species in WT and fakA-KO strains in the absence or presence of eFAs. All data represent means ± standard deviations for conditions measured in biological triplicate.

2.3. Discussion

2.3.1. *Geh is the primary lipase for the utilization of serum lipids by S. aureus.*

Although *S. aureus* is known to utilize serum lipids and is thought to depend on Geh to incorporate eFAs from lipoproteins, comprehensive lipidomic studies on the role of bacterial lipases and their substrate specificity on cholesteryl esters have not yet been performed (112, 113, 125, 154). We found that the incorporation of fatty acids from cholesteryl esters required Geh, but not Sal1 and 0641 (**Figure 2.2**). On the other hand, none of the lipase mutants grown in the presence of TGs showed a complete lack of UFA incorporation; however, UFAs were decreased in the Δ*geh* mutant compared to Δ*sal1* and Δ*0641.* This is consistent with previous studies that observed a *geh* mutant could still incorporate some UFAs into PG lipids in the presence of human low-density lipoproteins (113). It is likely that Sal1 or 0641 can hydrolyze FAs from TGs to compensate for the absence of Geh. PUFA-containing lipids were not seen at significant levels, whereas monounsaturated lipid species were abundant, implying that the 20:4 PUFA is not preferentially utilized from TGs. Thus, our data suggest that Geh is essential for hydrolyzing UFAs from CEs, whereas other lipases have overlapping functions to release fatty acids from TGs.

2.3.2. *eFA incorporation is inversely related to human serum albumin concentration.*

We determined that in addition to serum lipoproteins, human serum albumin can serve as a source of eFAs for the bacteria, primarily supplying oleic and linoleic acid (**Figure 2.6**). Although a previous report demonstrated that albumin could sequester exogenous oleic acid from *S. aureus,* preventing the inactivation of the antibiotic daptomycin, that study used fatty acid-free HSA at 10 mg/L (101). Furthermore, we observed that eFA utilization by *S. aureus* had an

inverse relationship with albumin concentration, where lower HSA levels promoted FFA incorporation whereas higher levels reduced incorporation. Hypoalbuminemia, diagnosed at albumin levels <35 mg/mL, has recently been significantly associated with increased risk and adverse outcomes of deep musculoskeletal *S. aureus* infections (155). Our findings of albumin concentration affecting eFA incorporation corroborate virulence pathways by which the bacteria utilize host fatty acids to promote survival during infection and tolerate antibiotic treatments (100, 113, 130). Although all lipid species displayed an overall decreasing abundance pattern with increasing albumin concentration, PG 15:0/20:4 levels remained comparatively high at 40 mg/mL, which may be a result of albumin preferentially binding to monounsaturated fatty acids, therefore leaving PUFAs such as arachidonic acid (20:4) and linoleic acid (18:2) more readily available.

2.3.3. *Cell membrane fluidity increases in eFA environment.*

As expected from incorporating host-derived fatty acids into its phospholipids, the membrane fluidity of *S. aureus* increased in eFA-rich environments (**Figure 2.9**). Consistent with previous studies of the Δ*fakA* mutant grown with oleic acid, Δ*fakA* had a significantly more rigid membrane at the 5 hour time point than the wild-type due to its lack of ability to incorporate eFAs (117, 130). On the other hand, the fluidity of Δ*fakA* strains also increased overall upon eFA and serum treatment (**Figure 2.9 A**). This provides evidence that differences in membrane fluidity are not entirely due to eFA incorporation, instead suggesting that these environments signal for altered endogenous fatty acid metabolism and composition (117, 156), such as the production of branched-chain fatty acids.

2.3.4. *AFN-1252 exposure leads to accumulation of unsaturated FASII intermediate.*

Therapeutic value of FASII inhibitors remains in debate, as *S. aureus* can bypass suppressed endogenous fatty acid synthesis by utilizing eFAs (98, 99, 101). Lipidomics of *S. aureus* grown with AFN-1252-only revealed a significant increase in the proportion of UFAs with abnormally long chains (C19:1) and phospholipids with various fatty acid combinations (C14:1, C16:1, C17:1, or C19:1), suggesting accumulation of the acyl-ACP intermediate at the inhibited FabI step (98, 151, 157). In the presence of eFAs and AFN-1252, the bacteria indeed incorporated more eFAs than eFAs alone, but the overall UFA content is lower than when treated with AFN-1252 only (**Figure 2.10**). This data indicates *S. aureus* preferably continued to initiate new acyl chains, leading to intermediate accumulation, rather than completely favor FASII bypass with eFA; however, preferred pathways and adaptive mechanisms differ based on experimental conditions such as fatty acid sources or FASII inhibitor concentrations (98, 100, 151, 158, 159). AFN-1252 has demonstrated promising synergistic effects when combined with daptomycin by blocking decoy phospholipid release or bacterial growth (101, 159). We speculate that the increased UFA ratio of *S. aureus* in the presence of AFN-1252 could also contribute to enhanced daptomycin activity, as daptomycin targets specific fluid areas of the membrane (121, 128, 160).

To summarize, using comprehensive lipidomics and genetic KOs, this work demonstrated the importance of various *S. aureus* lipases in the utilization of host-derived CEs and TGs, identified a surprising role of HSA as a buffer of eFAs, and revealed an underappreciated biological consequence of the FASII inhibitor AFN-1252, all of which could lead to new approaches to enhance *S. aureus* killing in a host environment.

2.4. Experimental

2.4.1. *Bacterial cultures and growth conditions.*

Studies were conducted using the USA300 LAC wild-type (WT) strain of *Staphylococcus aureus*, along with isogenic Δ*geh*, Δ*sal1*, Δ*0641*,and Δ*fakA* mutants. Each strain was grown in triplicate in 1 mL of tryptic soy broth (TSB) at 37℃ with shaking for 24 hours in Eppendorf tubes. For human serum treatments, TSB was supplemented with 20% heat-treated pooled gender human serum (BiolVT; Hicksville, NY). To determine lipase substrate specificity, the WT, lipase KOs, and Δ*geh*+*geh* complement strain were grown in the presence of pure cholesteryl ester and triglyceride lipid standards found in serum, containing the fatty acid mix: C18:1, C18:2, and C20:4 (Nu-Chek Prep, Inc., Elysian, MN) in ethanol each at 100 μM in TSB. To determine the effect of albumin on eFA sources, the WT and Δ*fakA* mutant were grown with fatty acid-containing and fatty acid-free HSA (Sigma-Aldrich, St. Louis, MO) at 10-40 mg/mL in TSB. To determine the effect of AFN-1252 (MIC 0.002 mg/L) on eFA incorporation and FASII pathway modifications, the WT was grown in the presence of 0.5 x the MIC of AFN-1252 (MedChemExpress LLC, Monmouth Junction, NJ) at 0.001 mg/L in TSB.

2.4.2. *Generation of bacterial mutant strains.*

Lipase deletion mutants (Δ*geh*, Δ*sal1*, Δ*0641*) and the Geh complement strain (Δ*geh*+*geh*) were generated in a previous study (64). To generate a Δ*fakA* mutant, five hundred-fifty base pair regions of homology upstream and downstream of the *fakA* open reading frame (SAUSA300_1119) were amplified from WT *S. aureus* genomic DNA using primer pairs *fakA*-SOE-1 (CCCGGTACCGGTGATTTAAGCGTAAGTCA) and *fakA*-SOE2 (GGTAGTTTTTTATTTTAAATTTTTCAAGTTGTCCTCCT) or *fakA*-SOE3

(AGGAGGACAACTTGAAAAATTTAAAATAAAAAACTACC) and *fakA*-SOE4 (CCCGAGCTCACCTTTAACAGTTATAGTTTG). The resulting amplicons were used in a splicing by overlap extension (SOE) PCR along with primer pair *fakA*-SOE-1 and *fakA*-SOE4. The final amplicon was subcloned into the pIMAY plasmid after digestion with restriction endonucleases KpnI and SacI (161). Allelic replacement was carried out as previously described (162). This series of knockouts (KOs) target individual lipases or FakA.

2.4.3. *Lipidomics analysis.*

Cultures were pelleted by centrifugation, washed by resuspension and centrifugation in phosphate-buffered saline (PBS), and dried in a vacuum concentrator. Total lipids were extracted by the method of Bligh and Dyer (163). Dried extracts were reconstituted in 2:1 acetonitrile-methanol. Extracts were analyzed by hydrophilic interaction liquid chromatography (HILIC) coupled with ion mobility-mass spectrometry (IM-MS). Chromatographic separations were carried out with a Phenomenex Kinetex HILIC column (50 x 2.1 mm, 1.7 μm) on a Waters Acquity FTN UPLC (Waters Corp., Milford, MA) (138). The solvent system consists of mobile phases (A) 95% acetonitrile/5% water with 5 mM ammonium acetate and (B) 50% acetonitrile/50% water with 5 mM ammonium acetate. A flow rate of 0.5 mL/min was used with the following linear gradient conditions: 0-0.5 min, 100% A; 2 min, 90% A; 3.5-4 min, 70% A; and 4.5-6 min, 100% A. Injection volumes were 5 μL for both positive and negative modes. CCS calibration was created with phosphatidylcholine and phosphatidylethanolamine CCS standards as previously described (138). IM-MS analysis was performed on a Waters Synapt XS HDMS (Water Corp., Milford, MA) in both positive and negative ionization modes as described previously (wave velocity, 500 m/s; wave height, 40 V) (137, 138). Additional targeted MS/MS

experiments were performed with a collision energy ramp of 30-45 eV to determine FA contents of selected DGDG (positive mode) and PG (negative mode) lipid species.

2.4.4. *Data analysis.*

Data alignment and peak detection were performed in Progenesis QI (Nonlinear Dynamics; Waters Corp., Milford MA) with normalization to all compounds. Retention time calibration and lipid identification were calculated with the Python package, LiPydomics (164). Multivariate statistics were created through LiPydomics and ClustVis (164, 165). MS/MS analysis and identification of the most abundant FAs was performed in Skyline utilizing a targeted lipid library generated with LipidCreator (166, 167).

2.4.5. *Cell membrane fluidity assay.*

The WT and Δ*fakA* mutant strains were grown to 5 hours and 24 hours in 20 mL of TSB at 37°C with shaking in Falcon tubes. Each strain was grown in the presence and absence of 20% human serum (v/v) or the fatty acid mix: oleic acid (18:1), linoleic acid (18:2), and arachidonic acid (20:4) (Nu-Chek Prep, Inc., Elysian, MN), each at a final concentration of 100 μM. Cultures were pelleted by centrifugation, washed, and resuspended in normal saline at a McFarland reading of 0.9. Cell membrane fluidity was measured by polarizing spectrofluorometry using a BioTek Synergy H1 plate reader (BioTek Instruments, Winooski, VT) with the fluorescent probe, 1,6-diphenyl-1,3,5-hexatriene (DPH).

2.4.6. *Growth curves.*

Overnight cultures of the WT and Δ*fakA* strains were diluted 1:100 in TSB for growth curve measurements. Cells were added to a Costar 96-well flat-bottom microplate and grown with the fatty acid mix (18:1, 18:2, 20:4) at 100 μM or α-tocopherol (Sigma-Aldrich, St. Louis,

MO) at 80 μM. Growth was monitored at 600 nm using a BioTek Synergy H1 plate reader (BioTek Instruments, Winooski, VT) set at 37°C with continuous, double orbital shaking.

2.4.7. *Reactive oxygen species measurements.*

The WT and Δ*fakA* mutant strain were grown in 7 mL of MHB50 at 37°C with shaking for 24 hours in Falcon tubes. Both strains were grown in the presence and absence of the fatty acid mix: oleic acid (18:1), linoleic acid (18:2), and arachidonic acid (20:4) (Nu-Chek Prep, Inc., Elysian, MN), each at a final concentration of 100 μM. Cultures were pelleted by centrifugation, resuspended in 7 mL MHB50 containing the fluorogenic dye, 2',7'-dichlorodihydrofluorescein diacetate (H_2DCFDA) at a concentration of 10 μM, and incubated for 45 minutes at 37°C protected from light. Cultures were pelleted by centrifugation, washed with saline, and resuspended in 7 mL of MHB50. Cells were added in triplicate to a black Nunc 96-well flat-bottom microplate in the presence or absence of the fatty acid mix with a final volume of 200 μL. Reactive oxygen species were measured by fluorescence readings (λ excitation=485 nm, λ emission=535 nm) using a BioTek Synergy H1 plate reader set at 37°C for 8 hours.

2.5. Acknowledgements

This work was supported by an NIH grant R01AI136979 (to L.X. and B.J.W.). F.A. acknowledges the support from NIH grant R01AI120994 and Burroughs Wellcome Fund Investigators in the Pathogenesis of Infectious Disease Award (1019120.01).

CHAPTER 3: Tracking the Metabolism of Unsaturated Fatty Acids in *S. aureus* Using Online Paternó-Büchi Reactions

3.1. Introduction

Antimicrobial resistance has become a substantial challenge to modern medicine and global health, with the gram-positive pathogen *Staphylococcus aureus* posing one of the most serious threats (12, 27). As a highly adaptive bacterium, *S. aureus* can utilize exogenous fatty acids found in the host environment to promote survival and enhance virulence (46, 61, 65, 74, 168). Lipids, particularly glycerophospholipids, are essential for various biological functions and cellular processes. Specific compositions of fatty acids and lipid isomers, such as *cis/trans* configuration (R versus S), acyl chain position (*sn*-1, *sn*-2, *and sn*-3), and location of carbon-carbon double bonds (C=C), distinctly affect cellular interactions and physiochemical properties of cell membranes (169, 170). *S. aureus* can only synthesize straight-chain or branched-chain fatty acids via the type II fatty acid synthesis pathway (FASII), but its ability to incorporate host fatty acids allows bacteria to reduce energy consumption, bypass innate immune responses, and withstand drug activity (46, 61, 62, 64, 65, 74, 168, 171). Structural and isomeric lipid variations can also affect the susceptibility of *S. aureus* to membrane-targeting antimicrobials, highlighting the importance of elucidating metabolic evolution and lipid modifications in resistant bacteria (46, 81, 172, 173).

Despite comprehensive studies on the effects of exogenous fatty acids on *S. aureus,* the complete molecular composition of the incorporated lipids has yet to be determined. Detailed lipid characterization could confirm which *sn* position is acylated by exogenous fatty acids, whether exogenous lipids undergo further elongation via FASII, and derive additional pathway modifications. While FASII elongation has previously been examined, these studies required extensive sample preparation, including additional fatty acid extractions after total lipid extraction and separate fatty acid analysis with gas chromatography (74, 97, 174, 175). Modern

mass spectrometry (MS) is a driving force for qualitative and quantitative lipidomic analyses; however, resolving the compositional isomers and distinguishing the C=C location of unsaturated lipids remains a challenge (169, 170, 176). Several methods have been explored to increase the structural sensitivity and efficiency of lipid ionization, including ozone-induced dissociation (OzID), ultraviolet photodissociation (UVPD), electron impact excitation of ions from organics (EIEIO), and photochemical reactions coupled with tandem MS (MS/MS) (177–192). One of the most effective photochemical derivatization methods for C=C identification is the Paternó-Büchi (PB) reaction, a [2+2] cycloaddition in which a photochemically excited carbonyl-containing compound forms a four-membered oxetane ring with a C=C bond (186, 193–195). Upon collision-induced dissociation (CID), ring cleavage produces fragment ions specific to the original double-bond location (**Figure 3.1**) (179, 181, 186–188, 196–198).

Unlike other double-bond assignment methods that require specialized or significantly modified instruments, the PB reaction method has been successfully integrated into shotgun, direct analysis, matrix-assisted laser desorption/ionization (MALDI), ion mobility (IM), and liquid chromatography-mass spectrometry (LC-MS) workflows but relies on identifying diagnostic fragment ions with very low abundances (184, 186, 188, 189, 196, 197, 199–201). Acetone was the most commonly used PB reagent in these studies; however, this solvent has adverse effects on lipid analysis because of its major Norrish type I side reactions that decrease the PB reaction yield, increase chemical interference, and its low molecular mass of 58 Da leads to overlap with other products (184, 187, 202). Alternatively, recent screening of various carbonyl compounds revealed 2-acetylpyridine (2-ACP) to be a better-suited PB reagent for enhancing reaction yields, increasing the intensity of *sn*-position diagnostic ions, and simplifying

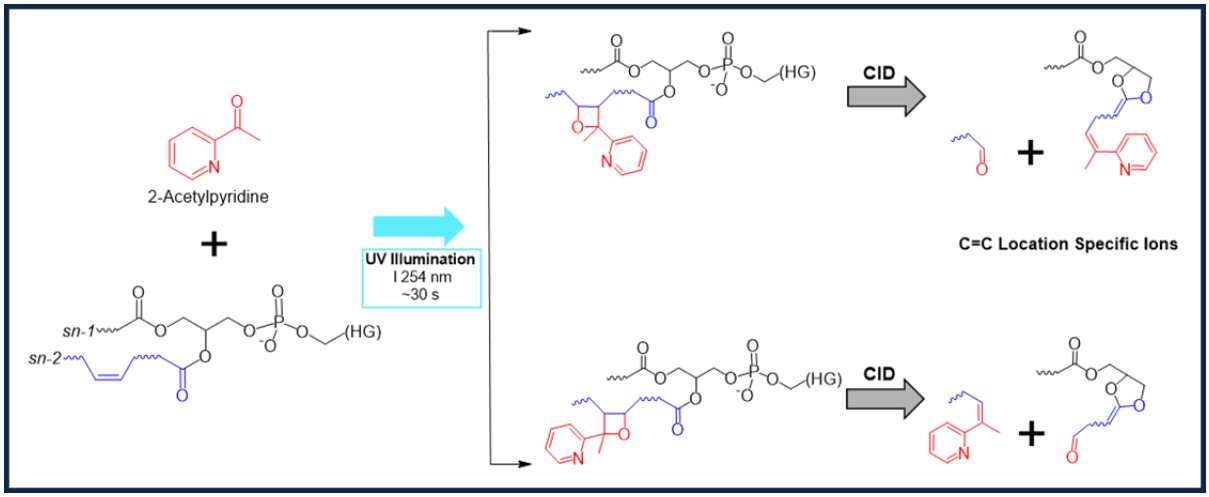

Figure 3.1. Schematic of the Paternó-Büchi reaction between the PB reagent, 2-acetylpyridine, and an unsaturated lipid. (HG) represents an unspecified lipid headgroup. Upon UV excitation, two possible regioisomers of the strained four-membered rings were produced. Collision-induced dissociation (CID) yields pairs of diagnostic fragment ions specific to the original C=C location.

spectral complexity owing to its molecular mass of 121.14 g mol^{-1}, which eliminates overlapping PB products (187, 187, 192, 203–205). The sensitivity of low-intensity diagnostic ions has been improved through the integration of hydrophilic interaction liquid chromatography (HILIC) and ion mobility spectrometry. HILIC is an advantageous method for coupling with MS because it can resolve lipid species on a scale of seconds, based on the polarity of the head groups, acyl chain length, and degree of unsaturation within the subclass. Ion mobility (IM) is an orthogonal gas-phase separation method that sorts identically charged ions according to their size and shape (105, 197, 206, 207). HILIC-PB-MS/MS workflows have been developed for complex biological sample analyses, including comparisons of C=C location isomers for disease phenotyping of human breast cancer tissues, type 2 diabetes plasma, and human bladder cancer tissues (189, 206, 208). However, these lipid profiling methods use acetone as the PB reagent or conduct PB derivatization offline prior to analysis.

In this study, we integrated the Paternó-Büchi reaction with our existing HILIC-IM-MS methods into a single workflow for comprehensive analysis of lipid metabolism in *S. aureus* at detailed structural levels. By implementing the PB reaction online and utilizing 2-acetylpyridine (2-ACP) as the PB reagent, we aimed to overcome the limitations of previous lipid profiling methods and enhance the efficiency of C=C location determination in bacterial lipids. In our experimental setup, the PB reagent 2-ACP was injected post-HILIC separation immediately before ESI, as illustrated in **Figure 3.2**. This approach maintained the retention times of the lipid classes and did not require changes in the mobile phase (ACN/H_2O). Online PB reactions allow for real-time derivatization of unsaturated lipid species, enabling the simultaneous characterization of the incorporation and modification of exogenous lipids in *S. aureus.* Analysis of the bacterial lipidome using HILIC-PB-MS/MS provided significant insights into the

utilization of host fatty acids, confirming that *S. aureus* elongates fatty acids from the carboxylic acid end. Additionally, integrated HILIC and IM techniques increased the sensitivity and precision of the identification of lipid structural features. Our findings demonstrate the potential of the online PB reaction in conjunction with advanced MS techniques to enhance the understanding of microbial lipid metabolism, particularly in the context of host-pathogen interactions and antimicrobial resistance. By refining methodologies for detailed lipid analysis and leveraging the capabilities of mass spectrometry, we are advancing toward a comprehensive elucidation of lipid metabolism in microbial systems. This progress has significant implications for the development of targeted antimicrobial strategies and effective countermeasures against bacterial resistance.

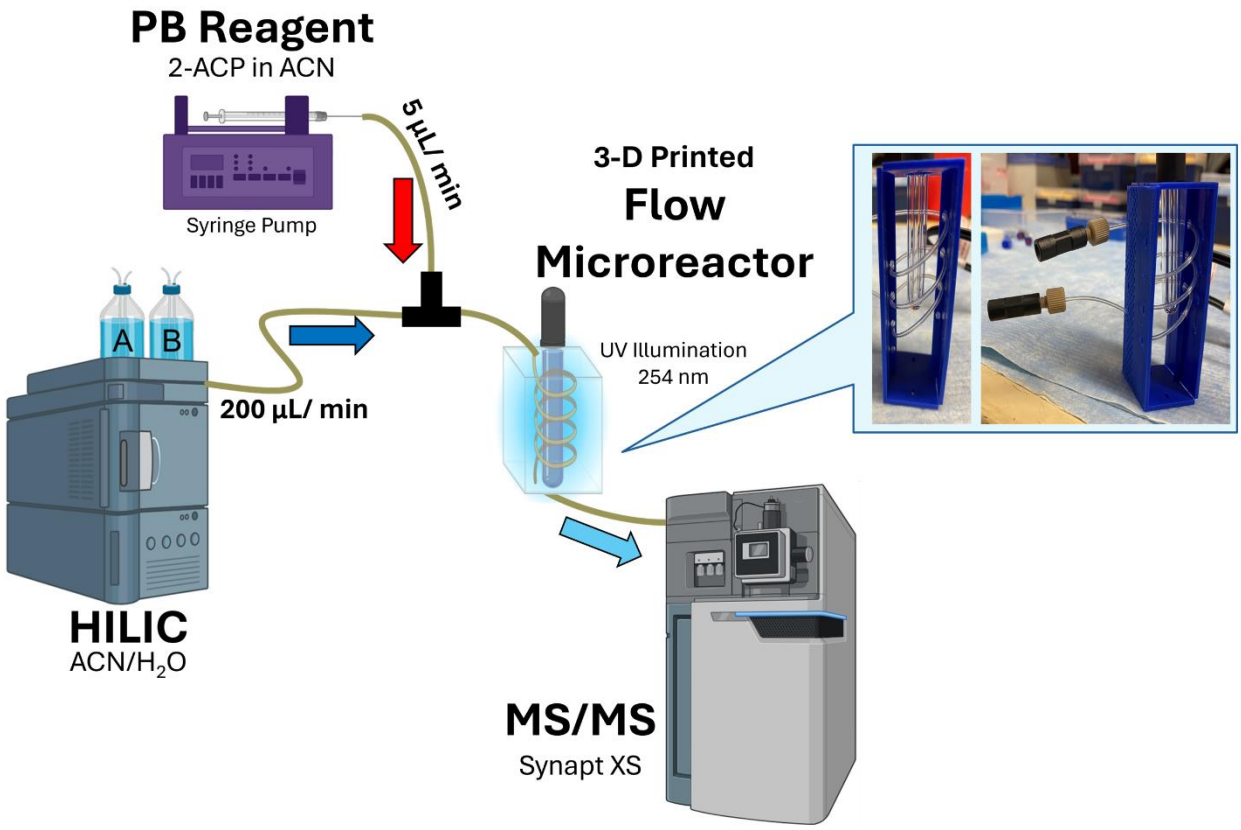

Figure 3.2. Schematic of the online HILIC-PB-MS/MS setup, including photos of the 3-D printed flow microreactor. This setup was adapted from Yang, X.; Xia, Y. Mapping Complex Disulfide Bonds via Implementing Photochemical Reduction Online with Liquid Chromatography–Mass Spectrometry. *J. Am. Soc. Mass Spectrom.* **2021**, *32* (1), 307–314.

3.2. Results and Discussion

3.2.1. *Comprehensive structural elucidation of lipids by HILIC-PB-MS/MS*

Glycerophospholipids are divided into distinct subclasses based on the polarity of their different headgroups, which affect the ionization efficiency of lipids in positive and negative ESI modes (207, 209). Although intact phosphatidylglycerols (PGs) and fatty acids (FAs) are preferentially analyzed in negative ESI mode, using the nitrogen-containing reagent 2-acetylpyridine for charge-tagging and PB derivatization has been shown to significantly improve signal abundance and sensitivity in positive mode for nonpolar lipids, presumably because of the higher proton affinity of the pyridine moiety (192, 204, 205, 207, 209–212). Therefore, positive ESI mode was used for subsequent online PB experiments.

Performance of the 3D-printed flow microreactor and PB reaction time were first evaluated using the model lipid PC 16:0/18:1(Δ9) (**Figure 3.3**). MS/MS spectra were first acquired with the UV lamp off, and then upon UV irradiation, successful derivatization was noted by the appearance of a peak at *m/z* 881.6, a signature 121-Da increase from the underivatized lipid (*m/z* 760.5), due to the addition of 2-ACP. Reaction product yields of 20-30% were achieved under optimized conditions with a flow rate of 200 μL/min and a reaction time of 30 s. As expected, chromatographic peak broadening occurred because of the slower flow rate; however, good separation of phospholipid classes was still obtained, as demonstrated with a standard mixture containing phosphatidylcholine (PC), phosphatidylethanolamine (PE), and phosphatidylglycerol (PG) lipids (**Figure 3.4)**.

Further method validation was performed by MS/MS experiments targeting the protonated PB reaction products of the monounsaturated lipid standards PC 16:0/18:1, PG 16:0/18:1, PE 16:0/18:1, and PE 18:0/18:1. Fragmentation ion structures and their subsequent

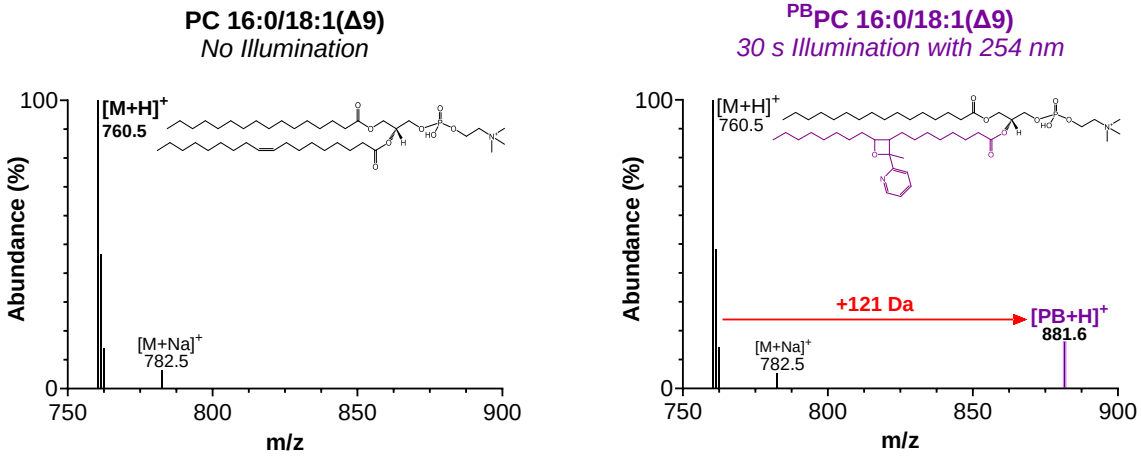

Figure 3.3. Mass spectrum of PC 16:0/18:1(Δ9) without 254 illumination and PB-MS spectrum of PC 16:0/18:1(Δ9) after 30 s of 254 nm illumination. PB derivatization by 2-ACP was indicated by the $[PB+H]^+$ peak at *m/z* 881, a signature 121-Da increase from the underivatized $[M+H]^+$ signal at *m/z* 760.

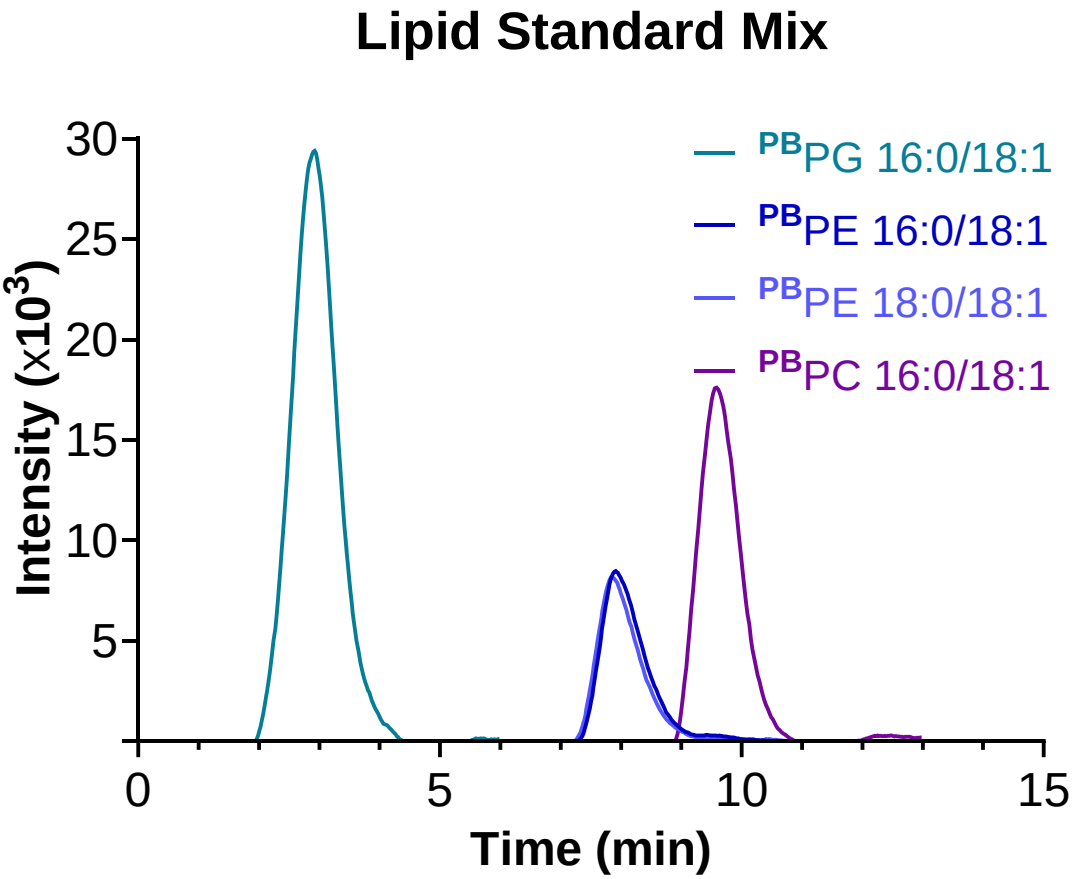

Figure 3.4. Extracted chromatograms of PB derivatized lipid standard mix: PG 16:0/18:1, PE 16:0/18:1, PE 18:0/18:1, and PC 16:0/18:1. PB reaction products were detected in positive ionization mode as [PB+H]+ adducts.

notations are depicted in **Figure 3.5,** with an example of PB-derivatized PG 16:0/18:1(Δ9). Upon CID, all lipid spectra displayed a subclass-specific headgroup-loss fragment ion ($[PB\text{-}HG]^+$) (**Figure 3.6**). Fully intact or $[PB\text{-}HG]^+$-derivatized lipids were expected to have C=C diagnostic fragment ion pairs 89-Da apart, indicating the formation of an olefin ($^{\Delta n}F_O$) and aldehyde ($^{\Delta n}F_A$) adduct at the cleavage site. For 16:0/18:1 lipids, *m/z* 556 ($^{\Delta 9}F_O$) and 467 ($^{\Delta 9}F_A$) revealed the C=C location at the Δ9 position, whereas the 18:0/18:1 containing lipid displayed a fragment pair at *m/z* 584 ($^{\Delta 9}F_O$) and 495 ($^{\Delta 9}F_A$) (188). Interestingly, the relative abundance of olefin fragment ions ($^{\Delta n}F_O$) was consistently higher than that of the corresponding aldehyde fragment ions ($^{\Delta n}F_A$). This displays a different pattern than the PB-MS/MS methods that use acetone or 2',4',6'-trifluoroacetophenone, as the C=C diagnostic fragments are expected to have similar ion signal intensities. However, this is not entirely unexpected; as opposed to the use of more neutral PB reagents, olefin fragment ions from 2-ACP contain a charged pyridine functional group (187, 212).

Fatty acyl-specific diagnostic ions were also observed from the cleavage of the two isomeric oxetanes, denoted as α- and ω-ions, based on the orientation of the pyridine moiety relative to the carboxylic acid (**Figure 3.5).** The formation of the photoproduct of oleic acid with 2-ACP ($[^{PB}C18{:}1]^+$) was confirmed by signals at *m/z* 404 and 386 ($[^{PB}C18{:}1\text{-}H_2O]^+$). Derivatized fatty acids of C18 yield a Δ9 specific α-ion at *m/z* 262 and ω-ion at *m/z* 232 (192). We again noted a difference in the relative abundance between this fragment pair, as ω-ions were consistently higher than α-ions, which may indicate preferential orientation of 2-ACP during the PB reaction (192). This phenomenon may also be correlated to preferential ionization, as the ω-ion is an olefin fragment containing the alkyl chain cleaved from the F_A ion.

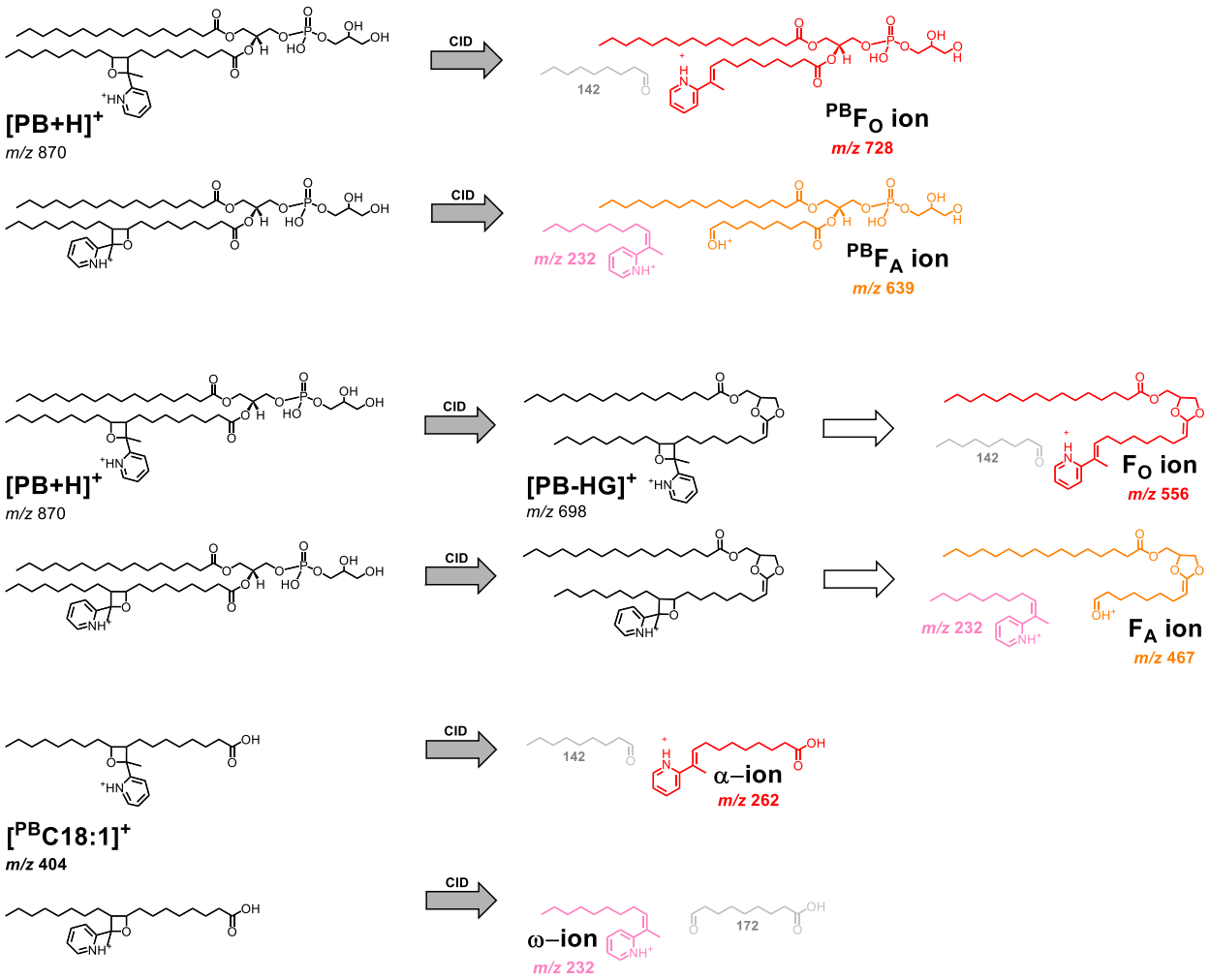

Figure 3.5. Fragmentation schematic for 2-ACP derivatized PG 16:0/18:1(Δ9) **Top Pair:** diagnostic C=C fragment ion structures of the intact lipid upon dissociation, where $^{PB}F_O$ and $^{PB}F_A$ indicate the presence of an olefin or aldehyde at the cleavage site. **Middle Pair:** F_O and F_A indicate the presence of an olefin or aldehyde, respectively, at the cleavage site after headgroup loss. **Bottom Pair**: Fatty acid ^{PB}C18:1 C=C specific α- and ω-fragment ions indicate the orientation of the pyridine moiety from the cleavage of the two isomeric oxetanes.

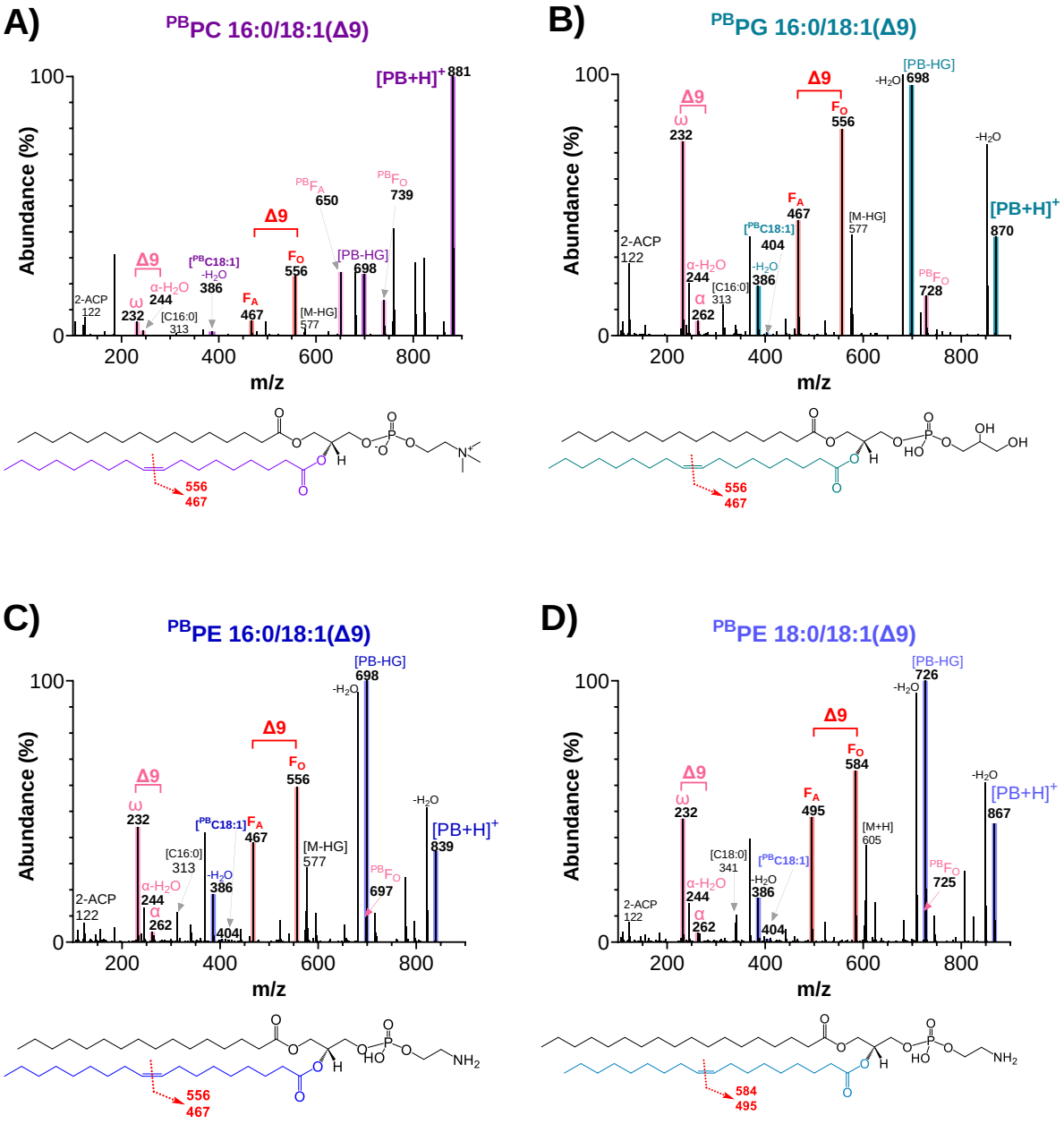

Figure 3.6. PB MS/MS spectra resulting from the PB reaction between 2-acetylpyridine and monounsaturated lipid standards. **A, B, C)** Each 16:0/18:1 spectrum is labeled with the derivatized lipid, $[PB+H]^+$; fragment corresponding to the loss of headgroup, $[PB\text{-}HG]^+$, (*m/z* 698); product ions at *m/z* 556 and 467, which were C=C specific diagnostic ions due to oxetane cleavage, indicating C=C at Δ9 (labeled in red); and functionalized oleic acid α- and ω- fragment ions at *m/z* 262 and 232 (labeled in pink). **D)** PB MS/MS spectrum of PE 18:0/18:1(Δ9).

3.2.2. *Application of Online HILIC-PB-MS/MS to Bacterial Lipidome Analysis*

To demonstrate the applicability of our online HILIC-PB-MS/MS method for the analysis of lipid isomers in the bacterial lipidome, we elucidated the modifications made by *S. aureus* to the C=C locations of the utilized exogenous FAs. *S. aureus* only synthesizes saturated fatty acids via FASII but can utilize host-derived fatty acids, including unsaturated fatty acids. In a recent study, we found that *S. aureus* displayed evidence of elongation of exogenous fatty acids C18:1 to C20:1, C18:2 to C20:2, and C20:4 to C22:4 when grown in the presence of human serum, cholesteryl esters, or triglycerides (213). Elongation of host-derived fatty acids has been observed in a multitude of studies on *S. aureus;* however, the exact mechanism behind eFA elongation has not yet been elucidated, and previous fatty acid composition analyses were reported on a gas chromatograph using fatty acid methyl esters prepared from extracted lipids with hydrolysis followed by methylation (168, 46, 74, 97, 102, 174).

In this study, we tracked the location of the modified C=C in PG lipids, which are the most abundant phospholipids in *S. aureus*. The wild-type (WT) strain was grown with oleic (C18:1), linoleic (C18:2), or arachidonic acid (C20:4) under separate conditions to avoid potential misidentification of source lipids. As polyunsaturated fatty acids can inhibit growth and inflict damage on *S. aureus* upon incorporation, bacterial growth was monitored to ensure that all conditions reached the stationary phase before the cultures were extracted for analysis (**Figure 3.7**). The total fatty acyl chain composition and degree of unsaturation of PG lipids containing total carbons C33-35 were identified using our HILIC-IM-MS and MS/MS methods prior to employing the online PB reaction (**Figure 3.8**).

Results of the targeted fragmentation of the PB reaction products of PG 33:1 and PG 35:1 are displayed in **Figure 3.9**. For PG 33:1, C=C fragment ions were observed at *m/z* 542 (F_O) and

453 (F_A), indicating C=C at Δ9 position. These ions are not fatty acyl-specific, as they only suggest the presence of Δ9 C=C originating from the terminal methyl group. However, a significant peak at *m/z* 386 confirmed the presence of PB-reacted C18:1, whereas the α-ion at *m/z* 262 (-H_2O, m/z 244) and ω-ion at *m/z* 232 validated C18:1(Δ9). For PG 35:1, C=C diagnostic ions were observed at *m/z* 570 (F_O) and 481 (F_A), with mass differences of +28 Da compared with PG 33:1 fragment ions, indicating C=C at the Δ9 position from the methyl end. Fatty acyl composition was determined to be15:0/20:1, as indicated by the MS/MS spectrum collected in negative mode prior to the PB reaction (**Figure 3.9 B**) and by the peaks at *m/z* 299 (C15:0) and *m/z* 414 (PB-derivatized C20:1). The α- and ω-ions observed at *m/z* 272 and 232, respectively, confirmed that the C=C location was C20:1(Δ11). This shift indicated that *S. aureus* elongated C18:1(Δ9) by two carbons at the carboxylic end of the fatty acid to C20:1(Δ11).

Polyunsaturated fatty acids incorporated into the PG lipids of WT strains grown in the presence of 18:2 and 20:4 were also investigated. When grown with linoleic acid, *S. aureus* incorporated C18:2 into PG 33:2, with C=C located at Δ9 and Δ12 (**Figure 3.10 C**), and elongated the exogenous fatty acid to C20:2(Δ11, Δ14) for PG 35:2 (**Figure 3.10 D**). In the presence of arachidonic acid, C=C diagnostic ions were observed but at much lower levels than those of oleic and linoleic acids (**Figure 3.11).** This is in accordance with previous Paternó-Büchi studies of 2-acetylpyridine with C20:4, which showed a higher PB reactivity of polyunsaturated FAs compared to monounsaturated FAs, leading to multiple attachments of PB reagents to arachidonic acid, and the reactivity of double bonds depends on the distance between carboxylic acid and double bonds (192).

Our findings indicated that *S. aureus* modifies the C=C locations of these exogenous FAs, enhancing its ability to adapt to and utilize host-derived lipids. By revealing the exact positions

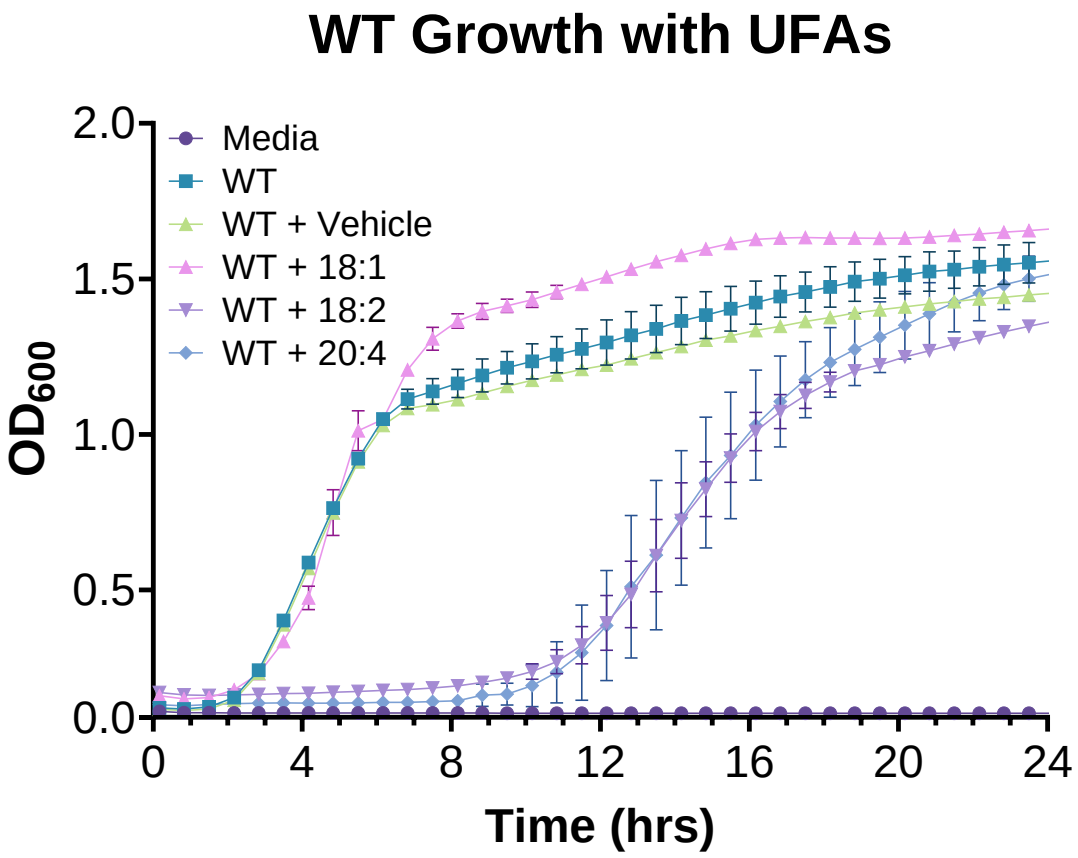

Figure 3.7. Growth curves of *S. aureus* WT (USA300 LAC) strain grown in the presence or absence of 100 μM oleic acid (18:1), linoleic acid (18:2), or arachidonic acid (20:4).

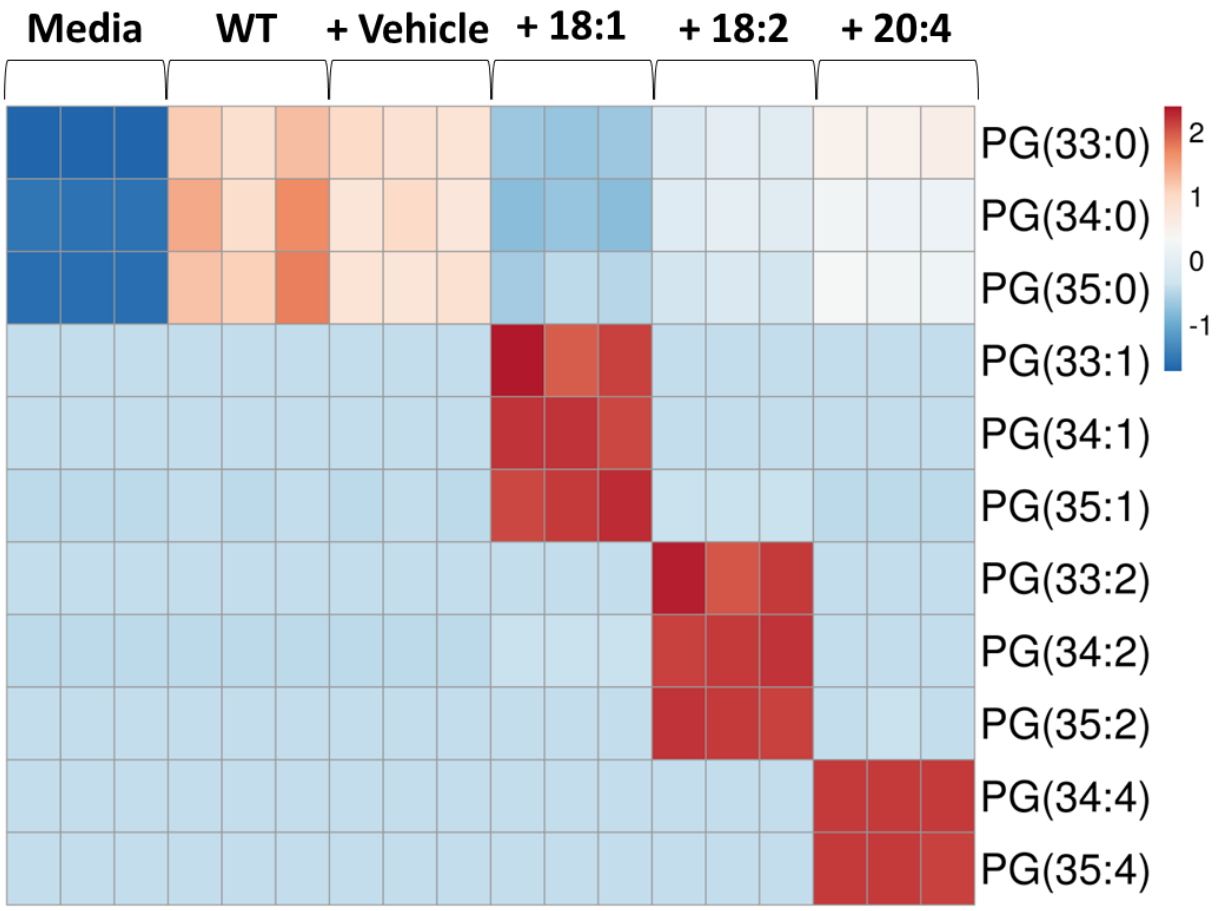

Figure 3.8. Heatmap depicting the relative abundance of PG lipids (33-35) in the *S. aureus* WT (USA300 LAC) strain grown in the presence or absence of 100 μM oleic (18:1), linoleic (18:2), or arachidonic (20:4) acid. Strains were grown in triplicate. Results are row centered and scaled by unit variance scaling.

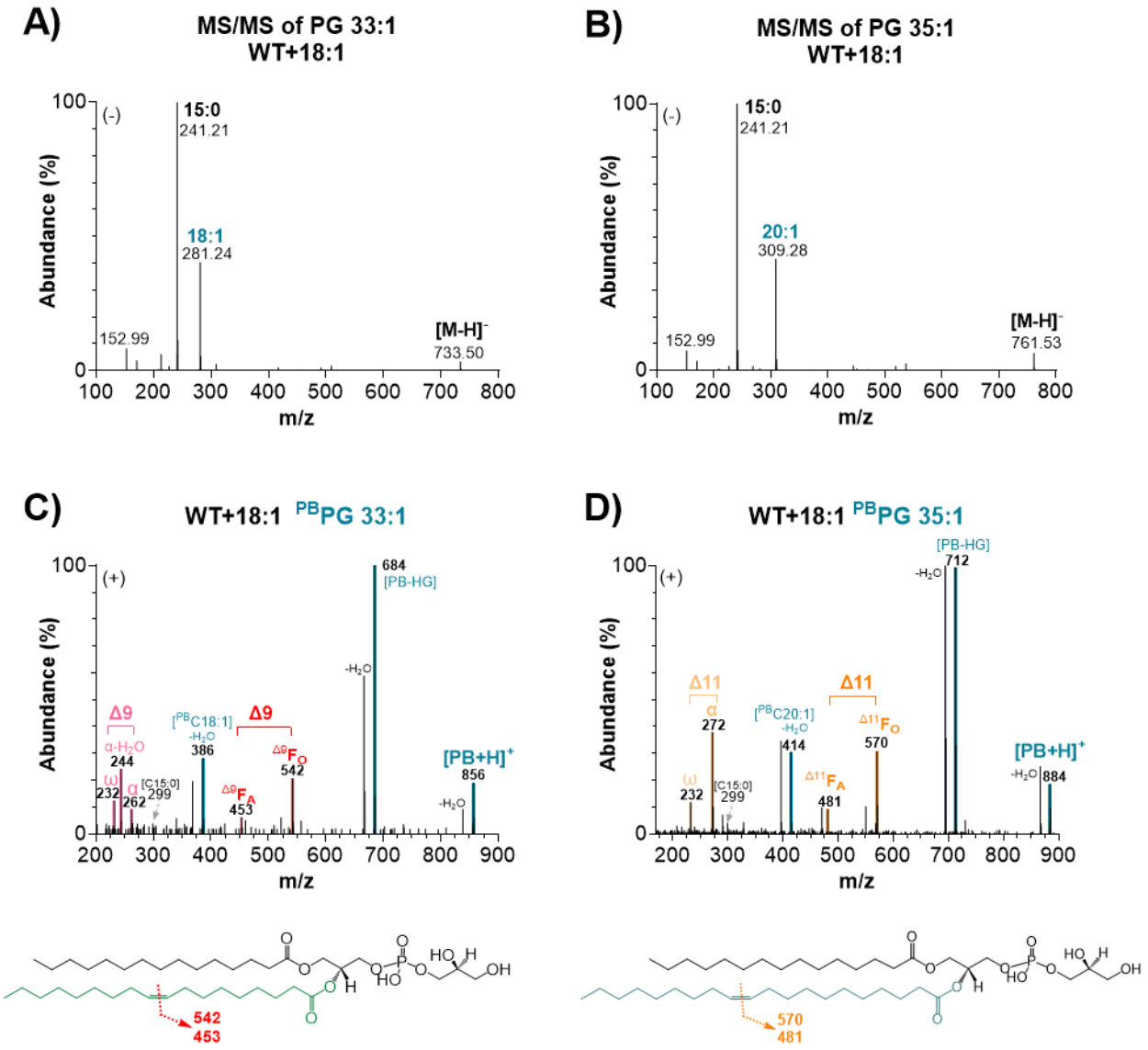

Figure 3.9. Spectra of PG 33:1 and PG 35:1 from *S. aureus* WT strain grown in the presence of oleic acid (18:1). **A and B)** MS/MS spectra collected in negative ionization mode without the PB setup to determine the PG fatty acyl composition. **C)** PB-MS/MS of PG 33:1, $[PB + H]^+$, at *m/z* 856. Product ions at *m/z* 542 and 453 were specific for C=C at Δ9 in PG 15:0/18:1. Diagnostic α- and ω-fragment ions for C18:1(Δ9) were identified at *m/z* 262 ($-H_2O$, *m/z* 244) and 232, respectively. **D)** PB-MS/MS of PG 35:1, $[PB + H]^+$ at *m/z* 884. The product ions at *m/z* 570 and 481 were specific for C=C at Δ11 in PG 15:0/20:1. The derivatized C20:1 fatty acid was confirmed at *m/z* 414, and diagnostic α- and ω- fragment ions for C20:1(Δ11) were identified at *m/z* 272 and 232.

453 (F_A), indicating C=C at Δ9 position. These ions are not fatty acyl-specific, as they only suggest the presence of Δ9 C=C originating from the terminal methyl group. However, a significant peak at *m/z* 386 confirmed the presence of PB-reacted C18:1, whereas the α-ion at *m/z* 262 (-H_2O, m/z 244) and ω-ion at *m/z* 232 validated C18:1(Δ9). For PG 35:1, C=C diagnostic ions were observed at *m/z* 570 (F_O) and 481 (F_A), with mass differences of +28 Da compared with PG 33:1 fragment ions, indicating C=C at the Δ9 position from the methyl end. Fatty acyl composition was determined to be15:0/20:1, as indicated by the MS/MS spectrum collected in negative mode prior to the PB reaction (**Figure 3.9 B**) and by the peaks at *m/z* 299 (C15:0) and *m/z* 414 (PB-derivatized C20:1). The α- and ω-ions observed at *m/z* 272 and 232, respectively, confirmed that the C=C location was C20:1(Δ11). This shift indicated that *S. aureus* elongated C18:1(Δ9) by two carbons at the carboxylic end of the fatty acid to C20:1(Δ11).

Polyunsaturated fatty acids incorporated into the PG lipids of WT strains grown in the presence of 18:2 and 20:4 were also investigated. When grown with linoleic acid, *S. aureus* incorporated C18:2 into PG 33:2, with C=C located at Δ9 and Δ12 (**Figure 3.10 C**), and elongated the exogenous fatty acid to C20:2(Δ11, Δ14) for PG 35:2 (**Figure 3.10 D**). In the presence of arachidonic acid, C=C diagnostic ions were observed but at much lower levels than those of oleic and linoleic acids (**Figure 3.11).** This is in accordance with previous Paternó-Büchi studies of 2-acetylpyridine with C20:4, which showed a higher PB reactivity of polyunsaturated FAs compared to monounsaturated FAs, leading to multiple attachments of PB reagents to arachidonic acid, and the reactivity of double bonds depends on the distance between carboxylic acid and double bonds (192).

Our findings indicated that *S. aureus* modifies the C=C locations of these exogenous FAs, enhancing its ability to adapt to and utilize host-derived lipids. By revealing the exact positions

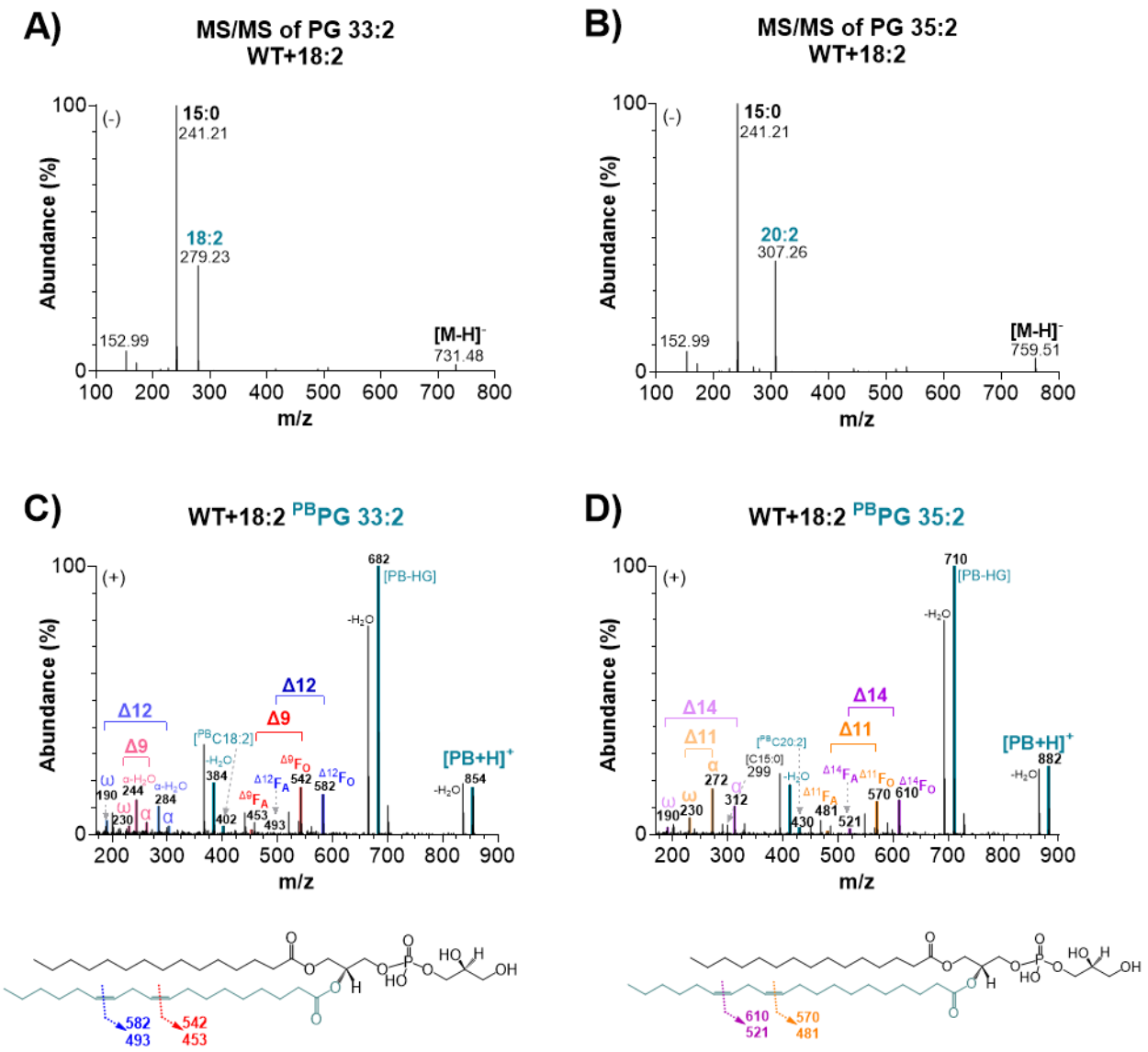

Figure 3.10. Spectra of PG 33:2 and PG 35:2 from the *S. aureus* WT strain grown in the presence of linoleic acid (18:2). **A and B)** MS/MS spectra collected in negative ionization mode without the PB setup to determine the PG fatty acyl composition. **C)** PB-MS/MS of PG 33:2, [PB + H]+ at *m/z* 854. The fragment ion pairs at *m/z* 542 and 453 were specific for C=C at Δ9 in C18:2, confirmed by diagnostic α- and ω-fragment ions at *m/z* 262 (-H_2O, *m/z* 244) and 232, respectively, and the fragment ion pairs at *m/z* 582 and 493 were specific for C=C at Δ12 in C18:2, confirmed by additional diagnostic α- and ω-fragment ions at *m/z* 302 (-H_2O, *m/z* 284) and 190. **D)** PB-MS/MS of PG 35:2, $[PB + H]^+$ at *m/z* 882. Product ions at *m/z* 570 and 481 were specific for C=C Δ11 in C20:2, confirmed by diagnostic α- and ω-fragment ions at *m/z* 272 and 230, respectively, and the fragment ion pairs at *m/z* 610 and 521 were specific for C=C at Δ14 in C20:2, confirmed by additional diagnostic α- and ω-fragment ions at *m/z* 312 and 190.

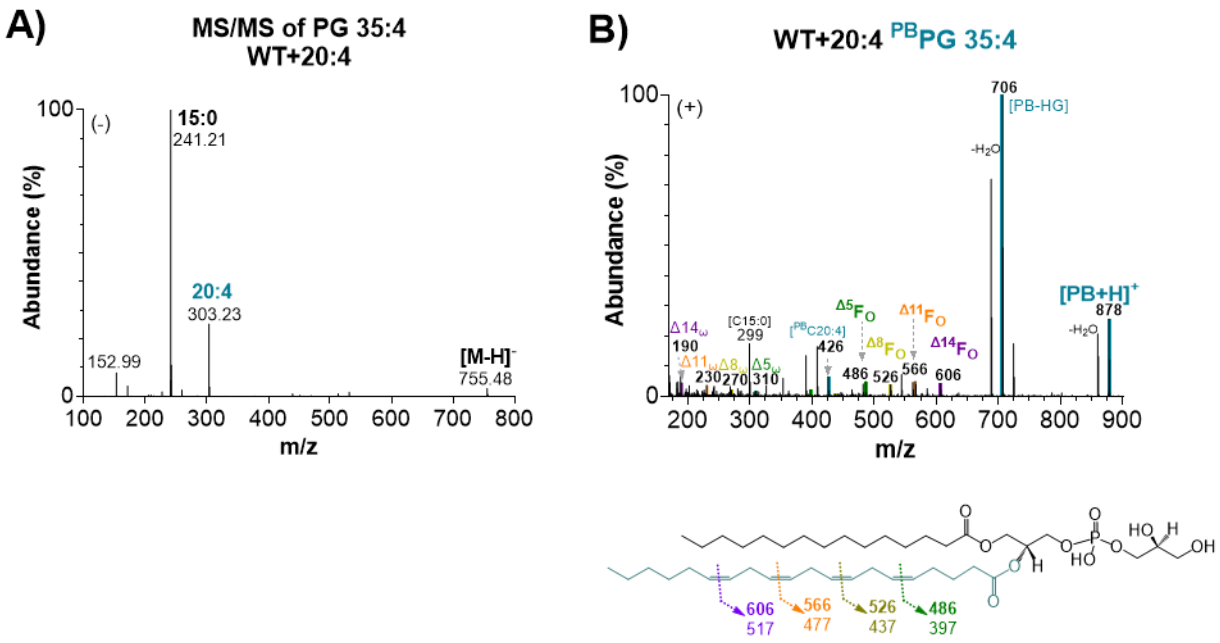

Figure 3.11. Spectra of PG 35:4 from the *S. aureus* WT strain grown in the presence of arachidonic acid (20:4). **A)** MS/MS spectra were collected in negative ionization mode without the PB setup to determine the PG fatty acyl composition. **B)** PB-MS/MS of PG 35:4, [PB + H]+ at *m/z* 878. The location of C = C in C20:4 was determined from the F_O peaks at m/z 606 ($\Delta14F_O$), 566 ($\Delta11F_O$), 526 ($\Delta8F_O$), and 486 ($\Delta5F_O$). Fragments specific for ω-ions were identified at *m/z* 310 (Δ5ω), 270 (Δ8ω), 230 (Δ11ω), and 190 (Δ14ω).

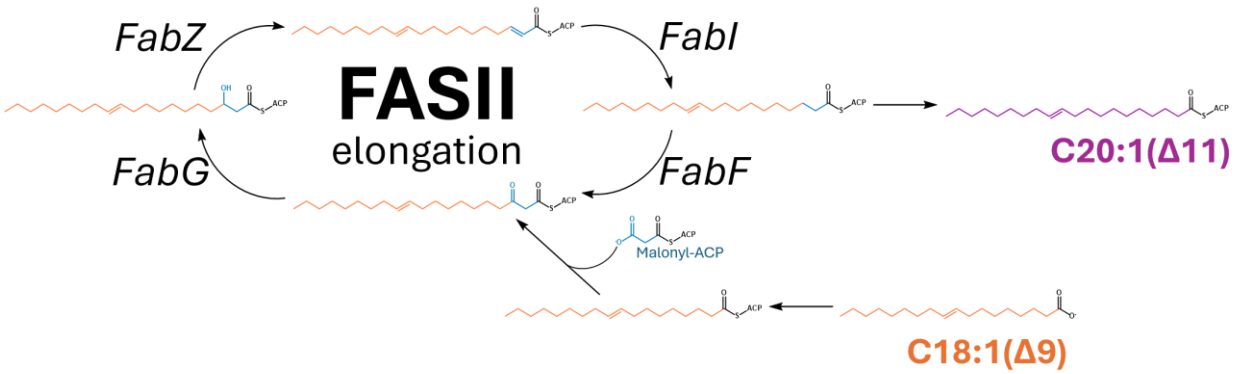

Figure 3.12. Modified type II fatty acid synthesis pathway (FASII) depicting the elongation of C18:1(Δ9) to C20:1(Δ11).

of C=C in the elongated fatty acids, our method provides critical insights into the metabolic adaptations of S. aureus. Detailed structural elucidation is crucial for understanding bacterial lipid metabolism, and could have significant implications for developing strategies to counteract bacterial infections.

3.2.3. *Ion Mobility Trends of Paternó-Büchi Derivatized Lipids*

We aimed to increase the sensitivity and specificity of our C=C location determination method by utilizing ion mobility to obtain collision-cross-section (CCS) values, enabling higher validation of lipid feature identification (197, 212, 214–216). Previous studies have shown that derivatization can alter the ionization properties and mobility of lipids, resulting in improved separation and structural differentiation (179, 197). Our analysis of phosphatidylcholine (PC) and phosphatidylethanolamine (PE) lipid standards (**Table 3.1**) using IM-MS revealed significant differences between underivatized and 2-ACP derivatized lipids (**Figure 3.13)**. The consistent increase in CCS values for 2-ACP derivatized lipids, compared to their underivatized counterparts, indicated a more significant molecular size and reduced mobility (**Figure 3.14**). This shift in drift time reflects the 121-Da mass increase and structural modifications introduced by the 2-ACP derivatization process. Enhanced resolution and separation of lipid species were clearly observed in the IM-MS plots, which is particularly beneficial for distinguishing between the isomeric forms.

The dimensionless compaction factor ([C]) was calculated to describe the relative change in ion mobility when lipids were derivatized with 2-ACP using the following equation:

$$\left(\frac{CCS_{underivatized}}{CCS_{\ derivatized}}\right) = c * \left(\frac{mass_{underivatized}}{mass_{\ derivatized}}\right)^{2/3}$$

Table 3.1. PC and PE lipid standards used in the HILIC-PB-MS/MS experiments.

Lipid	Adduct	m/z	Retention Time	Calibrated RT	CCS ($Å^2$)
PC 10:0/10:0	$[+H]^+$	566.4	10.3	7.0	245.4
PC 12:0/12:0	$[+H]^+$	622.4	10.3	6.9	258.4
PC 14:0/14:0	$[+H]^+$	678.5	10.2	6.7	270.4
PC 16:0/16:0	$[+H]^+$	734.6	10.2	6.7	282.5
PC 16:0/18:2	$[+H]^+$	758.6	10.2	6.7	284.5
PC 16:0/18:1	$[+H]^+$	760.6	10.2	6.7	281.5
PC 18:1/18:1	$[+H]^+$	786.6	10.2	6.7	288.6
PC 18:0/18:0	$[+H]^+$	790.6	10.2	6.7	294.5
PC 18:0/20:4	$[+H]^+$	810.6	10.2	6.7	291.1
PC 20:0/20:0	$[+H]^+$	846.7	10.2	6.7	306.4
PE 10:0/10:0	$[+H]^+$	524.3	8.6	5.8	233.0
PE 12:0/12:0	$[+H]^+$	580.4	8.7	5.8	246.7
PE 14:0/14:0	$[+H]^+$	636.5	8.5	5.7	259.2
PE 16:1/16:1	$[+H]^+$	688.5	8.2	5.5	263.5
PE 16:0/16:0	$[+H]^+$	692.5	8.4	5.7	271.5
PE 16:0/18:1	$[+H]^+$	718.5	8.0	5.4	274.1
PE 18:1/18:1	$[+H]^+$	744.6	8.1	5.5	276.5
PE 18:0/18:1	$[+H]^+$	746.6	8.1	5.5	279.0
PE 18:0/18:0	$[+H]^+$	748.6	8.2	5.5	282.7
PE 20:4/20:4	$[+H]^+$	788.5	7.8	5.3	277.4

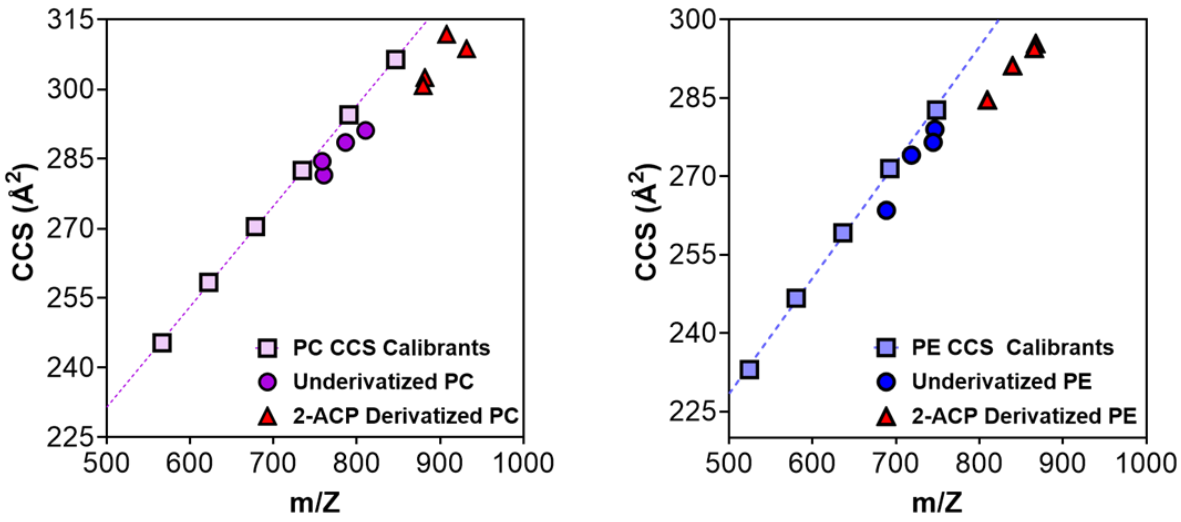

Figure 3.13. IM-MS plots of PC lipid and PE lipid standards. Saturated lipids (squares) were used to generate calibration curves. Underivatized lipids (circles) are unsaturated lipids and 2-ACP derivatized lipids (triangles) are their corresponding PB-reacted products. PE 20:4/20:4 was excluded from this graph because the number of double bonds present was >4x other PE standards.

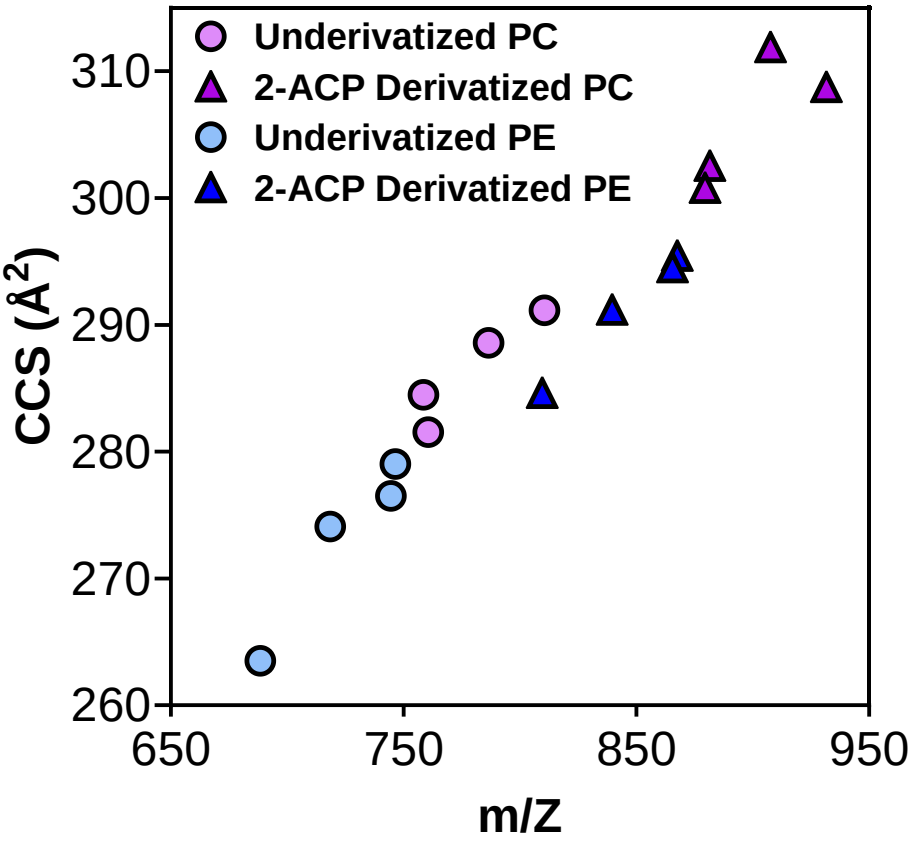

Figure 3.14. IM-MS plots of underivatized (circles) and 2-ACP derivatized (triangles) PC and PE lipids. Unsaturated lipid standards are shown in Table 1. PE 20:4/20:4 was excluded from this graph because the number of double bonds present was >4x other PE standards.

A compaction factor greater than 1 indicates that the derivatized lipid is more compact than the underivatized lipid, whereas a factor less than 1 indicates a less compact PB-derivatized lipid (62, 63). Consistent compaction factors across different lipid classes suggest a predictable impact of 2-ACP derivatization (**Table 3.2**). For both PC and PE lipids, compaction factors greater than 1 indicated that derivatization led to a more compact molecular conformation despite the increase in mass. This paradoxical effect occurs because the addition of the 2-ACP moiety causes the lipid molecule to adopt a more folded or compact conformation, reducing the overall volume occupied by the lipid molecule, and thus lowering its CCS trendline along with other PB products, despite the increased mass. Overall trends of CCS values of these lipid standards indicated that 2-ACP derivatization consistently increased the drift times of lipids, enhancing their separation in IM-MS. This improvement provides better resolution and structural differentiation of lipid species, facilitating more accurate lipidomic analysis.

Detailed isomer differentiation was achieved by identifying specific diagnostic ions, enabling the pinpointing of multiple double-bond positions within lipid molecules. Various C=C positions were detected in the PC (**Figures 3.15** and **3.16**) and PE (**Figures 3.17** and **3.18**) lipid standards containing 1–8 double bonds. This advanced structural elucidation of lipids with multiple unsaturations is vital for understanding the complexity of lipid compositions and their functional roles in biological systems. *S. aureus* samples and PG lipids from PB-MS/MS experiments were further analyzed by post-mobility fragmentation, where C=C diagnostic fragment ions were observed (**Figures 3.19** and **3.20**). While MS/MS spectra without ion mobility tended to exhibit pronounced water loss fragments ($-H_2O$), these adducts were notably absent or much less abundant in the spectra where ion mobility was employed. Post-mobility fragmentation also yielded an increase in PB products with intact lipid backbones, such as the

Table 3.2. Compaction factors of 2-ACP derivatized PC and PE lipid standards.

Underivatized Lipid	Derivatized Lipid	Compaction Factor [*C*]
PC 16:0/18:2	(2-ACP) PC 16:0/18:2	1.04
PC 16:0/18:1	(2-ACP) PC 16:0/18:1	1.03
PC 18:1/18:1	(2-ACP) PC 18:1/18:1	1.03
PC 18:0/20:4	(2-ACP) PC 18:0/20:4	1.02
PE 16:1/16:1	(2-ACP) PE 16:1/16:1	1.03
PE 16:0/18:1	(2-ACP) PE 16:0/18:1	1.04
PE 18:1/18:1	(2-ACP) PE 18:1/18:1	1.04
PE 18:0/18:1	(2-ACP) PE 18:0/18:1	1.04
PE 20:4/20:4	(2-ACP) PE 20:4/20:4	1.03

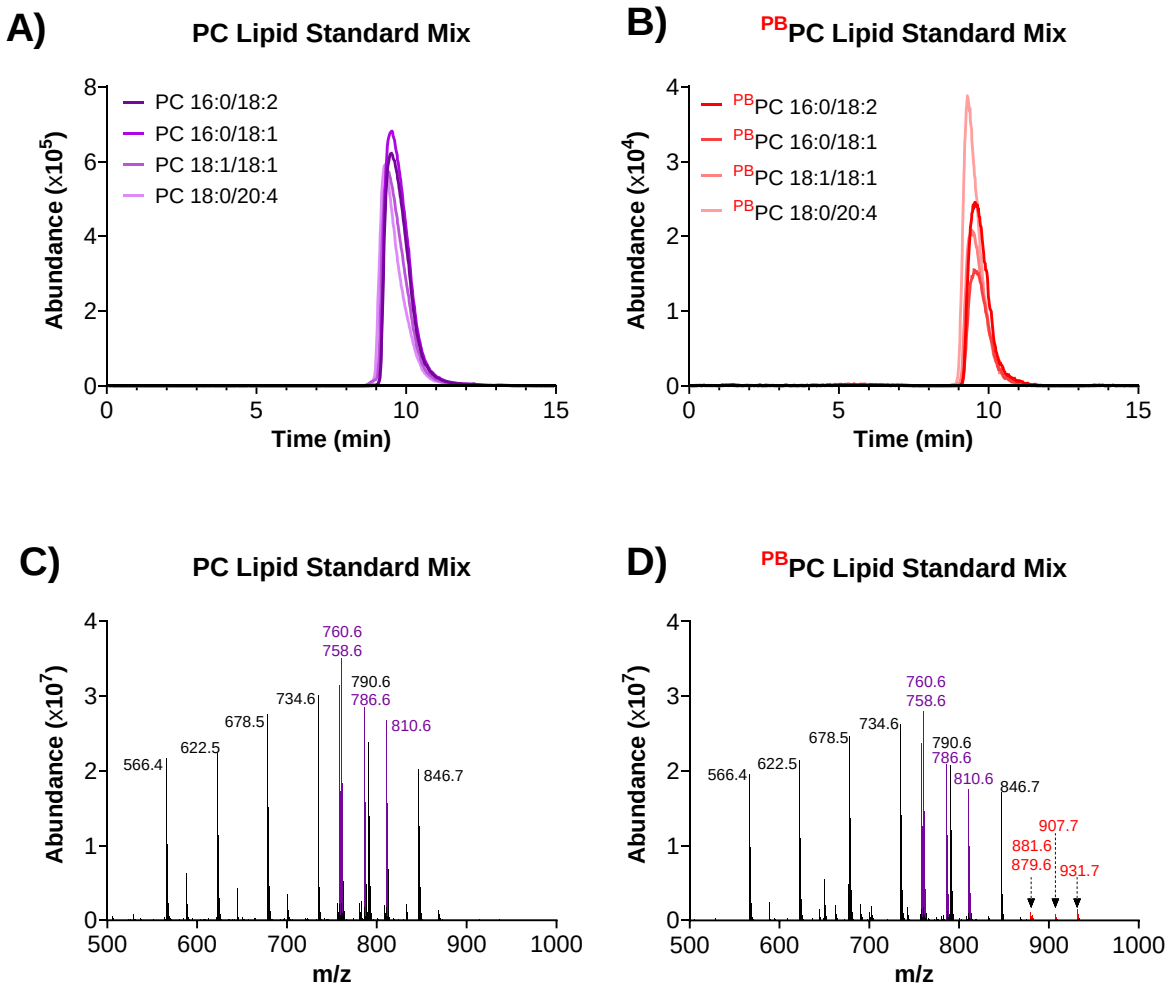

Figure 3.15. Extracted chromatograms and mass spectra of PC lipid standards **A and C)** underivatized and **B,D)** derivatized with 2-ACP. The peaks labeled in purple indicate the underivatized lipids, and the peaks labeled in red are their corresponding PB products, with a 121-Da mass increase. PC lipids 16:0/18:2 (*m/z* 758 → 879), 16:0/18:1 (*m/z* 760 → 881), 18:1/18:1 (*m/z* 786 → 907), and 18:0/20:4 (*m/z* 758 → 931) are represented.

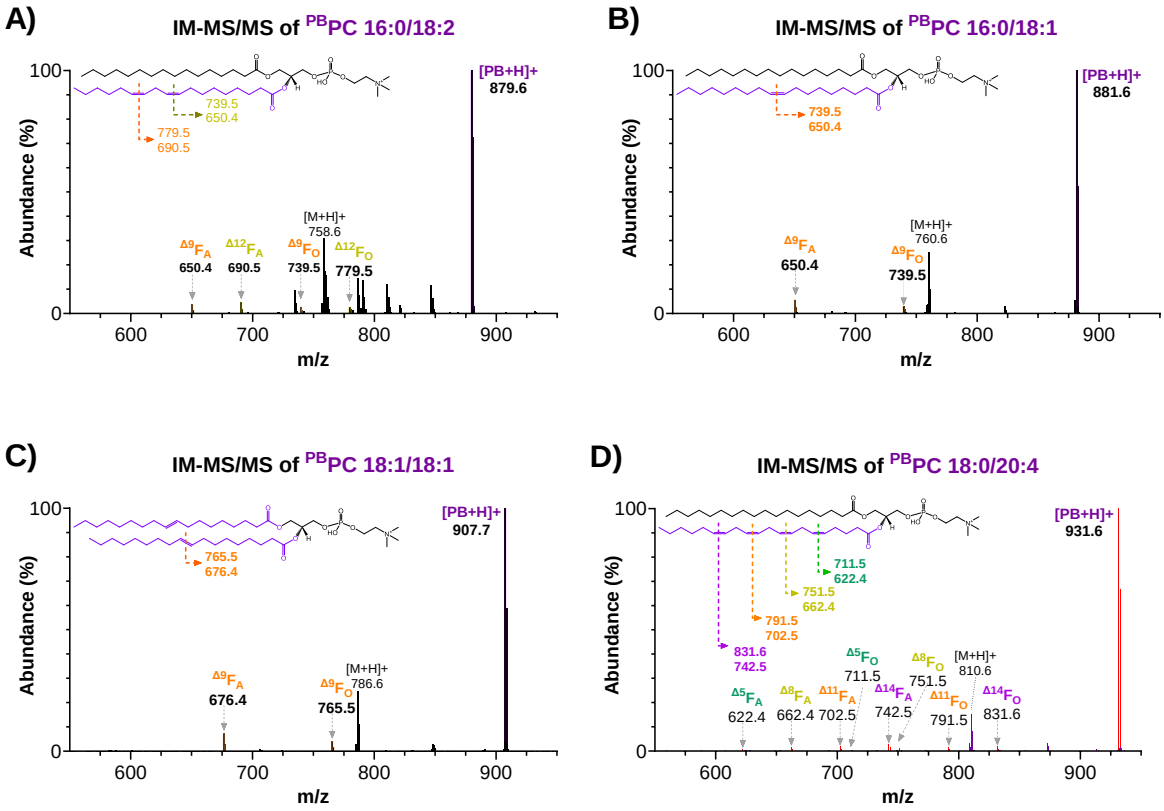

Figure 3.16. IM-MS/MS analysis of PB-derivatized PC lipid standards. The spectra highlight the fragmentation patterns and diagnostic ions resulting from the PB derivatization of various PC lipids. **A)** IM-MS/MS of PC 16:0/18:2 showing diagnostic ions at *m/z* 779 (Δ9F$_O$) and 739 (Δ9F$_A$) and *m/z* 690 (Δ12F$_O$) and 650 (Δ12F$_A$). **B)** IM-MS/MS of PC 16:0/18:1 displaying diagnostic ions at *m/z* 739 (Δ9F$_O$) and 650 (Δ9F$_A$). **C)** IM-MS/MS of PC 18:1/18:1, with highlighted diagnostic ions at *m/z* 765 (Δ9F$_O$) and 676 (Δ9F$_A$). **D)** IM-MS/MS of PC 18:0/20:4 highlighting olefin diagnostic ions at *m/z* 831 (Δ14F$_O$), 791 (Δ11F$_O$), 751 (Δ8F$_O$), and 711 (Δ5F$_O$), and the corresponding aldehyde-containing ions at *m/z* 742 (Δ14F$_A$), 702 (Δ11F$_A$), 662 (Δ8F$_A$), and 622 (Δ5F$_A$).

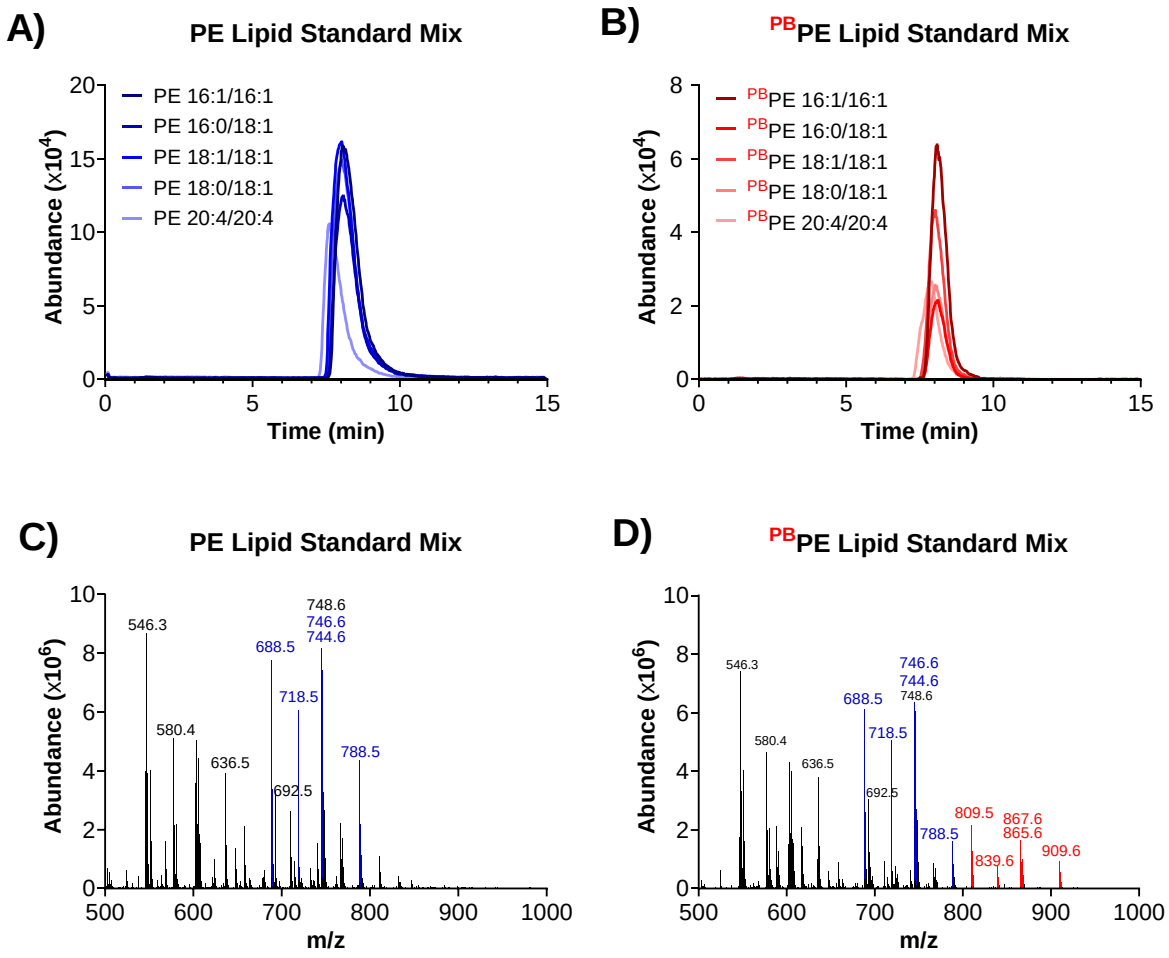

Figure 3.17. Extracted chromatograms and mass spectra of PE lipid standards A and C) underivatized and B,D) derivatized with 2-ACP. Peaks labeled in blue indicate underivatized lipids, and the peaks labeled in red are their corresponding PB products, with a 121-Da mass increase. PE lipids 16:1/16:1 (m/z 688 → 809), 16:0/18:1 (m/z 718 → 839), 18:1/18:1 (m/z 744 → 865), 18:0/18:1 (m/z 746 → 867) and 20:4/20:4 (m/z 788 → 909) are represented.

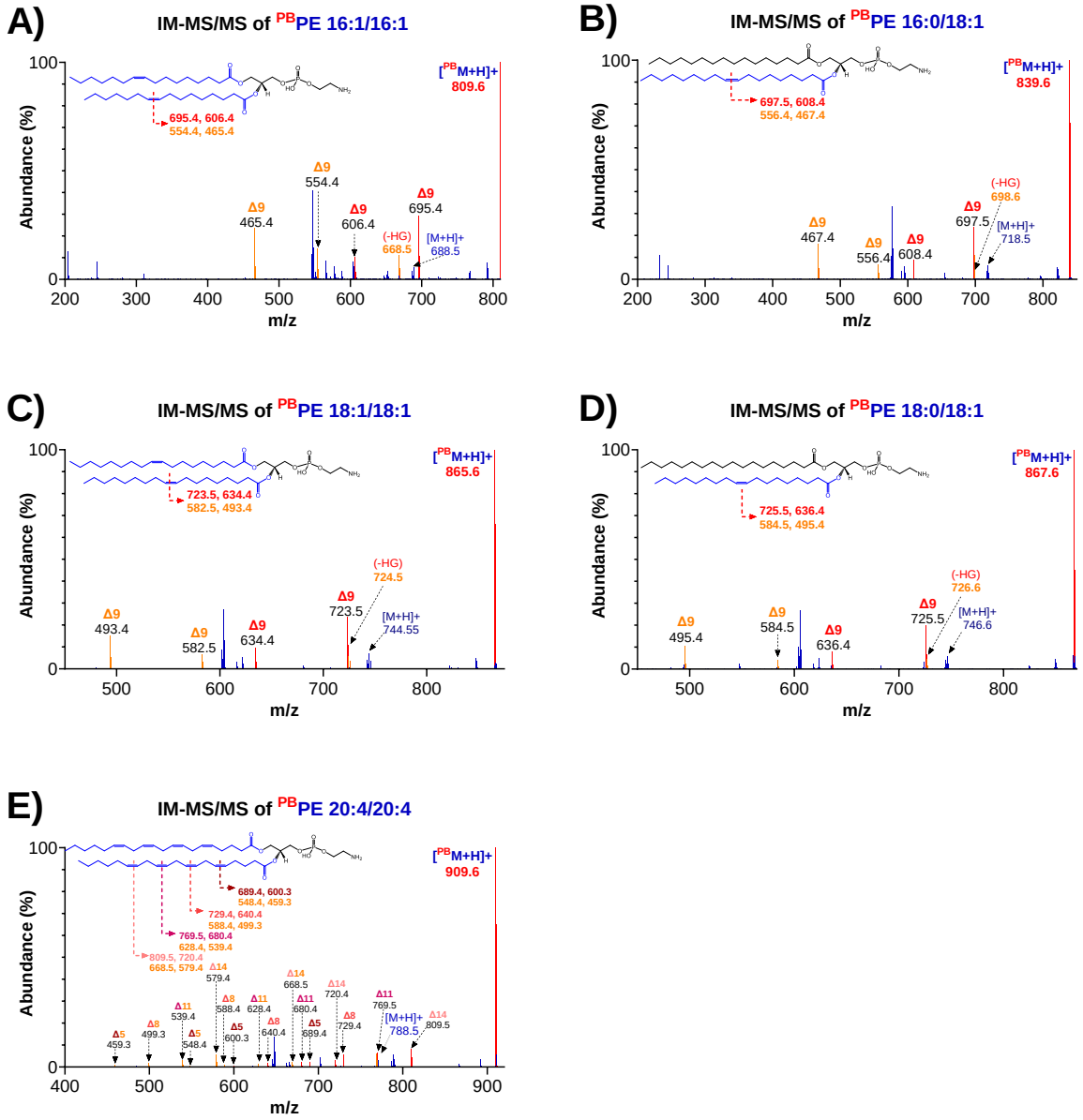

Figure 3.18. IM-MS/MS analysis of PB-derivatized PE lipid standards. The spectra highlight the fragmentation patterns and diagnostic ions resulting from PB derivatization of various PE lipids. **A)** IM-MS/MS of PE 16:1/16:1 showing diagnostic ion pairs at *m/z* 695 and 606 (Δ9) and *m/z* 554 and 465 (Δ9). **B)** IM-MS/MS of PE 16:0/18:1 showing diagnostic ion pairs at *m/z* 697 and 608 (Δ9) and *m/z* 556 and 467 (Δ9). **C)** IM-MS/MS of PE 18:1/18:1 showing diagnostic ion pairs at *m/z* 723 and 634 (Δ9) and *m/z* 582 and 493 (Δ9). **D)** IM-MS/MS of PE 18:0/18:1 showing diagnostic ion pairs at *m/z* 725 and 636 (Δ9) and *m/z* 584 and 495 (Δ9). **E)** IM-MS/MS of PE 20:4/20:4 showing diagnostic ion pairs at *m/z* 729 and 640 (Δ5), *m/z* 588 and 499 (Δ5), *m/z* 689 and 600 (Δ8), *m/z* 548 and 459 (Δ8), *m/z* 769 and 680 (Δ11), *m/z* 628 and 539 (Δ11), *m/z* 809 and 720 (Δ14), and *m/z* 668 and 579 (Δ14).

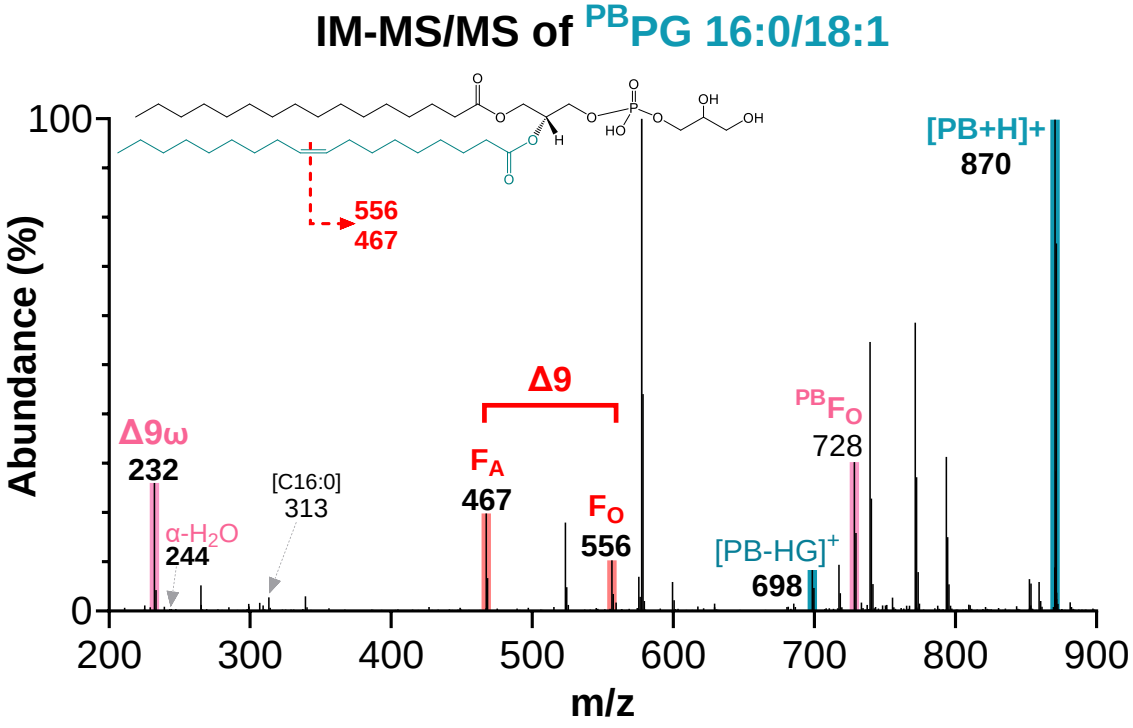

Figure 3.19. PB IM-MS/MS spectra resulting from the PB reaction between 2-acetylpyridine and the PG 16:0/18:1 standard. The highlighted peaks correspond to the derivatized lipid, $[PB+H]^+$ at *m/z* 870; loss of headgroup, $[PB-HG]^+$ at *m/z* 698; C=C specific diagnostic ions for Δ9 at *m/z* 556 and 467; loss of α-fragment at *m/z* 728; and ω-fragment at *m/z* 232.

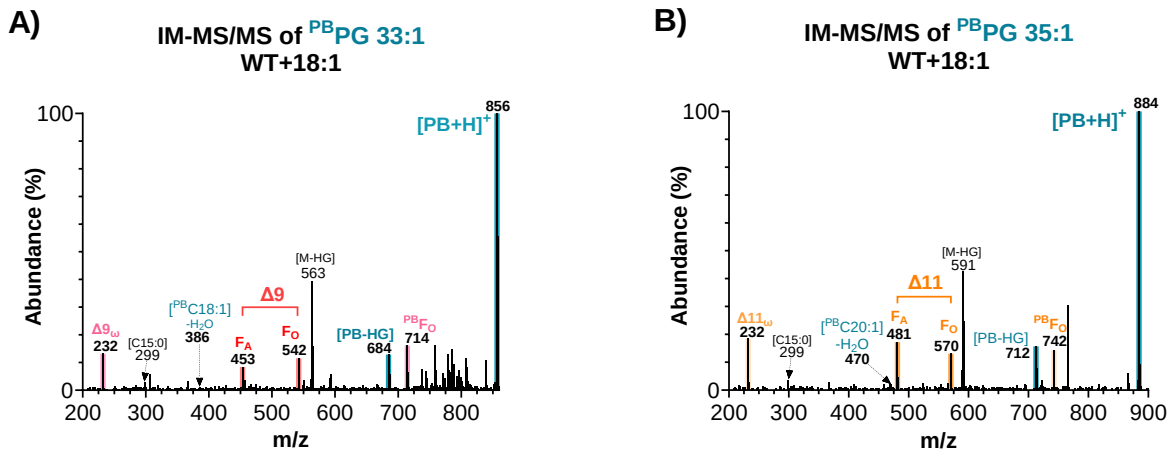

Figure 3.20. PB derivatized spectra of PG 33:1 and PG 35:1 from *S. aureus* WT strain grown in the presence of oleic acid (18:1). **A)** PB IM-MS/MS of PG 33:1, $[PB + H]^+$ at *m/z* 856. Product ions at *m/z* 542 and 453 were specific for C=C at Δ9 in PG 15:0/18:1. The diagnostic ω-fragment ion for C18:1(Δ9) was identified as *m/z* 232. **B)** PB IM-MS/MS of PG 35:1, $[PB + H]^+$ at *m/z* 884. The product ions at *m/z* 570 and 481 were specific for C=C at Δ11 in PG 15:0/20:1. The derivatized C20:1 fatty acid was confirmed at *m/z* 414, and the diagnostic ω-fragment ion for C20:1(Δ11) was identified at *m/z* 232.

peak at *m/z* 728 in PG 16:0/18:1 (**Figure 3.19**). This identified additional diagnostic ions that could be used to confirm the location of C = C in the lipids and potentially provide more detailed information on the derivatization process with 2-ACP. Online Paternó-Büchi reactions using 2-acetylpyridine in conjunction with IM-MS significantly improved analytical capabilities for studying lipid metabolism and structural diversity.

3.3. Conclusions

In tracking the metabolism of unsaturated fatty acids in *Staphylococcus aureus*, online Paternò-Büchi reactions present a promising avenue for streamlined analysis of the incorporation and modification of exogenous lipids. By integrating the PB reaction with HILIC-IM-MS and utilizing 2-acetylpyridine as the PB reagent, we overcame the limitations of previous lipid profiling methods and enhanced the efficiency of C=C location determination in bacterial lipids. Our experimental setup allowed for real-time derivatization of unsaturated lipid species, enabling simultaneous characterization of the incorporation and modification of exogenous lipids in *S. aureus*.

As ongoing research continues to refine lipid analysis methodologies and enhance the capabilities of mass spectrometry, the potential for comprehensive elucidation of lipid metabolism in *S. aureus* and other microbial systems is becoming increasingly attainable. Leveraging the PB reaction in conjunction with advanced HILIC and IM-MS techniques provides the ability to gain further insights into the specific isomeric and positional details of unsaturated fatty acids within the bacterial lipidome. This progress has significant implications for the development of targeted antimicrobial strategies and deciphering the mechanisms underlying microbial resistance to host immune responses and therapeutic interventions.

3.4. Experimental

3.4.1. *Materials and Chemicals*

Phosphatidylcholine (PC), phosphatidylethanolamine (PE), and phosphatidylglycerol (PG) standards were acquired from Avanti Polar Lipids (Alabaster, AL). Lipid standard solutions (5 μM) were prepared in 2:1 acetonitrile/methanol (ACN/MeOH) for analysis. 2-acetylpyridine (2-ACP) was purchased from Sigma Aldrich. The PB reagent solution was prepared using 20 mM 2-ACP in ACN and purged with nitrogen gas for 5 min immediately before use. Optima LC/MS grade acetonitrile (ACN), methanol (MeOH), water, and ammonium acetate were purchased from Fisher Scientific (Pittsburgh, PA). Fatty acids used in the bacterial growth experiments, oleic acid (C18:1), linoleic acid (C18:2), and arachidonic acid (C20:4), were purchased from Nu-Chek Prep, Inc. (Elysian, MN, USA).

3.4.2. *Bacterial Cultures and Growth Conditions*

Staphylococcus aureus USA300 LAC wild-type strain was grown in tryptic soy broth or on tryptic soy agar (TSA). Liquid cultures were prepared in 5 mL TSB in Falcon Tubes by suspending a single colony from TSA plates and incubating overnight at 37°C with shaking. Bacteria were subsequently diluted 1:100 in 5 mL of fresh TSB and grown in triplicate for 24 h with or without the addition of 100 μM oleic, linoleic, or arachidonic acid. Cultures were pelleted by centrifugation, washed by resuspension and centrifugation in phosphate-buffered saline, and total lipids were extracted using the method described by Bligh and Dyer (163). Extracts were dried in a vacuum concentrator and reconstituted in 2:1 acetonitrile-methanol for analysis.

For growth curve measurements, the bacterial cultures were diluted 1:100 in TSB and added to a Costar 96-well flat-bottom microplate. Growth was monitored at 600 nM using a BioTek Synergy H1 plate reader (BioTek Instruments) at 37°C with continuous double orbital shaking.

3.4.3. *Online Paternó-Büchi Reaction*

All chromatographic separations were carried out with a Phenomenex Kinetex HILIC column (50 x 2.1 mm, 1.7 μm) on a Waters Acquity FTN UPLC (Waters Corp., Milford, MA) (51). The solvent system consisted of the following mobile phases: A) 95% acetonitrile/5% water with 5 mM ammonium acetate, and B) 50% acetonitrile/50% water with 5 mM ammonium acetate. A constant flow rate of 200 μL/min was maintained throughout the 15-minute run time using the following linear gradient: 0-1.25 min, 100% A; 5 min, 90% A; 8.75 min; 70% A; and 11.25-15 min, 100% A. An injection volume of 5 μL was used in this study.

Similar to the design and setup of Yang et al. and Zhang et al., a flow microreactor was installed after HILIC separation before ESI, while the PB reagent solution (20 mM 2-ACP in ACN) was teed-in to the LC eluent at a flow rate of 5 μL/min using a 500 μL Hamilton syringe and Fisher Scientific syringe pump (189, 217). The reactor was designed using Tinkercad and 3D printed on a Creality CR-10 Series 3D printer (Shenzhen Creality 3D Technology Co., LTD.). BGB Analytik UV-transmitting FEP tubing (1/16” OD x 0.75 mm ID) was coiled around a BHK low-pressure mercury lamp (185/254 nm) for a reaction time of ~ 30 s (217, 218). After irradiation, the lipid solution was infused into the ESI source of the mass spectrometer.

3.4.4. *Mass Spectrometry Analysis*

All MS and MS/MS data were collected in positive or negative ionization mode on a Waters Synapt XS traveling-wave ion mobility-mass spectrometer (Water Corp.) with the following instrument parameters: capillary voltage, 2.5-3.0 kV; source temperature, 150°C; sampling cone, 100 V; source offset, 4 V; desolvation temperature, 250°C; cone gas flow, 10 L/hr; desolvation gas flow, 500 L/hr. Mass calibration and data acquisition were performed in resolution mode, as previously described (137, 207). Targeted MS/MS experiments were performed with a 0.5 s scan time over the range of 50-1200 m/z and quadrupole resolution of 15.0 (a.u.). Collision-induced dissociation was applied to the transfer region, with a collision energy ramp of 25-40 eV. To calculate the TWIM drift times into CCS values, drift times for the PC and PE standards were manually extracted from their respective mobiligrams in the arrival time distribution function of MassLynx, and correction calibration calculations were performed using custom Python scripts, as previously described (219).

3.5. Acknowledgements

We would like to thank Seth Sedberry for his contribution in building and designing the microreactor prototype, and Ryan Ngyuen for aiding in the calculation of standard CCS values.

CHAPTER 4: Summary and Future Directions

Staphylococcus aureus is an insidious pathogen that significantly contributes to the pandemic of antibiotic resistance and is increasingly threatening global healthcare systems. This dissertation expands our understanding of the adaptive metabolic strategies through which *S. aureus* exploits host-derived fatty acids for survival and virulence. **Chapter 2** explored the incorporation of host-derived eFAs, particularly unsaturated fatty acids, by *S. aureus* and their subsequent impact on bacterial membrane fluidity and antimicrobial susceptibility. We identified glycerol ester hydrolase (Geh) as the primary lipase that hydrolyzes cholesteryl esters, highlighting its pivotal role in the pathogen's eFA acquisition mechanism and offering a potential therapeutic target to disrupt the adaptability of *S. aureus* in host environments. Furthermore, interactions between *S. aureus* and human serum albumin (HSA) revealed a sophisticated regulatory mechanism: at lower concentrations, HSA serves as a source and enhances fatty acid availability to support bacterial growth, whereas at higher concentrations, it restricts access and potentially inhibits bacterial proliferation. We also demonstrated the potential of the FASII pathway inhibitor AFN-1252 to alter the bacterial lipid profile, suggesting a novel approach to undermine bacterial resistance through metabolic interference. Notably, the ability of AFN-1252 to enhance UFA content, even in the absence of exogenous lipids, suggests that modulation of membrane properties is part of its mechanism of action. These findings advocate further exploration of metabolic inhibitors as adjunctive therapies to counteract *S. aureus* adaptation to the host environment. **Chapter 3** integrates online Paternò-Büchi reactions with HILIC-IM-MS methods to locate carbon-carbon double bonds (C=C) in unsaturated lipid species. This chapter describes the simultaneous characterization of the incorporation and modification of exogenous lipids in *S. aureus.* Understanding the isomeric and positional details of the fatty acids and lipids used by bacteria is essential for deciphering *S. aureus* adaptations

within the host environment and the underlying evolutionary mechanisms of antimicrobial resistance.

Further investigation of the findings of this study is warranted. Increased levels of saturated lipid species were observed in the *Δgeh* strain grown in the presence of human serum or triglycerides (**Chapter 2, Figures 2.2—2.5**). This increase was attributed to the upregulation of *de novo* fatty acid synthesis in the lipase knockout. Given the emerging interest in the role of Geh as a key player in lipid metabolism and its potential impact on pathogenicity, future studies should focus on elucidating its precise function and mechanism. It may be beneficial to investigate whether the increase in saturated lipids under these conditions is due to endogenous biosynthesis, or whether *S. aureus* incorporates more host-derived saturated fatty acids without Geh.

Lipid analysis of *S. aureus* grown with AFN-1252 (**Chapter 2, Figures 2.12, 2.13, and 2.15**) revealed an unusual fatty acid composition. This possible modulation of membrane properties as part of AFN-1252's mechanism of action would be intriguing to investigate. Although not presented in Chapter 3, we subjected AFN-1252 treated samples to the PB reaction (**Figure 4.1**). We indeed observed the molecular ion of $[PB+H]^+$; however, the PB-MS/MS spectra did not display the expected fragmentation pattern. This further suggests that double-bond positions influence this pattern and that AFN-1252 modifies endogenous fatty acids. Unpublished growth curve experiments (**Figure 4.2**) comparing WT and AFN-1252 in the presence of 18:1, 18:2, and 20:4 fatty acid standards demonstrated that AFN-1252 might aid in the rescue of *S. aureus* growth in the presence of toxic PUFAs. These exogenous PUFAS are prone to lipid peroxidation, which is the reason for their inhibition of the growth of *S. aureus.* In addition, these

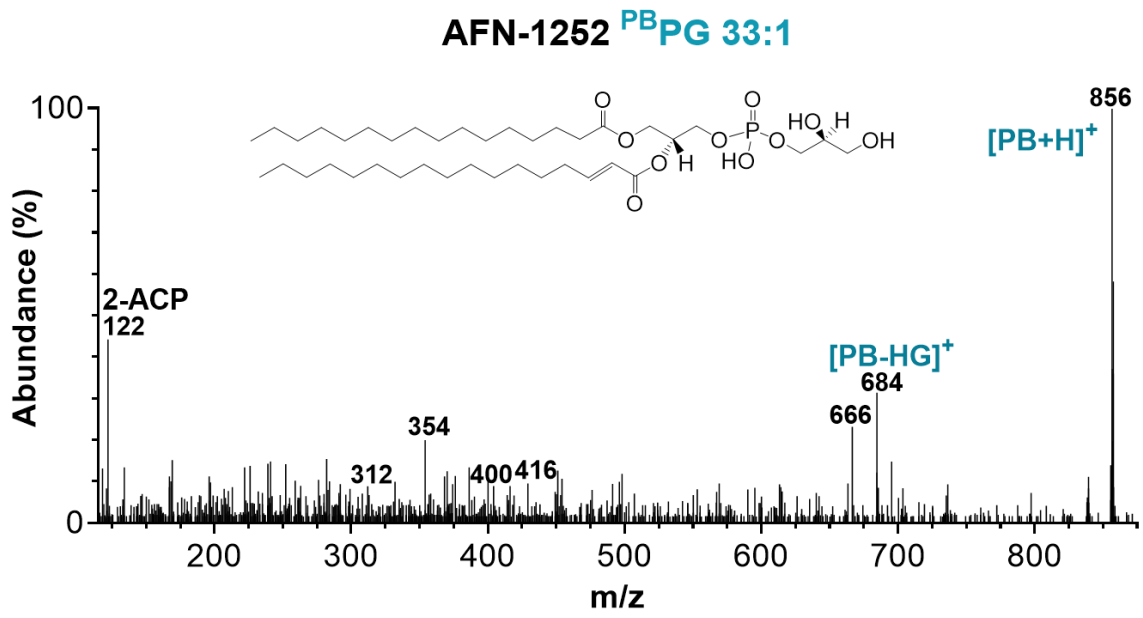

Figure 4.1. PB-MS/MS of PG 33:1 from *S. aureus* growth with AFN-1252 only. $[PB + H]^+$, at *m/z* 856, $[PB - HG]^+$, at *m/z* 684, and $[2\text{-ACP} + H]^+$, at *m/z* 122 were successfully identified.

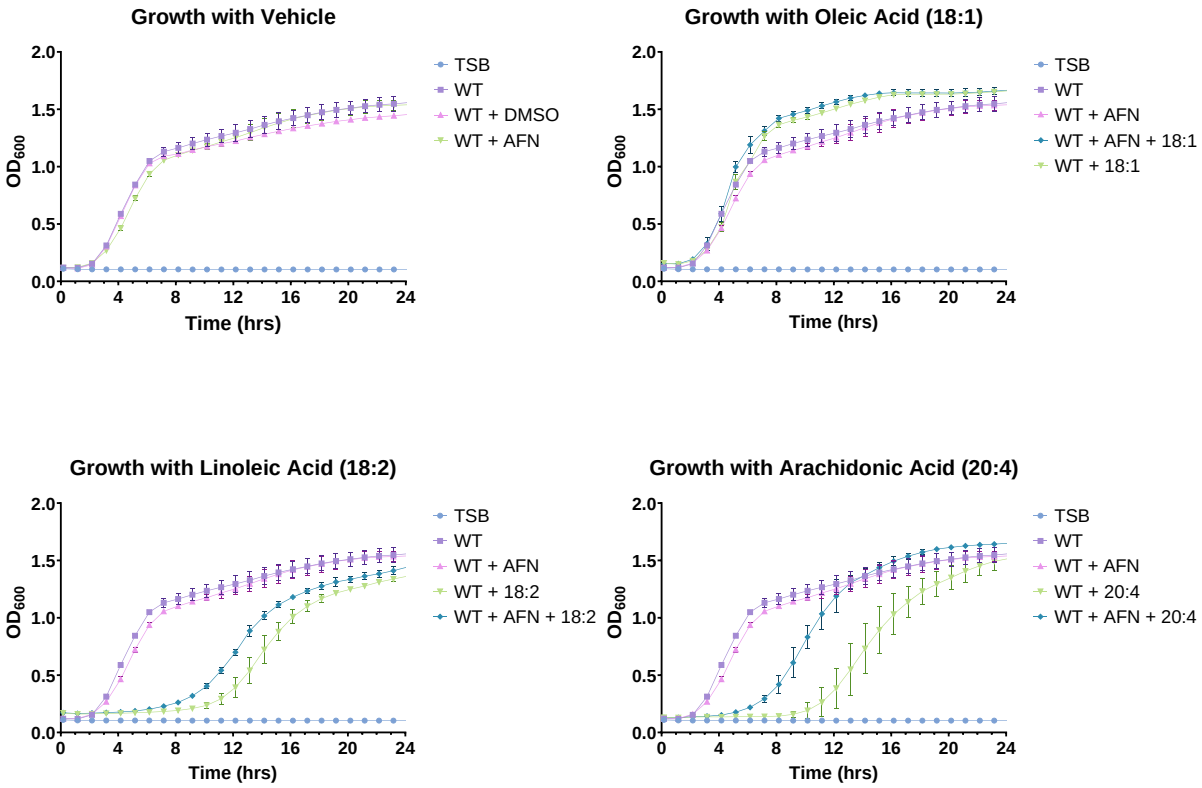

Figure 4.2. Growth curves of *S. aureus* WT treated with AFN-1252 in the presence or absence of 100 μM oleic acid (18:1), linoleic acid (18:2), or arachidonic acid (20:4).

cis double bond-containing PUFAs induce stronger changes in membrane fluidity than *trans* fatty acids. However, the exact mechanisms that AFN-1252 confers protection of *S. aureus* against these PUFAs remains to be elucidated. Overall, future research should consider the effect of AFN-1252 on ROS formation and explore the use of other PB reagents to obtain an accurate identification of these modified C=C configurations, providing significant implications for membrane properties and bacterial adaptation.

BIBLIOGRAPHY

1. Ogston A. 1880. Über Abscesse. Arch Klin Chir 25:588–600.

2. Ogston A. 1882. Micrococcus Poisoning. J Anat Physiol 17:24–58.

3. Rosenbach FJ. 1884. Mikro-organismen bei den Wund-Infections-Krankheiten des Menschen. J.F. Bergmann, Wiesbaden.

4. David Skinner, Chester S. Keefer. 1941. Significance of bacteremia caused by Staphylococcus aureus: a study of one hundred and twenty-two cases and a review of the literature concerned with experimental infection in animals. Arch Intern Med (Chic) 68:851.

5. Fleming A. 1941. Penicillin. Br Med J 2:386.

6. Fleming A. 1944. The Discovery of Penicillin. British Medical Bulletin 2:4–5.

7. Kirby WMM. 1944. Extraction of a Highly Potent Penicillin Inactivator from Penicillin Resistant Staphylococci. Science 99:452–453.

8. Barber M, Rozwadowska-Dowzenko M. 1948. Infection by Penicillin-Resistant Staphylococci. The Lancet 252:641–644.

9. Chambers HF. 2001. The changing epidemiology of Staphylococcus aureus? Emerg Infect Dis 7:178–182.

10. Thompson RL, Cabezudo I, Wenzel RP. 1982. Epidemiology of nosocomial infections caused by methicillin-resistant Staphylococcus aureus. Ann Intern Med 97:309–317.

11. David MZ, Daum RS. 2010. Community-Associated Methicillin-Resistant Staphylococcus aureus: Epidemiology and Clinical Consequences of an Emerging Epidemic. Clinical Microbiology Reviews 23:616–687.

12. Antimicrobial Resistance Collaborators. 2022. Global burden of bacterial antimicrobial resistance in 2019: a systematic analysis. Lancet 399:629–655.

13. Wertheim HF, Melles DC, Vos MC, van Leeuwen W, van Belkum A, Verbrugh HA, Nouwen JL. 2005. The role of nasal carriage in *Staphylococcus aureus* infections. The Lancet Infectious Diseases 5:751–762.

14. Tong SYC, Davis JS, Eichenberger E, Holland TL, Fowler VG. 2015. Staphylococcus aureus Infections: Epidemiology, Pathophysiology, Clinical Manifestations, and Management. Clin Microbiol Rev 28:603–661.

15. Laux C, Peschel A, Krismer B. 2019. Staphylococcus aureus Colonization of the Human Nose and Interaction with Other Microbiome Members. Microbiology Spectrum 7:10.1128/microbiolspec.gpp3-0029–2018.

16. Howden BP, Giulieri SG, Wong Fok Lung T, Baines SL, Sharkey LK, Lee JYH, Hachani A, Monk IR, Stinear TP. 2023. Staphylococcus aureus host interactions and adaptation. Nat Rev Microbiol 21:380–395.

17. Gorwitz RJ, Kruszon-Moran D, McAllister SK, McQuillan G, McDougal LK, Fosheim GE, Jensen BJ, Killgore G, Tenover FC, Kuehnert MJ. 2008. Changes in the Prevalence of Nasal Colonization with *Staphylococcus aureus* in the United States, 2001–2004. J INFECT DIS 197:1226–1234.

18. Kumar N, David MZ, Boyle-Vavra S, Sieth J, Daum RS. 2015. High Staphylococcus aureus Colonization Prevalence among Patients with Skin and Soft Tissue Infections and Controls in an Urban Emergency Department. J Clin Microbiol 53:810–815.

19. Lopez MS, Tan IS, Yan D, Kang J, McCreary M, Modrusan Z, Austin CD, Xu M, Brown EJ. 2017. Host-derived fatty acids activate type VII secretion in *Staphylococcus aureus*. 42. Proc Natl Acad Sci USA 114:11223–11228.

20. Thomer L, Schneewind O, Missiakas D. 2016. Pathogenesis of Staphylococcus aureus Bloodstream Infections. Annual Review of Pathology: Mechanisms of Disease 11:343–364.

21. Turner NA, Sharma-Kuinkel BK, Maskarinec SA, Eichenberger EM, Shah PP, Carugati M, Holland TL, Fowler VG. 2019. Methicillin-resistant Staphylococcus aureus: an overview of basic and clinical research. Nat Rev Microbiol 17:203–218.

22. Rivera ES, Weiss A, Migas LG, Freiberg JA, Djambazova KV, Neumann EK, Van de Plas R, Spraggins JM, Skaar EP, Caprioli RM. 2022. Imaging mass spectrometry reveals complex lipid distributions across *Staphylococcus aureus* biofilm layers. Journal of Mass Spectrometry and Advances in the Clinical Lab 26:36–46.

23. Richards MJ, Edwards JR, Culver DH, Gaynes RP. 1999. Nosocomial infections in medical intensive care units in the United States. Critical Care Medicine 27:887.

24. Hogan S, Stevens NT, Humphreys H, O'Gara JP, O'Neill E. 2014. Current and Future Approaches to the Prevention and Treatment of Staphylococcal Medical Device-Related Infections. CPD 21:100–113.

25. Balasubramanian D, Harper L, Shopsin B, Torres VJ. 2017. Staphylococcus aureus pathogenesis in diverse host environments. Pathog Dis 75:ftx005.

26. Pietrocola G, Campoccia D, Motta C, Montanaro L, Arciola CR, Speziale P. 2022. Colonization and Infection of Indwelling Medical Devices by Staphylococcus aureus with an Emphasis on Orthopedic Implants. Int J Mol Sci 23:5958.

27. Kourtis AP, Hatfield K, Baggs J, Mu Y, See I, Epson E, Nadle J, Kainer MA, Dumyati G, Petit S, Ray SM, Emerging Infections Program MRSA author group, Ham D, Capers C, Ewing H, Coffin N, McDonald LC, Jernigan J, Cardo D. 2019. *Vital Signs:* Epidemiology and Recent Trends in Methicillin-Resistant and in Methicillin-Susceptible *Staphylococcus aureus* Bloodstream Infections — United States. 9. MMWR Morb Mortal Wkly Rep 68:214–219.

28. Suaya JA, Mera RM, Cassidy A, O'Hara P, Amrine-Madsen H, Burstin S, Miller LG. 2014. Incidence and cost of hospitalizations associated with Staphylococcus aureus skin and soft tissue infections in the United States from 2001 through 2009. BMC Infect Dis 14:296.

29. Klevens RM, Morrison MA, Nadle J, Petit S, Gershman K, Ray S, Harrison LH, Lynfield R, Dumyati G, Townes JM, Craig AS, Zell ER, Fosheim GE, McDougal LK, Carey RB, Fridkin SK, Active Bacterial Core surveillance (ABCs) MRSA Investigators for the. 2007. Invasive Methicillin-Resistant Staphylococcus aureus Infections in the United States. JAMA 298:1763–1771.

30. Diekema DJ, Richter SS, Heilmann KP, Dohrn CL, Riahi F, Tendolkar S, McDanel JS, Doern GV. 2014. Continued Emergence of USA300 Methicillin-Resistant *Staphylococcus*

aureus in the United States: Results from a Nationwide Surveillance Study. Infect Control Hosp Epidemiol 35:285–292.

31. Cheung GYC, Bae JS, Otto M. 2021. Pathogenicity and virulence of *Staphylococcus aureus*. Virulence 12:547–569.

32. Slavetinsky CJ, Hauser JN, Gekeler C, Slavetinsky J, Geyer A, Kraus A, Heilingbrunner D, Wagner S, Tesar M, Krismer B, Kuhn S, Ernst CM, Peschel A. 2022. Sensitizing Staphylococcus aureus to antibacterial agents by decoding and blocking the lipid flippase MprF. eLife. eLife Sciences Publications Limited. https://elifesciences.org/articles/66376. Retrieved 2 June 2024.

33. World Health Organization. 2024. WHO bacterial priority pathogens list, 2024: Bacterial pathogens of public health importance to guide research, development and strategies to prevent and control antimicrobial resistance. World Health Organization, Geneva.

34. Subramanian C, Frank MW, Batte JL, Whaley SG, Rock CO. 2019. Oleate hydratase from Staphylococcus aureus protects against palmitoleic acid, the major antimicrobial fatty acid produced by mammalian skin. J Biol Chem 294:9285–9294.

35. Peschel A, Jack RW, Otto M, Collins LV, Staubitz P, Nicholson G, Kalbacher H, Nieuwenhuizen WF, Jung G, Tarkowski A, Van Kessel KPM, Van Strijp JAG. 2001. *Staphylococcus aureus* Resistance to Human Defensins and Evasion of Neutrophil Killing via the Novel Virulence Factor Mprf Is Based on Modification of Membrane Lipids with L -Lysine. The Journal of Experimental Medicine 193:1067–1076.

36. Ernst CM, Kuhn S, Slavetinsky CJ, Krismer B, Heilbronner S, Gekeler C, Kraus D, Wagner S, Peschel A. 2015. The Lipid-Modifying Multiple Peptide Resistance Factor Is an Oligomer Consisting of Distinct Interacting Synthase and Flippase Subunits. mBio 6:e02340-14.

37. Al-Mebairik NF, El-Kersh TA, Al-Sheikh YA, Marie MAM. 2016. A review of virulence factors, pathogenesis, and antibiotic resistance in Staphylococcus aureus. Reviews and Research in Medical Microbiology 27:50.

38. DeMars ZR, Krute CN, Ridder MJ, Gilchrist AK, Menjivar C, Bose JL. 2021. Fatty acids can inhibit Staphylococcus aureus SaeS activity at the membrane independent of alterations in respiration. Mol Microbiol 116:1378–1391.

39. Radka CD, Batte JL, Frank MW, Rosch JW, Rock CO. 2021. Oleate Hydratase (OhyA) Is a Virulence Determinant in Staphylococcus aureus. Microbiology Spectrum 9:e01546-21.

40. Marrakchi H, Zhang Y-M, Rock CO. 2002. Mechanistic diversity and regulation of Type II fatty acid synthesis. Biochemical Society Transactions 30:1050–1055.

41. White SW, Zheng J, Zhang Y-M, Rock CO. 2005. The structural biology of type II fatty acid biosynthesis. Annu Rev Biochem 74:791–831.

42. Sen S, Sirobhushanam S, Johnson SR, Song Y, Tefft R, Gatto C, Wilkinson BJ. 2016. Growth-Environment Dependent Modulation of Staphylococcus aureus Branched-Chain to Straight-Chain Fatty Acid Ratio and Incorporation of Unsaturated Fatty Acids. 10. PLoS ONE 11:e0165300.

43. Kuhn S, Slavetinsky CJ, Peschel A. 2015. Synthesis and function of phospholipids in Staphylococcus aureus. International Journal of Medical Microbiology 305:196–202.

44. Ratledge C, Wilkinson SG (ed). 1988. Microbial Lipids. Academic Press, London, United Kingdom.

45. Jiang J-H, Bhuiyan MS, Shen H-H, Cameron DR, Rupasinghe TWT, Wu C-M, Le Brun AP, Kostoulias X, Domene C, Fulcher AJ, McConville MJ, Howden BP, Lieschke GJ, Peleg AY. 2019. Antibiotic resistance and host immune evasion in *Staphylococcus aureus* mediated by a metabolic adaptation. 9. Proc Natl Acad Sci USA 116:3722–3727.

46. Hines KM, Alvarado G, Chen X, Gatto C, Pokorny A, Alonzo F, Wilkinson BJ, Xu L. 2020. Lipidomic and Ultrastructural Characterization of the Cell Envelope of *Staphylococcus aureus* Grown in the Presence of Human Serum. 3. mSphere 5:e00339-20, /msphere/5/3/mSphere339-20.atom.

47. Joyce GH, Hammond RK, White DC. 1970. Changes in Membrane Lipid Composition in Exponentially Growing Staphylococcus aureus During the Shift from 37 to 25 C. Journal of Bacteriology 104:323–330.

48. Singh VK, Hattangady DS, Giotis ES, Singh AK, Chamberlain NR, Stuart MK, Wilkinson BJ. 2008. Insertional Inactivation of Branched-Chain α-Keto Acid Dehydrogenase in Staphylococcus aureus Leads to Decreased Branched-Chain Membrane Fatty Acid Content and Increased Susceptibility to Certain Stresses. Appl Environ Microbiol 74:5882–5890.

49. Zhang Y-M, Rock CO. 2008. Membrane lipid homeostasis in bacteria. Nat Rev Microbiol 6:222–233.

50. Tsai M, Ohniwa RL, Kato Y, Takeshita SL, Ohta T, Saito S, Hayashi H, Morikawa K. 2011. Staphylococcus aureus requires cardiolipin for survival under conditions of high salinity. BMC Microbiol 11:13.

51. Albanesi D, Reh G, Guerin ME, Schaeffer F, Debarbouille M, Buschiazzo A, Schujman GE, Mendoza D de, Alzari PM. 2013. Structural Basis for Feed-Forward Transcriptional Regulation of Membrane Lipid Homeostasis in Staphylococcus aureus. PLOS Pathogens 9:e1003108.

52. Perez-Lopez MI, Mendez-Reina R, Trier S, Herrfurth C, Feussner I, Bernal A, Forero-Shelton M, Leidy C. 2019. Variations in carotenoid content and acyl chain composition in exponential, stationary and biofilm states of *Staphylococcus aureus*, and their influence on membrane biophysical properties. Biochimica et Biophysica Acta (BBA) - Biomembranes 1861:978–987.

53. Zamudio-Chávez L, Suesca E, López G-D, Carazzone C, Manrique-Moreno M, Leidy C. 2023. Staphylococcus aureus Modulates Carotenoid and Phospholipid Content in Response to Oxygen-Restricted Growth Conditions, Triggering Changes in Membrane Biophysical Properties. Int J Mol Sci 24:14906.

54. Kraus D, Herbert S, Kristian SA, Khosravi A, Nizet V, Götz F, Peschel A. 2008. The GraRS regulatory system controls Staphylococcus aureus susceptibility to antimicrobial host defenses. BMC Microbiol 8:85.

55. Peleg AY, Miyakis S, Ward DV, Earl AM, Rubio A, Cameron DR, Pillai S, Moellering RC, Eliopoulos GM. 2012. Whole Genome Characterization of the Mechanisms of Daptomycin

Resistance in Clinical and Laboratory Derived Isolates of Staphylococcus aureus. PLoS ONE 7:e28316.

56. Parsons JB, Frank MW, Jackson P, Subramanian C, Rock CO. 2014. Incorporation of extracellular fatty acids by a fatty acid kinase-dependent pathway in *S taphylococcus aureus*: Fatty acid metabolism in *S. aureus*. 2. Molecular Microbiology 92:234–245.

57. Parsons JB, Rock CO. 2013. Bacterial Lipids: Metabolism and Membrane Homeostasis. Prog Lipid Res 52:249–276.

58. Kaiser JC, Sen S, Sinha A, Wilkinson BJ, Heinrichs DE. 2016. The role of two branched-chain amino acid transporters in Staphylococcus aureus growth, membrane fatty acid composition and virulence. Molecular Microbiology 102:850–864.

59. DeMars Z, Singh VK, Bose JL. 2020. Exogenous Fatty Acids Remodel Staphylococcus aureus Lipid Composition through Fatty Acid Kinase. 14. J Bacteriol 202.

60. Parsons JB, Broussard TC, Bose JL, Rosch JW, Jackson P, Subramanian C, Rock CO. 2014. Identification of a two-component fatty acid kinase responsible for host fatty acid incorporation by Staphylococcus aureus. 29. Proceedings of the National Academy of Sciences 111:10532–10537.

61. Morvan C, Halpern D, Kénanian G, Hays C, Anba-Mondoloni J, Brinster S, Kennedy S, Trieu-Cuot P, Poyart C, Lamberet G, Gloux K, Gruss A. 2016. Environmental fatty acids enable emergence of infectious Staphylococcus aureus resistant to FASII-targeted antimicrobials. 1. Nat Commun 7:12944.

62. Gloux K, Guillemet M, Soler C, Morvan C, Halpern D, Pourcel C, Vu Thien H, Lamberet G, Gruss A. 2017. Clinical Relevance of Type II Fatty Acid Synthesis Bypass in Staphylococcus aureus. 5. Antimicrob Agents Chemother 61:e02515-16, e02515-16.

63. Delekta PC, Shook JC, Lydic TA, Mulks MH, Hammer ND. 2018. *Staphylococcus aureus* Utilizes Host-Derived Lipoprotein Particles as Sources of Fatty Acids. 11. J Bacteriol 200:e00728-17, /jb/200/11/e00728-17.atom.

64. Chen X, Alonzo F. 2019. Bacterial lipolysis of immune-activating ligands promotes evasion of innate defenses. 9. Proc Natl Acad Sci USA 116:3764–3773.

65. Kénanian G, Morvan C, Weckel A, Pathania A, Anba-Mondoloni J, Halpern D, Solgadi A, Dupont L, Henry C, Poyart C, Fouet A, Lamberet G, Gloux K, Gruss A. 2019. Permissive Fatty Acid Incorporation in Host Environments Promotes Staphylococcal Adaptation to FASII Antibiotics. Cell Rep 29:3974-3982.e4.

66. Frank MW, Whaley SG, Rock CO. 2021. Branched-chain amino acid metabolism controls membrane phospholipid structure in Staphylococcus aureus. Journal of Biological Chemistry 297:101255.

67. Lu Y-J, Zhang Y-M, Grimes KD, Qi J, Lee RE, Rock CO. 2006. Acyl-Phosphates Initiate Membrane Phospholipid Synthesis in Gram-Positive Pathogens. Molecular Cell 23:765–772.

68. Oku Y, Kurokawa K, Ichihashi N, Sekimizu K. 2004. Characterization of the Staphylococcus aureus mprF gene, involved in lysinylation of phosphatidylglycerol. Microbiology 150:45–51.

69. Koprivnjak T, Zhang D, Ernst CM, Peschel A, Nauseef WM, Weiss JP. 2011. Characterization of Staphylococcus aureus Cardiolipin Synthases 1 and 2 and Their Contribution to Accumulation of Cardiolipin in Stationary Phase and within Phagocytes. 16. J Bacteriol 193:4134–4142.

70. Rollof J, Hedström SA, Nilsson-Ehle P. 1987. Purification and characterization of a lipase from Staphylococcus aureus. 2. Biochimica et Biophysica Acta (BBA) - Lipids and Lipid Metabolism 921:364–369.

71. Simons J-WFA, Adams H, Cox RC, Dekker N, Gotz F, Slotboom AJ, Verheij HM. 1996. The Lipase from Staphylococcus aureus. Expression in Escherichia coli, Large-scale Purification and Comparison of Substrate Specificity to Staphylococcus hyicus Lipase. 3. Eur J Biochem 242:760–769.

72. Cadieux B, Vijayakumaran V, Bernards MA, McGavin MJ, Heinrichs DE. 2014. Role of Lipase from Community-Associated Methicillin-Resistant Staphylococcus aureus Strain USA300 in Hydrolyzing Triglycerides into Growth-Inhibitory Free Fatty Acids. 23. J Bacteriol 196:4044–4056.

73. Kumar NG, Contaifer D, Wijesinghe DS, Jefferson KK. 2021. Staphylococcus aureus Lipase 3 (SAL3) is a surface-associated lipase that hydrolyzes short chain fatty acids. 10. PLoS ONE 16:e0258106.

74. Parsons JB, Frank MW, Jackson P, Subramanian C, Rock CO. 2014. Incorporation of extracellular fatty acids by a fatty acid kinase-dependent pathway in *S taphylococcus aureus*: Fatty acid metabolism in *S. aureus*. 2. Molecular Microbiology 92:234–245.

75. Zhao W, Róg T, Gurtovenko AA, Vattulainen I, Karttunen M. 2008. Role of phosphatidylglycerols in the stability of bacterial membranes. Biochimie 90:930–938.

76. Nikolic P, Mudgil P. 2023. The Cell Wall, Cell Membrane and Virulence Factors of Staphylococcus aureus and Their Role in Antibiotic Resistance. 2. Microorganisms 11:259.

77. Peschel A, Sahl H-G. 2006. The co-evolution of host cationic antimicrobial peptides and microbial resistance. Nat Rev Microbiol 4:529–536.

78. Ernst CM, Staubitz P, Mishra NN, Yang S-J, Hornig G, Kalbacher H, Bayer AS, Kraus D, Peschel A. 2009. The Bacterial Defensin Resistance Protein MprF Consists of Separable Domains for Lipid Lysinylation and Antimicrobial Peptide Repulsion. PLoS Pathog 5:e1000660.

79. Perry WJ, Grunenwald CM, Van De Plas R, Witten JC, Martin DR, Apte SS, Cassat JE, Pettersson GB, Caprioli RM, Skaar EP, Spraggins JM. 2022. Visualizing Staphylococcus aureus pathogenic membrane modification within the host infection environment by multimodal imaging mass spectrometry. Cell Chemical Biology 29:1209-1217.e4.

80. Foster TJ. 2017. Antibiotic resistance in Staphylococcus aureus. Current status and future prospects. FEMS Microbiology Reviews 41:430–449.

81. Boudjemaa R, Cabriel C, Dubois-Brissonnet F, Bourg N, Dupuis G, Gruss A, Lévêque-Fort S, Briandet R, Fontaine-Aupart M-P, Steenkeste K. 2018. Impact of Bacterial Membrane Fatty Acid Composition on the Failure of Daptomycin To Kill *Staphylococcus aureus*. 7. Antimicrob Agents Chemother 62:e00023-18, /aac/62/7/e00023-18.atom.

82. Miller WR, Bayer AS, Arias CA. 2016. Mechanism of Action and Resistance to Daptomycin in *Staphylococcus aureus* and Enterococci. Cold Spring Harb Perspect Med 6:a026997.

83. Müller A, Wenzel M, Strahl H, Grein F, Saaki TNV, Kohl B, Siersma T, Bandow JE, Sahl H-G, Schneider T, Hamoen LW. 2016. Daptomycin inhibits cell envelope synthesis by interfering with fluid membrane microdomains. 45. Proc Natl Acad Sci USA 113:E7077–E7086.

84. Nguyen AH, Hood KS, Mileykovskaya E, Miller WR, Tran TT. 2022. Bacterial cell membranes and their role in daptomycin resistance: A review. Front Mol Biosci 9.

85. Hines KM, Waalkes A, Penewit K, Holmes EA, Salipante SJ, Werth BJ, Xu L. 2017. Characterization of the Mechanisms of Daptomycin Resistance among Gram-Positive Bacterial Pathogens by Multidimensional Lipidomics. 6. mSphere 2:mSphere.00492-17, e00492-17.

86. Beriashvili D, Taylor R, Kralt B, Abu Mazen N, Taylor SD, Palmer M. 2018. Mechanistic studies on the effect of membrane lipid acyl chain composition on daptomycin pore formation. Chemistry and Physics of Lipids 216:73–79.

87. Kengmo Tchoupa A, Peschel A. 2020. Staphylococcus aureus Releases Proinflammatory Membrane Vesicles To Resist Antimicrobial Fatty Acids. 5. mSphere 5:e00804-20.

88. Pader V, Hakim S, Painter KL, Wigneshweraraj S, Clarke TB, Edwards AM. 2016. Staphylococcus aureus inactivates daptomycin by releasing membrane phospholipids. Nat Microbiol 2:16194.

89. Shen T, Hines KM, Ashford NK, Werth BJ, Xu L. 2021. Varied Contribution of Phospholipid Shedding From Membrane to Daptomycin Tolerance in Staphylococcus aureus. Front Mol Biosci 8.

90. Hernández-Villa L, Manrique-Moreno M, Leidy C, Jemioła-Rzemińska M, Ortíz C, Strzałka K. 2018. Biophysical evaluation of cardiolipin content as a regulator of the membrane lytic effect of antimicrobial peptides. Biophysical Chemistry 238:8–15.

91. Campbell JW, Jr JEC. 2001. Bacterial Fatty Acid Biosynthesis: Targets for Antibacterial Drug Discovery. Annual Review of Microbiology 55:305–332.

92. Zhang Y-M, White SW, Rock CO. 2006. Inhibiting Bacterial Fatty Acid Synthesis *. Journal of Biological Chemistry 281:17541–17544.

93. Parsons JB, Rock CO. 2011. Is bacterial fatty acid synthesis a valid target for antibacterial drug discovery? Current Opinion in Microbiology 14:544–549.

94. Hafkin B, Kaplan N, Murphy B. 2016. Efficacy and Safety of AFN-1252, the First Staphylococcus-Specific Antibacterial Agent, in the Treatment of Acute Bacterial Skin and Skin Structure Infections, Including Those in Patients with Significant Comorbidities. Antimicrob Agents Chemother 60:1695–1701.

95. Brinster S, Lamberet G, Staels B, Trieu-Cuot P, Gruss A, Poyart C. 2009. Type II fatty acid synthesis is not a suitable antibiotic target for Gram-positive pathogens. Nature 458:83–86.

96. Balemans W, Lounis N, Gilissen R, Guillemont J, Simmen K, Andries K, Koul A. 2010. Essentiality of FASII pathway for Staphylococcus aureus. Nature 463:E3–E3.

97. Parsons JB, Frank MW, Subramanian C, Saenkham P, Rock CO. 2011. Metabolic basis for the differential susceptibility of Gram-positive pathogens to fatty acid synthesis inhibitors. 37. Proc Natl Acad Sci USA 108:15378–15383.

98. Morvan C, Halpern D, Kénanian G, Hays C, Anba-Mondoloni J, Brinster S, Kennedy S, Trieu-Cuot P, Poyart C, Lamberet G, Gloux K, Gruss A. 2016. Environmental fatty acids enable emergence of infectious Staphylococcus aureus resistant to FASII-targeted antimicrobials. Nat Commun 7:12944.

99. Gloux K, Guillemet M, Soler C, Morvan C, Halpern D, Pourcel C, Vu Thien H, Lamberet G, Gruss A. 2017. Clinical Relevance of Type II Fatty Acid Synthesis Bypass in Staphylococcus aureus. Antimicrob Agents Chemother 61:e02515-16, e02515-16.

100. Kénanian G, Morvan C, Weckel A, Pathania A, Anba-Mondoloni J, Halpern D, Solgadi A, Dupont L, Henry C, Poyart C, Fouet A, Lamberet G, Gloux K, Gruss A. 2019. Permissive Fatty Acid Incorporation in Host Environments Promotes Staphylococcal Adaptation to FASII Antibiotics https://doi.org/10.1101/635698.

101. Pee CJE, Pader V, Ledger EVK, Edwards AM. 2019. A FASII Inhibitor Prevents Staphylococcal Evasion of Daptomycin by Inhibiting Phospholipid Decoy Production. Antimicrob Agents Chemother 63:e02105-18, /aac/63/4/AAC.02105-18.atom.

102. Frank MW, Yao J, Batte JL, Gullett JM, Subramanian C, Rosch JW, Rock CO. 2020. Host Fatty Acid Utilization by Staphylococcus aureus at the Infection Site. 3. mBio 11:e00920-20.

103. Fahy E, Subramaniam S, Brown HA, Glass CK, Merrill AH, Murphy RC, Raetz CRH, Russell DW, Seyama Y, Shaw W, Shimizu T, Spener F, van Meer G, VanNieuwenhze MS, White SH, Witztum JL, Dennis EA. 2005. A comprehensive classification system for lipids. J Lipid Res 46:839–861.

104. Cífková E, Holčapek M, Lísa M, Ovčačíková M, Lyčka A, Lynen F, Sandra P. 2012. Nontargeted quantitation of lipid classes using hydrophilic interaction liquid chromatography-electrospray ionization mass spectrometry with single internal standard and response factor approach. Anal Chem 84:10064–10070.

105. Li A, Hines KM, Xu L. 2020. Lipidomics by HILIC-Ion Mobility-Mass Spectrometry, p. 119–132. *In* Paglia, G, Astarita, G (eds.), Ion Mobility-Mass Spectrometry. Humana, New York, NY.

106. Appala K, Bimpeh K, Freeman C, Hines KM. 2020. Recent applications of mass spectrometry in bacterial lipidomics. Anal Bioanal Chem 412:5935–5943.

107. Hines KM, Herron J, Xu L. 2017. Assessment of altered lipid homeostasis by HILIC-ion mobility-mass spectrometry-based lipidomics. 4. Journal of Lipid Research 58:809–819.

108. Baker PRS, Armando AM, Campbell JL, Quehenberger O, Dennis EA. 2014. Three-dimensional enhanced lipidomics analysis combining UPLC, differential ion mobility spectrometry, and mass spectrometric separation strategies1[S]. Journal of Lipid Research 55:2432–2442.

109. Hines KM, May JC, McLean JA, Xu L. 2016. Evaluation of Collision Cross Section Calibrants for Structural Analysis of Lipids by Traveling Wave Ion Mobility-Mass Spectrometry. Anal Chem 88:7329–7336.

110. Murray CJ, Ikuta KS, Sharara F, Swetschinski L, Robles Aguilar G, Gray A, Han C, Bisignano C, Rao P, Wool E, Johnson SC, Browne AJ, Chipeta MG, Fell F, Hackett S, Haines-Woodhouse G, Kashef Hamadani BH, Kumaran EAP, McManigal B, Agarwal R, Akech S, Albertson S, Amuasi J, Andrews J, Aravkin A, Ashley E, Bailey F, Baker S, Basnyat B, Bekker A, Bender R, Bethou A, Bielicki J, Boonkasidecha S, Bukosia J, Carvalheiro C, Castañeda-Orjuela C, Chansamouth V, Chaurasia S, Chiurchiù S, Chowdhury F, Cook AJ, Cooper B, Cressey TR, Criollo-Mora E, Cunningham M, Darboe S, Day NPJ, De Luca M, Dokova K, Dramowski A, Dunachie SJ, Eckmanns T, Eibach D, Emami A, Feasey N, Fisher-Pearson N, Forrest K, Garrett D, Gastmeier P, Giref AZ, Greer RC, Gupta V, Haller S, Haselbeck A, Hay SI, Holm M, Hopkins S, Iregbu KC, Jacobs J, Jarovsky D, Javanmardi F, Khorana M, Kissoon N, Kobeissi E, Kostyanev T, Krapp F, Krumkamp R, Kumar A, Kyu HH, Lim C, Limmathurotsakul D, Loftus MJ, Lunn M, Ma J, Mturi N, Munera-Huertas T, Musicha P, Mussi-Pinhata MM, Nakamura T, Nanavati R, Nangia S, Newton P, Ngoun C, Novotney A, Nwakanma D, Obiero CW, Olivas-Martinez A, Olliaro P, Ooko E, Ortiz-Brizuela E, Peleg AY, Perrone C, Plakkal N, Ponce-de-Leon A, Raad M, Ramdin T, Riddell A, Roberts T, Robotham JV, Roca A, Rudd KE, Russell N, Schnall J, Scott JAG, Shivamallappa M, Sifuentes-Osornio J, Steenkeste N, Stewardson AJ, Stoeva T, Tasak N, Thaiprakong A, Thwaites G, Turner C, Turner P, van Doorn HR, Velaphi S, Vongpradith A, Vu H, Walsh T, Waner S, Wangrangsimakul T, Wozniak T, Zheng P, Sartorius B, Lopez AD, Stergachis A, Moore C, Dolecek C, Naghavi M. 2022.

Global burden of bacterial antimicrobial resistance in 2019: a systematic analysis. The Lancet 399:629–655.

111. Kourtis AP, Hatfield K, Baggs J, Mu Y, See I, Epson E, Nadle J, Kainer MA, Dumyati G, Petit S, Ray SM, Emerging Infections Program MRSA author group, Ham D, Capers C, Ewing H, Coffin N, McDonald LC, Jernigan J, Cardo D. 2019. *Vital Signs:* Epidemiology and Recent Trends in Methicillin-Resistant and in Methicillin-Susceptible *Staphylococcus aureus* Bloodstream Infections — United States. MMWR Morb Mortal Wkly Rep 68:214–219.

112. Hines KM, Alvarado G, Chen X, Gatto C, Pokorny A, Alonzo F, Wilkinson BJ, Xu L. 2020. Lipidomic and Ultrastructural Characterization of the Cell Envelope of *Staphylococcus aureus* Grown in the Presence of Human Serum. mSphere 5:e00339-20, /msphere/5/3/mSphere339-20.atom.

113. Delekta PC, Shook JC, Lydic TA, Mulks MH, Hammer ND. 2018. *Staphylococcus aureus* Utilizes Host-Derived Lipoprotein Particles as Sources of Fatty Acids. J Bacteriol 200:e00728-17, /jb/200/11/e00728-17.atom.

114. Chen X, Alonzo F. 2019. Bacterial lipolysis of immune-activating ligands promotes evasion of innate defenses. Proc Natl Acad Sci USA 116:3764–3773.

115. Parsons JB, Frank MW, Jackson P, Subramanian C, Rock CO. 2014. Incorporation of extracellular fatty acids by a fatty acid kinase-dependent pathway in *S taphylococcus aureus*: Fatty acid metabolism in *S. aureus*. Molecular Microbiology 92:234–245.

116. Parsons JB, Broussard TC, Bose JL, Rosch JW, Jackson P, Subramanian C, Rock CO. 2014. Identification of a two-component fatty acid kinase responsible for host fatty acid incorporation by Staphylococcus aureus. Proceedings of the National Academy of Sciences 111:10532–10537.

117. DeMars Z, Singh VK, Bose JL. 2020. Exogenous Fatty Acids Remodel Staphylococcus aureus Lipid Composition through Fatty Acid Kinase. J Bacteriol 202.

118. Garber ED. 1960. The Host As A Growth Medium. Annals of the New York Academy of Sciences 88:1187–1194.

119. Krismer B, Liebeke M, Janek D, Nega M, Rautenberg M, Hornig G, Unger C, Weidenmaier C, Lalk M, Peschel A. 2014. Nutrient Limitation Governs Staphylococcus aureus Metabolism and Niche Adaptation in the Human Nose. PLoS Pathog 10:e1003862.

120. Valentino MD, Foulston L, Sadaka A, Kos VN, Villet RA, Santa Maria J, Lazinski DW, Camilli A, Walker S, Hooper DC, Gilmore MS. 2014. Genes Contributing to Staphylococcus aureus Fitness in Abscess- and Infection-Related Ecologies. mBio 5.

121. Sen S, Sirobhushanam S, Johnson SR, Song Y, Tefft R, Gatto C, Wilkinson BJ. 2016. Growth-Environment Dependent Modulation of Staphylococcus aureus Branched-Chain to Straight-Chain Fatty Acid Ratio and Incorporation of Unsaturated Fatty Acids. PLoS ONE 11:e0165300.

122. Altenbern RA. 1977. Cerulenin-Inhibited Cells of *Staphylococcus aureus* Resume Growth When Supplemented with Either a Saturated or an Unsaturated Fatty Acid. Antimicrob Agents Chemother 11:574–576.

123. van der Vusse GJ. 2009. Albumin as Fatty Acid Transporter. Drug Metabolism and Pharmacokinetics 24:300–307.

124. Rollof J, Hedström SA, Nilsson-Ehle P. 1987. Purification and characterization of a lipase from Staphylococcus aureus. Biochimica et Biophysica Acta (BBA) - Lipids and Lipid Metabolism 921:364–369.

125. Cadieux B, Vijayakumaran V, Bernards MA, McGavin MJ, Heinrichs DE. 2014. Role of Lipase from Community-Associated Methicillin-Resistant Staphylococcus aureus Strain USA300 in Hydrolyzing Triglycerides into Growth-Inhibitory Free Fatty Acids. J Bacteriol 196:4044–4056.

126. Simons J-WFA, Adams H, Cox RC, Dekker N, Gotz F, Slotboom AJ, Verheij HM. 1996. The Lipase from Staphylococcus aureus. Expression in Escherichia coli, Large-scale Purification and Comparison of Substrate Specificity to Staphylococcus hyicus Lipase. Eur J Biochem 242:760–769.

127. Kumar NG, Contaifer D, Wijesinghe DS, Jefferson KK. 2021. Staphylococcus aureus Lipase 3 (SAL3) is a surface-associated lipase that hydrolyzes short chain fatty acids. PLoS ONE 16:e0258106.

128. Boudjemaa R, Cabriel C, Dubois-Brissonnet F, Bourg N, Dupuis G, Gruss A, Lévêque-Fort S, Briandet R, Fontaine-Aupart M-P, Steenkeste K. 2018. Impact of Bacterial Membrane Fatty Acid Composition on the Failure of Daptomycin To Kill *Staphylococcus aureus*. Antimicrob Agents Chemother 62:e00023-18, /aac/62/7/e00023-18.atom.

129. Nishi H, Komatsuzawa H, Fujiwara T, McCallum N, Sugai M. 2004. Reduced Content of Lysyl-Phosphatidylglycerol in the Cytoplasmic Membrane Affects Susceptibility to Moenomycin, as Well as Vancomycin, Gentamicin, and Antimicrobial Peptides, in *Staphylococcus aureus*. Antimicrob Agents Chemother 48:4800–4807.

130. Lopez MS, Tan IS, Yan D, Kang J, McCreary M, Modrusan Z, Austin CD, Xu M, Brown EJ. 2017. Host-derived fatty acids activate type VII secretion in *Staphylococcus aureus*. Proc Natl Acad Sci USA 114:11223–11228.

131. Mishra NN, Rubio A, Nast CC, Bayer AS. 2012. Differential Adaptations of Methicillin-Resistant *Staphylococcus aureus* to Serial *In Vitro* Passage in Daptomycin: Evolution of Daptomycin Resistance and Role of Membrane Carotenoid Content and Fluidity. International Journal of Microbiology 2012:1–6.

132. Krute CN, Ridder MJ, Seawell NA, Bose JL. 2019. Inactivation of the exogenous fatty acid utilization pathway leads to increased resistance to unsaturated fatty acids in Staphylococcus aureus. Microbiology 165:197–207.

133. Chamberlain NR, Mehrtens BG, Xiong Z, Kapral FA, Boardman JL, Rearick JI. 1991. Correlation of carotenoid production, decreased membrane fluidity, and resistance to oleic acid killing in Staphylococcus aureus 18Z. Infect Immun 59:4332–4337.

134. Greenway DLA, Dyke KGH. 1979. Mechanism of the Inhibitory Action of Linoleic Acid on the Growth of Staphylococcus aureus. Journal of General Microbiology 115:233–245.

135. Knapp HR, Melly MA. 1986. Bactericidal Effects of Polyunsaturated Fatty Acids. Journal of Infectious Diseases 154:84–94.

136. Beavers WN, Monteith AJ, Amarnath V, Mernaugh RL, Roberts LJ, Chazin WJ, Davies SS, Skaar EP. 2019. Arachidonic Acid Kills Staphylococcus aureus through a Lipid Peroxidation Mechanism. mBio 10.

137. Li A, Hines KM, Xu L. 2020. Lipidomics by HILIC-Ion Mobility-Mass Spectrometry, p. 119–132. *In* Paglia, G, Astarita, G (eds.), Ion Mobility-Mass Spectrometry. Humana, New York, NY.

138. Hines KM, Herron J, Xu L. 2017. Assessment of altered lipid homeostasis by HILIC-ion mobility-mass spectrometry-based lipidomics. Journal of Lipid Research 58:809–819.

139. Hines KM, Waalkes A, Penewit K, Holmes EA, Salipante SJ, Werth BJ, Xu L. 2017. Characterization of the Mechanisms of Daptomycin Resistance among Gram-Positive Bacterial Pathogens by Multidimensional Lipidomics. mSphere 2:mSphere.00492-17, e00492-17.

140. Ratledge C, Wilkinson SG (ed). 1988. Microbial Lipids. Academic Press, London, United Kingdom.

141. Kuhn S, Slavetinsky CJ, Peschel A. 2015. Synthesis and function of phospholipids in Staphylococcus aureus. International Journal of Medical Microbiology 305:196–202.

142. Brenna JT, Plourde M, Stark KD, Jones PJ, Lin Y-H. 2018. Best practices for the design, laboratory analysis, and reporting of trials involving fatty acids. The American Journal of Clinical Nutrition 108:211–227.

143. Buchanan CDC, Lust CAC, Burns JL, Hillyer LM, Martin SA, Wittert GA, Ma DWL. 2021. Analysis of major fatty acids from matched plasma and serum samples reveals highly comparable absolute and relative levels. Prostaglandins, Leukotrienes and Essential Fatty Acids 168:102268.

144. Peters, Jr T. 1995. All About Albumin: Biochemistry, genetics, and Medical Applications. Academic Press, San Diego, CA. https://doi.org/10.1016/B978-0-12-552110-9.X5000-4.

145. Weaving G, Batstone GF, Jones RG. 2016. Age and sex variation in serum albumin concentration: an observational study. Ann Clin Biochem 53:106–111.

146. Cojutti PG, Candoni A, Ramos-Martin V, Lazzarotto D, Zannier ME, Fanin R, Hope W, Pea F. 2017. Population pharmacokinetics and dosing considerations for the use of daptomycin in adult patients with haematological malignancies. Journal of Antimicrobial Chemotherapy 72:2342–2350.

147. Saifer A, Goldman L. 1961. The free fatty acids bound to human serum albumin. Journal of Lipid Research 2:268–270.

148. Petitpas I, Grüne T, Bhattacharya AA, Curry S. 2001. Crystal structures of human serum albumin complexed with monounsaturated and polyunsaturated fatty acids. Journal of Molecular Biology 314:955–960.

149. Koprivnjak T, Zhang D, Ernst CM, Peschel A, Nauseef WM, Weiss JP. 2011. Characterization of Staphylococcus aureus Cardiolipin Synthases 1 and 2 and Their Contribution to Accumulation of Cardiolipin in Stationary Phase and within Phagocytes. J Bacteriol 193:4134–4142.

150. Parsons JB, Kukula M, Jackson P, Pulse M, Simecka JW, Valtierra D, Weiss WJ, Kaplan N, Rock CO. 2013. Perturbation of Staphylococcus aureus Gene Expression by the Enoyl-Acyl Carrier Protein Reductase Inhibitor AFN-1252. Antimicrob Agents Chemother 57:2182–2190.

151. Parsons JB, Frank MW, Subramanian C, Saenkham P, Rock CO. 2011. Metabolic basis for the differential susceptibility of Gram-positive pathogens to fatty acid synthesis inhibitors. Proc Natl Acad Sci USA 108:15378–15383.

152. Abuaita BH, Schultz TL, O'Riordan MX. 2018. Mitochondria-Derived Vesicles Deliver Antimicrobial Reactive Oxygen Species to Control Phagosome-Localized Staphylococcus aureus. Cell Host & Microbe 24:625-636.e5.

153. Dwyer DJ, Belenky PA, Yang JH, MacDonald IC, Martell JD, Takahashi N, Chan CTY, Lobritz MA, Braff D, Schwarz EG, Ye JD, Pati M, Vercruysse M, Ralifo PS, Allison KR, Khalil AS, Ting AY, Walker GC, Collins JJ. 2014. Antibiotics induce redox-related physiological alterations as part of their lethality. Proc Natl Acad Sci USA 111.

154. Teoh WP, Chen X, Laczkovich I, Alonzo F. 2021. *Staphylococcus aureus* adapts to the host nutritional landscape to overcome tissue-specific branched-chain fatty acid requirement. Proc Natl Acad Sci USA 118:e2022720118.

155. Campbell MP, Mott MD, Owen JR, Reznicek JE, Beck CA, Muthukrishnan G, Golladay GJ, Kates SL. 2022. Low albumin level is more strongly associated with adverse outcomes and *Staphylococcus aureus* infection than hemoglobin A1C or smoking tobacco. Journal Orthopaedic Research jor.25282.

156. DeMars Z, Bose JL. 2018. Redirection of Metabolism in Response to Fatty Acid Kinase in Staphylococcus aureus. J Bacteriol 200.

157. Parsons JB, Yao J, Jackson P, Frank M, Rock CO. 2013. Phosphatidylglycerol homeostasis in glycerol-phosphate auxotrophs of Staphylococcus aureus. BMC Microbiol 13:260.

158. Frank MW, Yao J, Batte JL, Gullett JM, Subramanian C, Rosch JW, Rock CO. 2020. Host Fatty Acid Utilization by Staphylococcus aureus at the Infection Site. mBio 11:e00920-20.

159. Pathania A, Anba-Mondoloni J, Gominet M, Halpern D, Dairou J, Dupont L, Lamberet G, Trieu-Cuot P, Gloux K, Gruss A. 2021. (p)ppGpp/GTP and Malonyl-CoA Modulate Staphylococcus aureus Adaptation to FASII Antibiotics and Provide a Basis for Synergistic Bi-Therapy. mBio 12:e03193-20.

160. Müller A, Wenzel M, Strahl H, Grein F, Saaki TNV, Kohl B, Siersma T, Bandow JE, Sahl H-G, Schneider T, Hamoen LW. 2016. Daptomycin inhibits cell envelope synthesis by interfering with fluid membrane microdomains. Proc Natl Acad Sci USA 113:E7077–E7086.

161. Monk IR, Shah IM, Xu M, Tan M-W, Foster TJ. 2012. Transforming the Untransformable: Application of Direct Transformation To Manipulate Genetically Staphylococcus aureus and Staphylococcus epidermidis. mBio 3:e00277-11.

162. Grayczyk JP, Harvey CJ, Laczkovich I, Alonzo F. 2017. A Lipoylated Metabolic Protein Released by Staphylococcus aureus Suppresses Macrophage Activation. Cell Host Microbe 22:678-687.e9.

163. Bligh EG, Dyer WJ. 1959. A rapid method of total lipid extraction and purification. 8. Can J Biochem Physiol 37:911–917.

164. Ross DH, Cho JH, Zhang R, Hines KM, Xu L. 2020. LiPydomics: A Python Package for Comprehensive Prediction of Lipid Collision Cross Sections and Retention Times and Analysis of Ion Mobility-Mass Spectrometry-Based Lipidomics Data. Anal Chem 92:14967–14975.

165. Metsalu T, Vilo J. 2015. ClustVis: a web tool for visualizing clustering of multivariate data using Principal Component Analysis and heatmap. Nucleic Acids Res 43:W566–W570.

166. Adams KJ, Pratt B, Bose N, Dubois LG, St. John-Williams L, Perrott KM, Ky K, Kapahi P, Sharma V, MacCoss MJ, Moseley MA, Colton CA, MacLean BX, Schilling B, Thompson JW, Alzheimer's Disease Metabolomics Consortium. 2020. Skyline for Small Molecules: A Unifying Software Package for Quantitative Metabolomics. J Proteome Res 19:1447–1458.

167. Peng B, Kopczynski D, Pratt BS, Ejsing CS, Burla B, Hermansson M, Benke PI, Tan SH, Chan MY, Torta F, Schwudke D, Meckelmann SW, Coman C, Schmitz OJ, MacLean B, Manke M-C, Borst O, Wenk MR, Hoffmann N, Ahrends R. 2020. LipidCreator workbench to probe the lipidomic landscape. Nat Commun 11:2057.

168. DeMars Z, Singh VK, Bose JL. 2020. Exogenous Fatty Acids Remodel Staphylococcus aureus Lipid Composition through Fatty Acid Kinase. 14. J Bacteriol 202.

169. Porta Siegel T, Ekroos K, Ellis SR. 2019. Reshaping Lipid Biochemistry by Pushing Barriers in Structural Lipidomics. Angewandte Chemie International Edition 58:6492–6501.

170. Kyle JE, Zhang X, Weitz KK, Monroe ME, Ibrahim YM, Moore RJ, Cha J, Sun X, Lovelace ES, Wagoner J, Polyak SJ, Metz TO, Dey SK, Smith RD, Burnum-Johnson KE, Baker ES. 2016. Uncovering biologically significant lipid isomers with liquid chromatography, ion mobility spectrometry and mass spectrometry. Analyst 141:1649–1659.

171. Delekta PC, Shook JC, Lydic TA, Mulks MH, Hammer ND. 2018. *Staphylococcus aureus* Utilizes Host-Derived Lipoprotein Particles as Sources of Fatty Acids. 11. J Bacteriol 200:e00728-17, /jb/200/11/e00728-17.atom.

172. Nishi H, Komatsuzawa H, Fujiwara T, McCallum N, Sugai M. 2004. Reduced Content of Lysyl-Phosphatidylglycerol in the Cytoplasmic Membrane Affects Susceptibility to Moenomycin, as Well as Vancomycin, Gentamicin, and Antimicrobial Peptides, in *Staphylococcus aureus*. 12. Antimicrob Agents Chemother 48:4800–4807.

173. Mishra NN, Rubio A, Nast CC, Bayer AS. 2012. Differential Adaptations of Methicillin-Resistant *Staphylococcus aureus* to Serial *In Vitro* Passage in Daptomycin: Evolution of Daptomycin Resistance and Role of Membrane Carotenoid Content and Fluidity. International Journal of Microbiology 2012:1–6.

174. Nguyen MT, Hanzelmann D, Härtner T, Peschel A, Götz F. 2015. Skin-Specific Unsaturated Fatty Acids Boost the Staphylococcus aureus Innate Immune Response. Infect Immun 84:205–215.

175. Parsons JB, Yao J, Frank MW, Jackson P, Rock CO. 2012. Membrane Disruption by Antimicrobial Fatty Acids Releases Low-Molecular-Weight Proteins from Staphylococcus aureus. Journal of Bacteriology 194:5294–5304.

176. Rustam YH, Reid GE. 2018. Analytical Challenges and Recent Advances in Mass Spectrometry Based Lipidomics. Anal Chem 90:374–397.

177. Thomas MC, Mitchell TW, Harman DG, Deeley JM, Nealon JR, Blanksby SJ. 2008. Ozone-Induced Dissociation: Elucidation of Double Bond Position within Mass-Selected Lipid Ions. Anal Chem 80:303–311.

178. Poad BLJ, Pham HT, Thomas MC, Nealon JR, Campbell JL, Mitchell TW, Blanksby SJ. 2010. Ozone-induced dissociation on a modified tandem linear ion-trap: Observations of different reactivity for isomeric lipids. J Am Soc Mass Spectrom 21:1989–1999.

179. Harris RA, May JC, Craig A. Stinson, Stinson CA, Yu Xia, Xia Y, McLean JA. 2018. Determining Double Bond Position in Lipids Using Online Ozonolysis Coupled to Liquid Chromatography and Ion Mobility-Mass Spectrometry. Analytical Chemistry 90:1915–1924.

180. Poad BLJ, Zheng X, Mitchell TW, Smith RD, Baker ES, Blanksby SJ. 2018. Online Ozonolysis Combined with Ion Mobility-Mass Spectrometry Provides a New Platform for Lipid Isomer Analyses. Analytical Chemistry 90:1292–1300.

181. Wäldchen F, Becher S, Esch P, Kompauer M, Heiles S. 2017. Selective phosphatidylcholine double bond fragmentation and localisation using Paternò–Büchi reactions and ultraviolet photodissociation. Analyst 142:4744–4755.

182. Klein DR, Feider CL, Garza KY, Lin JQ, Eberlin LS, Brodbelt JS. 2018. Desorption Electrospray Ionization Coupled with Ultraviolet Photodissociation for Characterization of Phospholipid Isomers in Tissue Sections. Anal Chem 90:10100–10104.

183. Campbell JL, Baba T. 2015. Near-Complete Structural Characterization of Phosphatidylcholines Using Electron Impact Excitation of Ions from Organics. Anal Chem 87:5837–5845.

184. Stinson CA, Xia Y. 2016. A method of coupling the Paternò–Büchi reaction with direct infusion ESI-MS/MS for locating the C□C bond in glycerophospholipids. The Analyst 141:3696–3704.

185. Ma X, Zhao X, Li J, Zhang W, Cheng J-X, Ouyang Z, Xia Y. 2016. Photochemical Tagging for Quantitation of Unsaturated Fatty Acids by Mass Spectrometry. Anal Chem 88:8931–8935.

186. Ma X, Xia Y. 2014. Pinpointing Double Bonds in Lipids by Paternò-Büchi Reactions and Mass Spectrometry. Angewandte Chemie 53:2592–2596.

187. Zhao J, Xie X, Lin Q, Ma X, Su P, Xia Y. 2020. Next-Generation Paternò–Büchi Reagents for Lipid Analysis by Mass Spectrometry. Anal Chem 92:13470–13477.

188. Cao W, Cheng S, Yang J, Feng J, Zhang W, Li Z, Chen Q, Xia Y, Ouyang Z, Ma X. 2020. Large-scale lipid analysis with C=C location and sn-position isomer resolving power. Nat Commun 11:375.

189. Zhang W, Donghui Zhang, Zhang D, Chen Q, Qinhua Chen, Chen Q, Wu J, Zheng Ouyang, Ouyang Z, Ouyang Z, Xia Y, Yu Xia. 2019. Online photochemical derivatization enables comprehensive mass spectrometric analysis of unsaturated phospholipid isomers. Nature Communications 10:79–79.

190. Feng G, Hao Y, Wu L, Chen S. A visible-light activated [2 + 2] cycloaddition reaction enables pinpointing carbon–carbon double bonds in lipids. Chem Sci 11:7244–7251.

191. Cetraro N, Cody RB, Yew JY. 2019. Carbon–carbon double bond position elucidation in fatty acids using ozone-coupled direct analysis in real time mass spectrometry. Analyst 144:5848–5855.

192. Esch P, Heiles S. 2018. Charging and Charge Switching of Unsaturated Lipids and Apolar Compounds Using Paternò-Büchi Reactions. J Am Soc Mass Spectrom 29:1971–1980.

193. Paterno E, Chieffi G. 1909. Sintesi in chimica organica per mezzo della luce. Nota II. Composti degli idrocarburi non saturi con aldeidi e chetoni. Gazz chim ital 39:341–361.

194. Büchi G, Inman CG, Lipinsky ES. 1954. Light-catalyzed Organic Reactions. I. The Reaction of Carbonyl Compounds with 2-Methyl-2-butene in the Presence of Ultraviolet Light. J Am Chem Soc 76:4327–4331.

195. Yang NC, Nussim M, Jorgenson MJ, Murov S. 1964. Photochemical reactions of carbonyl compounds in solution The Paterno-Büchi reaction. Tetrahedron Letters 5:3657–3664.

196. Ma X, Chong L, Rong Tian, Ran Tian, Tian R, Shi R, Hu Y, Hu TY, Zheng Ouyang, Ouyang Z, Xia Y. 2016. Identification and quantitation of lipid C=C location isomers: A

shotgun lipidomics approach enabled by photochemical reaction. Proceedings of the National Academy of Sciences of the United States of America 113:2573–2578.

197. Hynds HM, Hines KM. 2022. Ion Mobility Shift Reagents for Lipid Double Bonds Based on Paternò–Büchi Photoderivatization with Halogenated Acetophenones. J Am Soc Mass Spectrom 33:1982–1989.

198. Murphy RC, Okuno T, Johnson CA, Barkley RM. 2017. Determination of Double Bond Positions in Polyunsaturated Fatty Acids Using the Photochemical Paternò-Büchi Reaction with Acetone and Tandem Mass Spectrometry. Anal Chem 89:8545–8553.

199. Bednařík A, Bölsker S, Soltwisch J, Dreisewerd K. 2018. An On-Tissue Paternò–Büchi Reaction for Localization of Carbon–Carbon Double Bonds in Phospholipids and Glycolipids by Matrix-Assisted Laser-Desorption–Ionization Mass-Spectrometry Imaging. Angewandte Chemie International Edition 57:12092–12096.

200. Wäldchen F, Spengler B, Heiles S. 2019. Reactive Matrix-Assisted Laser Desorption/Ionization Mass Spectrometry Imaging Using an Intrinsically Photoreactive Paternò–Büchi Matrix for Double-Bond Localization in Isomeric Phospholipids. J Am Chem Soc 141:11816–11820.

201. Jeck V, Korf A, Vosse C, Hayen H. 2019. Localization of double-bond positions in lipids by tandem mass spectrometry succeeding high-performance liquid chromatography with post-column derivatization. Rapid Commun Mass Spectrom 33:86–94.

202. Tang S, Cheng H, Yan X. 2020. On-Demand Electrochemical Epoxidation in Nano-Electrospray Ionization Mass Spectrometry to Locate Carbon–Carbon Double Bonds. Angewandte Chemie International Edition 59:209–214.

203. Ren H, Alexander Triebl, Triebl A, Muralidharan S, Markus R. Wenk, Wenk MR, Xia Y, Federico Torta, Torta F. 2021. Mapping the distribution of double bond location isomers in lipids across mouse tissues. Analyst 146:3899–3907.

204. Li Z, Cheng S, Lin Q, Cao W, Yang J, Zhang M, Shen A, Zhang W, Xia Y, Ma X, Ouyang Z. 2021. Single-cell lipidomics with high structural specificity by mass spectrometry. Nat Commun 12:2869.

205. Xie X, Zhao J, Lin M, Zhang J-L, Xia Y. 2020. Profiling of Cholesteryl Esters by Coupling Charge-Tagging Paternò–Büchi Reaction and Liquid Chromatography–Mass Spectrometry. Anal Chem 92:8487–8496.

206. Wenpeng Zhang, Ruijun Jian, Jing Zhao, Yikun Liu, Yu Xia. 2022. Deep-lipidotyping by mass spectrometry: recent technical advances and applications. Journal of Lipid Research 100219–100219.

207. Hines KM, Herron J, Xu L. 2017. Assessment of altered lipid homeostasis by HILIC-ion mobility-mass spectrometry-based lipidomics. 4. Journal of Lipid Research 58:809–819.

208. Xia T, Zhou F, Zhang D, Jin X, Shi H, Yin H, Gong Y, Xia Y. 2023. Deep-profiling of phospholipidome via rapid orthogonal separations and isomer-resolved mass spectrometry. Nat Commun 14:4263.

209. Ivanova PT, Cerda BA, Horn DM, Cohen JS, McLafferty FW, Brown HA. 2001. Electrospray ionization mass spectrometry analysis of changes in phospholipids in RBL-2H3 mastocytoma cells during degranulation. Proceedings of the National Academy of Sciences of the United States of America 98:7152.

210. Koivusalo M, Haimi P, Heikinheimo L, Kostiainen R, Somerharju P. 2001. Quantitative determination of phospholipid compositions by ESI-MS: effects of acyl chain length, unsaturation, and lipid concentration on instrument response. Journal of Lipid Research 42:663–672.

211. Esch P, Heiles S. 2020. Investigating C□C positions and hydroxylation sites in lipids using Paternò–Büchi functionalization mass spectrometry. Analyst 145:2256–2266.

212. Xia T, Yuan M, Xu Y, Zhou F, Yu K, Xia Y. 2021. Deep Structural Annotation of Glycerolipids by the Charge-Tagging Paterno–Büchi Reaction and Supercritical Fluid Chromatography–Ion Mobility Mass Spectrometry. Anal Chem 93:8345–8353.

213. Pruitt EL, Zhang R, Ross DH, Ashford NK, Chen X, Alonzo F, Bush MF, Werth BJ, Xu L. Elucidating the impact of bacterial lipases, human serum albumin, and FASII inhibition on the utilization of exogenous fatty acids by Staphylococcus aureus. mSphere 8:e00368-23.

214. Picache JA, Rose BS, Balinski A, Leaptrot KL, Sherrod SD, May JC, McLean JA. 2019. Collision cross section compendium to annotate and predict multi-omic compound identities. Chem Sci 10:983–993.

215. Xie X, Yu Xia, Xia Y. 2019. Analysis of Conjugated Fatty Acid Isomers by the Paternò-Büchi Reaction and Trapped Ion Mobility Mass Spectrometry. Analytical Chemistry 91:7173–7180.

216. Kuo S-T, Tang S, Russell DH, Yan X. 2022. Characterization of lipid carbon–carbon double-bond isomerism via ion mobility-mass spectrometry (IMS-MS) combined with cuprous ion-induced fragmentation. International Journal of Mass Spectrometry 479:116889.

217. Yang X, Xia Y. 2021. Mapping Complex Disulfide Bonds via Implementing Photochemical Reduction Online with Liquid Chromatography–Mass Spectrometry. J Am Soc Mass Spectrom 32:307–314.

218. Cao W, Cheng S, Yang J, Feng J, Zhang W, Li Z, Chen Q, Xia Y, Ouyang Z, Ma X. 2020. Large-scale lipid analysis with C=C location and sn-position isomer resolving power. Nat Commun 11:375.

219. Nguyen R, Seguin RP, Ross DH, Chen P, Richardson S, Liem J, Lin YS, Xu L. 2024. Development and Application of a Multidimensional Database for the Detection of Quaternary Ammonium Compounds and Their Phase I Hepatic Metabolites in Humans. Environ Sci Technol 58:6236–6249.